CRANFIELD UNIVERSITY

ANDREW LORENTZ

DESIGN, CONSTRUCTION AND TESTING OF AN ASCENDING MICROPENETROMETER TO MEASURE SOIL CRUST RESISTANCE

SCHOOL OF ENGINEERING
MSc in Engineering by Research

MSc
Academic Year: 2013 - 2014

Supervisor: Prof. F. BRENNAN
Co-supervisors: Dr. M. COLLU and Prof. K. RITZ
Advisor: Dr. E. ARMENISE
February 2014

CRANFIELD UNIVERSITY

ANDREW LORENTZ

DESIGN, CONSTRUCTION AND TESTING OF AN ASCENDING MICROPENETROMETER TO MEASURE SOIL CRUST RESISTANCE

SCHOOL OF ENGINEERING
MSc in Engineering by Research

MSc
Academic Year: 2013 - 2014

Supervisor: Prof. F. BRENNAN
Co-supervisors: Dr. M. COLLU and Prof. K. RITZ
Advisor: Dr. E. ARMENISE
February 2014

ABSTRACT

The increasing world population is putting pressure on global food production. Agriculture must meet these growing demands by increasing crop yields. One phenomenon which prevents seedling emergence and damages crop yield is soil crusting. Understanding of soil crusting and the factors which influence it is fundamental to ensuring good crop production. An instrument which will test soil crust strength in a novel way, mimicking seedling growth, may lead to pre-emptive agricultural soil management which could increase crop production. This work details the process of design, construction and testing of an ascending penetrometer to measure soil crust strength. The full design process is discussed from concept generation and evaluation, using experimental methods and a multi-criteria decision making tool, through to final design configuration, specification, manufacture and testing.

Traditionally, soil penetrometers measure soil strength by forcing a probe from the surface of the soil into the bulk soil below. To more accurately measure the direct impedance a seedling would experience a device should measure impedance from the bulk soil upwards and into the soil crust, mimicking what a growing seedling would experience. Results prove that the manufactured ascending penetrometer with a force resolution of 0.01N and displacement resolution of 0.0004mm is capable of detecting differences in soil crusts. At these resolutions and accuracy to 0.1N and 0.1mm excellent repeatability was achieved. The machine is therefore a useful and realistic tool for quantitatively comparing soil crusts in soil. It is hoped that being able to compare soil crust strength will lead to improved soil management techniques.

Keywords: penetration resistance, TOPSIS, seedling emergence, instrument design

ACKNOWLEDGEMENTS

I have been lucky enough to have had amazing support around me during my MSc. The work would never have been completed without this support and so I would like to acknowledge their contributions. Dr. Elena Armenise has been my advisor, she has taught me so much about soil science and kept ideas flowing for me. I am extremely grateful for all the discussions we have had and her advice on how to progress. I would like to thank Prof. Feargal Brennan and Dr. Maurizio Collu for allowing me to take on the MSc by research; the experience has been life changing for me. Thank you Maurizio for all the meetings and setting time aside for me every week. I would also like to thank Mr. Stan Collins for taking extra time at the end of several days to help me with LabView programming. Dr. Rob Simmons and Prof. Karl Ritz, thank you to you both for the creative meetings; I hope that the machine will allow you and your team to make some great discoveries. To Mr. Ian Hakon, Derek Brown and the workshop team thank you for turning my machine into reality; it is a great piece of kit. Louise Lam designed the guide system for the penetrometer and it works perfectly, thank you.

My friends and family have also supported me through my journey. Thank you to Mark von Maltzahn, because you need a philosopher friend to keep life in perspective. Jiri Fajtl thanks for showing me what can be done with electronics. My father has given me sound advice throughout the project and I have enjoyed our discussions, thanks Dad. To my Mum and sisters for making sure I have had fun and good spirit during the MSc. Thanks to Dr. Liam Lorentz for being my "kop" doctor. Thanks too to my new family Jack, Riet and Stijn for your support and encouragement. Thank you Granny because of the penguins; yes, they just do their own thing.

Finally I would like to acknowledge my beautiful wife Merel. She has been an inspiration to me; she has always pushed me to discover new things and at the same time made my life full of joy. Merel you make things happen.

TABLE OF CONTENTS

LIST OF FIGURES

LIST OF TABLES

LIST OF EQUATIONS

LIST OF ABBREVIATIONS

PR	Penetration Resistance
FEA	Finite Element Analysis
ADC	Analogue to Digital Converter
ASAE	American Society of Agricultural Engineers

1 Introduction

1.1 Context

The availability of arable land is fast becoming a world crisis. Population growth is putting huge amounts of pressure on farming to become more efficient at using reduced land resources to feed the world and increasingly to produce biofuels. Any measure that is able to maximise crop yield is beneficial in ensuring that agriculture will meet the growing demands for food and energy. Many studies and investments have been made to understand conditions that lead to the best crop yield. Understanding soil properties, conditions and how different soil managements might affect crop development will increase crop profitability, crop production, maintain and improve soil fertility and minimise soil erosion (Davies et al., 1993).

Soil is a thin layer that covers the Earth's surface. It was formed from the weathering of rocks and minerals as a result of the interaction of five factors: 1) parent material, 2) climate, 3) living organisms (especially native vegetation), 4) topography and 5) time. Soil is a crucial constituent of the biosphere, functioning not only in the production of food and fibre, but also in the maintenance of environmental quality (Doran and Parkin, 1994). More specifically, soil provides an environment for seed germination, root growth as well as ensuring the functioning of roots to provide anchorage and absorb water and nutrients (Powlson et al., 2011). Adverse soil conditions can lead to the development of soil crusting which prevents the emergence and growth of seedlings during early development. The current study aims to develop a method to accurately quantify soil crust strength; an important soil property which directly influences seedling emergence, in a new and revolutionary way. It is envisaged that this method will allow for development pre-emptive soil management techniques for increasing seedling emergence.

Soil compaction increases soil strength and this is of major concern in agriculture. A high strength in soils means that more energy must be expended to make the soil viable for plant growth (Smith, 2000). The mechanical properties of soil including strength can be determined using several standard geotechnical tests. These tests include the tri-axial compression and shear tests. From these tests the relationship between stress and strain of the soil are obtained (Atkinson, 2007). The tests are good at determining the bulk soil

properties; however, knowing the effect on soil strength of the compaction caused by rainfall and soil tillage is very important. This compaction causes variable strength values within the top layers of soil. Soil strength in environmental science is generally measured by penetration resistance (PR) using penetrometers. These instruments are used to determine PR at discrete depth intervals, leading to an understanding of the change in soil strength per unit depth. A penetrometer generally consists of a conical tip attached to a shaft that is pushed into the soil. The force is measured during insertion into the soil using various force sensing methods.

Soil crusts are associated with crop loss and low crop yields causing agricultural hardship. A soil crust is a thin layer, with higher density, high shear strength, finer pores and lower saturated hydraulic conductivity than the bulk soil underneath. Bare soils exposed to rainfall can develop crusts due to the kinetic action of falling rain drops. Subsequent drying of the soil following rainfall further adds to the hardening of the crust (Baumhardt and Schwartz, 2005). The dense surface crust that forms prevents seedlings from emerging or hinders the development of the seedling due to loss of energy reserves. The effort the seedling exerts to emerge through the hard crust can cause uneven crop development (Jury et al., 2004; Monsanto Company, 2013). Soil crusting also has other indirect detrimental effects on seedling and crop growth as it increases soil erosion, nutrient depletion, pollution and water run-off, and decreases water infiltration (Batey, 2009). It is therefore important to study the soil crust strength and the parameters that effect crust formation in order to understand how to prevent soil crusting thus ensure maximum crop yield.

1.2 Rationale for current research

There is a gap in knowledge for studies which measure the ascending forces through a crust for a growing seedling. Traditionally, as in the study by Bedaiwy (2008), penetrometers measure soil and crust strength by forcing the probe from the surface into the bulk soil below. An ascending penetrometer would reproduce more accurately the forces that a growing seedling would experience. An attempt to develop such a type of penetrometer was made by Aubertot et al. (2002). Since then, to the author's knowledge, no studies have tried to recreate an ascending penetrometer to understand the impact that soil crust strength has on the emergence of seedlings.

The purpose of the present research is to design and construct an instrument to measure the PR that a seedling would encounter during emergence. Unlike Aubertot et al. (2002), the instrument will not be used to predict the emergence rate of seedlings, but to develop a detailed understanding of the location and magnitude of the forces that a seedling would encounter during emergence through a crust. The instrument would need to be able to detect changes in strength within the soil crust strength to a suitable resolution. By improving the resolution and accuracy of the measurement, the ascending penetrometer would be an improvement compared to the Aubertot et al. (2002) device and lead to a tool which would be effective at quantitatively comparing crusting of laboratory prepared soil samples.

1.3 Aim and objectives

The main aim of this project is to deliver a laboratory instrument that is capable of accurately measuring the soil crust strength within laboratory prepared soil samples. By designing and building a soil penetrometer which is ascending in force application, the device will more accurately measure the forces an emerging seedling encounters. A clear understanding of the factors involved in formation of soil crusts and their resultant strengths relative to emergent seedlings could then be developed. There are two mechanisms which cause crust formation due to rainfall. Firstly, the impact of the rain drops compacts the uppermost layer of the soil forming a thin layer of higher density soil (Sumner and Stewart, 1992). The skin is typically 0.1mm thick (Jury et al., 2004). Secondly, the impact of the rainfall causes the breakup of aggregates into finer particles. Physiochemical processes cause dispersion of the fine particles into the soil immediately below the surface. These finer particles clog the pores below the surface forming a "washed-in" zone which is typically 0.5mm – 3.0mm thick (Baumhardt and Schwartz, 2005). The resolution of the soil penetrometer should be fine enough to detect microstructure strength characteristics of the soil crust. Ideally the instrument should be able to detect changes in mechanical resistance between the crust, the washed-in zone, and the interface between the washed-in zone and the bulk soil.

In order to achieve this aim, the project has been broken down into several objectives:

- Propose a starting point for the design of a penetrometer that will be used in laboratory studies investigating the crust strength and properties which influence its formation. Verify the ability of ascending-type penetrometers to measure forces within soil samples (Chapter 4).
- To design concepts, critical evaluation of the designs, design choice, final design configuration and drawings and finally manufacture of the instrument (Chapter 5 and 6).
- Test and calibrate the device to ensure that PR was being accurately measured and changes in soil crust strength could be detected (Chapter 7).

1.4 Methodology

The design, manufacture and testing of the ascending micropenetrometer was broken down into methodical stages aimed at developing an understanding of the mechanics and design parameters. Stages of the project were defined as follows:

- **Literature review**

  To increase the understanding of current technology, theory and physical methods used to determine soil strength, first a literature study was conducted. Once a base knowledge was established a literature review, critically comparing the design and results of current penetrometers, was completed. (Chapter 2)

- **Theory**

  The main factors affecting soil crust formation and strength are explored and discussed. Fundamental understanding of these properties was important so that their effect on penetrometer design could be assessed. (Chapter 3)

- **Design requirements**

  Using the knowledge gained through the literature review technical requirements of the ascending micropenetrometer were discussed with the end user from a soil science perspective. These requirements would form the basis for all future work. Ultimately the micropenetrometer would need to meet these technical specifications. (Chapter 4)

- **Preliminary experiment – validation study**

  Following the literature review it was clear that a preliminary laboratory experiment to validate the applicability of ascending-type penetrometers was required. A preliminary experiment, designed to develop an understanding of the ascending penetration method as well as explore certain fundamental design characteristics for the micropenetrometer was conducted. (Chapter 4)

- **Finite element analysis model**

  The results of the experiment revealed some very interesting observations which warranted further investigation. To explore and further understand the mechanisms at work during soil penetration a Finite Element Analysis (FEA) of the dynamic ascending and descending penetrometer was conducted. (Chapter 4 and Appendix B)

- **Concept generation and evaluation**

  Once design parameters were explored and validated concept designs for the ascending micropenetrometer were developed. Using knowledge gained from the preliminary experiment, FEA, reviewed components and devices from existing literature a total of five concepts were proposed. Critical analysis of the proposed concepts was important to be able to select the design most likely to produce results which met the technical requirements. Concept evaluation was carried out using a multi-criteria decision making tool. (Chapter 5)

Final design

- Final design selection, following design concept choice three possible systems were proposed using various commercially available components. Once the final design and components were selected, the ascending micropenetrometer was manufactured and control software developed. (Chapter 6)

- **Testing and analysis**

  Finally the ascending micropenetrometer needed to be tested to ensure correct functionality. Calibration and testing results are discussed which led to the proposal of some future work. (Chapter 7)

2 Literature Review

The aim of this review is to critically analyse the types of soil penetrometers and componentry currently used to measure soil strength and in particular penetrometers which attempt to measure surface and crust strength.

2.1 Micropenetrometers

The most commonly used penetrometer for environmental applications is the static cone penetrometer (Herrick and Jones, 2002). These traditional penetrometers are mostly used to describe the macroscopic soil strength of large soil bodies only (Liu et al., 2006). Soils which behave homogeneously on a macroscopic level contain spatial variations in strength on a smaller, microscopic scale (Smith, 2000). General tillage and compaction effects can be measured using traditional penetrometers designed largely around the ASAE (American Society of Agricultural Engineers) standard S313.3 FEB04 described in section 3.3. For studies where bulk soil characteristics and generalised effects such us bulk density and soil texture are investigated, finer resolution in the measurement is required. The micropenetrometer should have a high rigidity and constant penetration velocity. The measuring probe should have a small diameter and small length dimensions. These properties will allow detection of thin layers and breaking of soil bonds rather than producing a primarily compressive failure (Schneebeli and Johnson, 1998).

Bedaiwy (2008) successfully investigated the effect of rainfall duration on the formation of a soil crust and its corresponding strength. The micropenetrometer used in the afore mentioned study was capable of determining differences in crust strength after 10min of rainfall, with the smallest change in strength recorded equal to 1.2N (approx. 100grams). The crust strength was measured as an average throughout the crust profile, therefore no information on the forces within the crust itself was obtained.

Smith et al. (1997) determined the textural influence of soil on the soil strength in 29 South African soils. The device used in Smith et al. (1997) was made from a Universal Testing Machine to determine average penetration resistance of soils. Again here in this study no information of strength characteristics at discrete depths throughout the penetration was created. To understand soil crust strength characteristics in more detail a finer resolution measurement of depth and load is required.

Liu et al. (2006) suggested that the microscopic strength variation of a soil can be used to better model the soil behaviour. The micropenetrometer developed by Liu et al. (2006) was able to measure at finer force resolution and smaller depth increments and could therefore measure surface strength variations more accurately. Another example is the micropenetrometer developed by Rolston et al. (1991) which measured the soil surface strength and the microfabric of the soil in situ. The aim of the study was to determine the instrument capability in detecting differences in surface characteristics induced by different soils physical properties and irrigation management (Rolston et al., 1991).

Liu et al. (2006) developed a micropenetrometer to analyse the microstructural strength of soils with different texture. The study does not specifically mention application of soil crust strength, however, with a depth resolution measurement of 0.1mm and force resolution of 0.1N it is suggested that this could easily be achieved. There are still some improvements that could be made to this design though. The motor used resulted in a movement resolution of only 0.5mm while the depth measurement transducer was capable of 0.1mm resolution. Finer motor control, down to at least the level of the transducer, would greatly improve the smoothness and resolution of the measurement. The micropenetrometer was used to determine soft soil microstructural strength for applications in civil engineering. This micropenetrometer differed from other devices in that instead of moving the probe into the soil the soil sample was forced onto a static probe. Having a static probe allowed the sensitive load cell to remain fixed behind the probe. It is suggested that this is a very good solution leading to greater measurement accuracy through reduction of signal noise which may be produced by a moving probe attached directly to the motor or drive.

The results from the micropenetrometer in Liu et al. (2006) clearly shows the force measured throughout the soil depth (Figure 1a). Good resolution is shown in Figure 1b which helps to understand the microstructure and strength variations of the soil. From Figure 1b it can be seen that in a layer of soil with similar average strength, particles in the soil cause localised peaks in strength that must be overcome by the advancing probe. These peaks form waves of variation in end resistance. The waveform has a relatively uniform wavelength and wave heights, thus indicating the relatively homogeneous nature of the sandy soil. The peaks are caused by the hard sand particles in the homogeneous soil

and a force of 0.5N – 1.5N is required to force the probe past these particles. The microstructure of the soil and the microscopic mechanical properties of the soil can be determined by being able to measure low load variations. Displacement resolution is, however, quite coarse and this means that detail within a short penetration depth is limited. To determine forces within a crust of 3-5mm finer position resolution is required. Finer resolution would most likely also smooth the measurement.

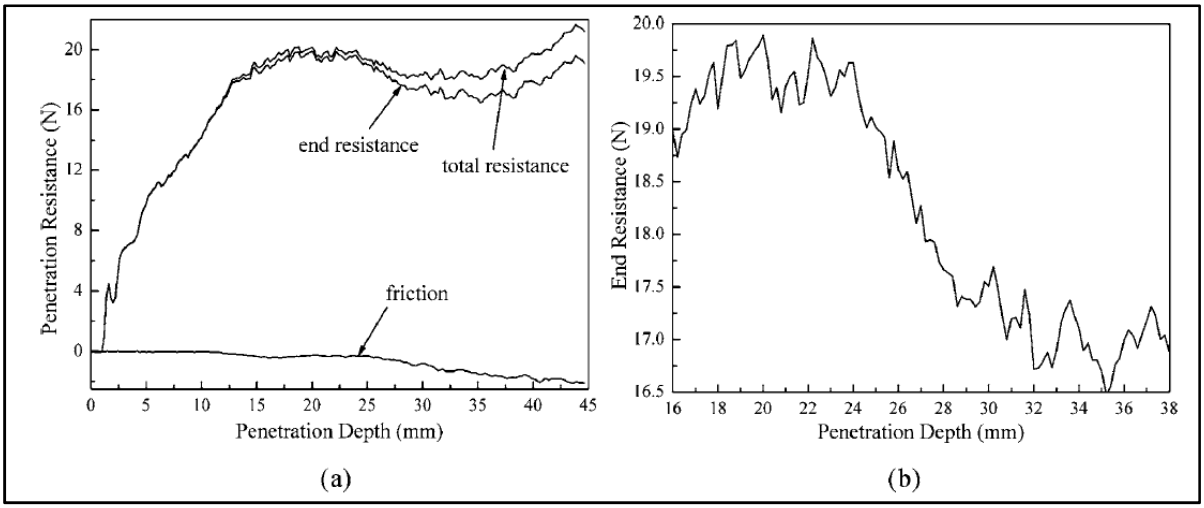

Figure 1 - Penetration resistance curves of a sandy soil. (a) General resistance curve and (b) Enlarged detail of end resistance. Reproduced from Liu et al. (2006)

Drahorad and Felix-Henningsen (2012) developed a high resolution micropenetrometer that was capable of detecting changes in crust strength on a sub-millimetre range. Figure 2 shows that at a fine force resolution of 0.0192N (2.0g) distinct layers in the crust can be identified, namely a top-crust and a sub-crust.

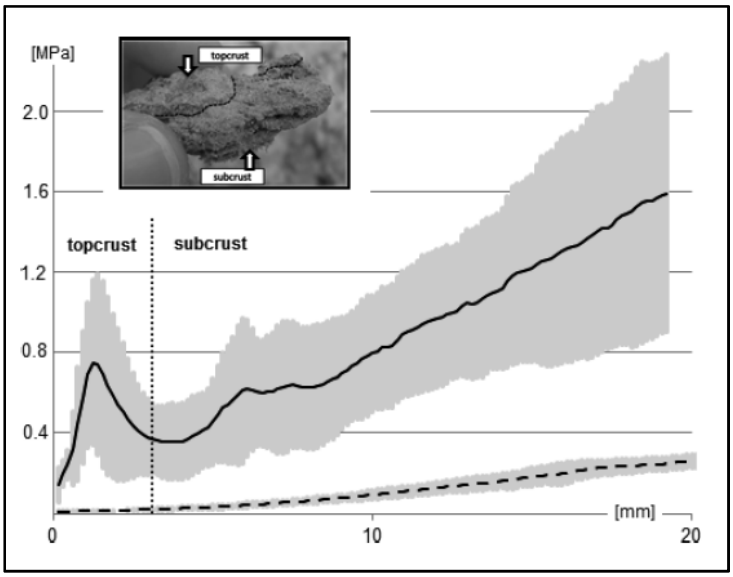

Figure 2 Penetration resistance of a biological soil crust (Drahorad and Felix-Henningsen, 2012)

In this study a number of measurements were taken and post processing averaged the results. The range of measured results is also displayed. For this kind of measurement small scale depth increments of 0.039mm are required. The fine resolution achieved here is impressive, however, with such tiny increments a lot of signal variation is produced during measurement. This highly variable measurement can make it difficult to analyse in post-processing, requiring complicated signal averaging to determine strength trends.

Aubertot et al. (2002) typical force measurement is shown in Figure 3. Results range from 0.05N (0.005g) to 0.80N (0.082g) for the force to break the crust; taken as the peak minus the plateau deemed the frictional force. Aubertot et al. (2002) does not consider the effect of depth on the penetration resistance. Instead force is measured over time with force recorded every 0.5 seconds at a penetration speed of 20mm/min, resulting in a position resolution of 0.17mm. The resulting curve clearly indicates the peak value of the crust PR, however, again the position resolution is relatively course. Better motor technology and position measurement would offer greater insight into the strength within the crust layer.

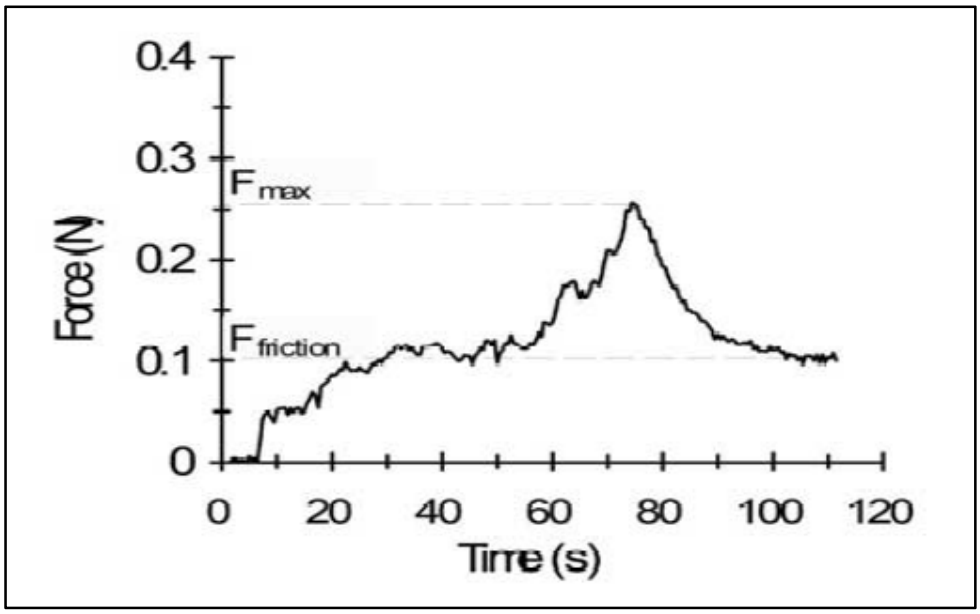

Figure 3 - Typical force measured by ascending probe.
Reproduced from Aubertot et al. (2002)

Rolston et al. (1991) demonstrated that some variation in the soil surface strength could be detected with a resolution of 0.016mm and force resolution of 0.054N (5.5g). Results from the study indicate that a peak in crust strength occurs near the surface and reduces to a steady state (Figure 4). The variation is, however, not very detailed since it would be desirable to have better resolution leading to the peak value. The authors did not attempt to measure the frictional effects, which likely leaded to a further over estimation of the surface strength. Results, however, still showed measureable differences in penetration resistance of different soils, although to a level seen as inadequate for crust strength variations.

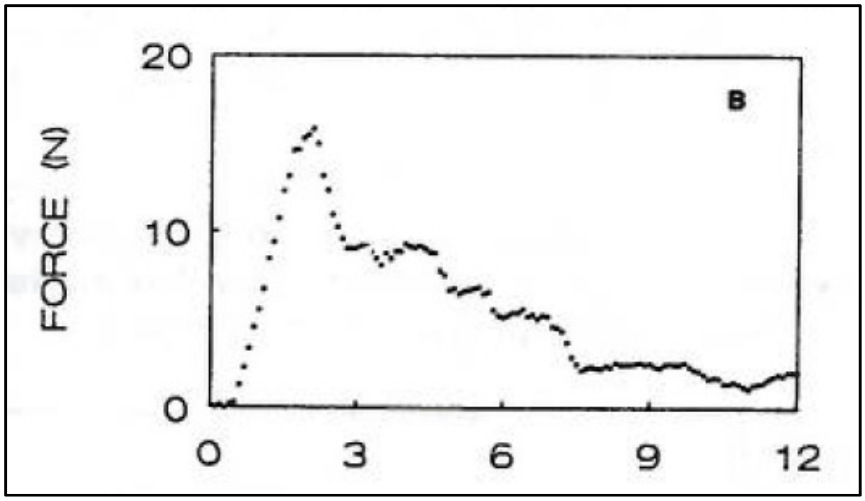

Figure 4 - For-depth curve for a shallow crust over loose soil (Rolston et al., 1991)

2.2 Ascending micropenetrometer

During its natural growth, a seedling penetrates the soil crust from underneath. The forces exerted on the crust by emerging seedlings differ depending on the shape of the hypocotyl. Monocotyledonous crops, such as grasses and cereals, exert a point load while dicotyledonous crops have larger hypocotyls which distribute the load over a small area (Goyal et al., 1979). During emergence seedlings, such as beetroot and wheat, are able to exert forces between 0.2N (20g) and 0.29N (30g) putting the crust under bending stress, creating tension on the top surface (Bouaziz et al., 1990; Aubertot et al., 2002). If the modulus of rupture of the soil is lower than this stress created, the crust will break and allow the seedling to push through (Goyal et al., 1979).

All the micropenetrometers apart from Aubertot et al. (2002) described in section 2.1 force the probe through the soil from above. Studies have shown that this greatly overestimates the strength of the soil, usually in the order of two to eight times greater than the force exerted by growing roots (Bengough and Mullins, 1990). This overestimation is due to the soil being compacted in front of the advancing probe thus providing further resistance. Therefore in order to accurately measure the forces experienced by emerging seedlings a new method of force application is required.

Therefore, an ascending penetrometer is suggested to better reproduce seedling growth. Aubertot et al. (2002) is the only study that has developed a micropenetrometer that mimics seedling emergence. With ascending penetration the soil is free to move in the

direction of the force, this significantly reduces the compaction in front of advancing probe and should produce PR forces more similar to that which a seedling experiences (Aubertot et al., 2002). A potential disadvantage of the ascending micropenetrometer is that it can only be used in the laboratory, where soil can be exposed from below the surface. Laboratory conditions should therefore reproduce field conditions as close as possible (Rolston et al., 1991).

There are several potential improvements to the ascending micropenetrometer designed by Aubertot et al. (2002) that have been identified:

- Aubertot et al. (2002) placed the soil to test in relatively large tanks (0.58 x 0.58 x 0.11 m) with soil depth of 9mm. With such a large area, the controllability of the soil properties such as water content and bulk density is reduced. Individual samples would allow better control, increased repeatability and analytical repetitions.

- Greater accuracy in positioning and load measurement by making use of modern technology, such as accurate stepper motors and control systems, would enhance the capability of the micropenetrometer to detect structural changes in the crust strength. Liu et al. (2006) achieved this goal effectively by using a load cell sensitive enough to detect 0.1N force changes within the soil.

- A load cell attached to the probe and driven into the soil produces higher noise in the signal due to vibrations of the motor. A better solution would be to fix the load cell and move the soil onto the probe. The effectiveness of this method was demonstrated by Liu et al. (2006)

- Fundamentally the aim of Aubertot et al. (2002) to predict the emergence rate of seedlings using a penetrometer is difficult to achieve. Seedlings grow following the path of least resistance and will therefore find cracks in the soil matrix which a ridgid probe cannot. A better aim for the study is to understand the structural nature of the crust strength and what is influencing it.

2.3 Design parameters for micropenetrometers

Design specifications for various micropenetrometers are compared in Table 1. From the table it is possible to identify the kind of resolution, probe diameter and configurations that have been used in studies thus far.

Table 1 - Micropenetrometer specifications

Journal Article	Probe Specifications 1. Diameter 2. Cone/Tip Properties 3. Material	Load Cell Specifications 1. Capacity 2. Resolution 3. Sampling period 4. Type	Displacement Transducer Specifications 1. Depth range 2. Resolution	Motor Drive Specifications 1. Type 2. Penetration speed 3. Step increment 4. Drive train 5. Power
Drahorad 2012	1. ϕ = 3mm 2. Flat tip 3. Stainless steel	1. 20N 2. 19.2mN (0.02% nonleararity) 3. 39µm (by depth) 4. Althen, Germany	1. 0 – 40mm 2. 39µm	1. Stepper motor 2. 16mm/min 3. 39µm 4. Gear and rack (Leitz, Germany) 5. 62 Nm Torque
Liu 2006	1. ϕ = 0.3 –1mm 2. Flat tip (assumed)	1. 100N 2. 0.1N 3. 0.01s	1. 0 – 50mm 2. 0.1mm	1. Constant speed electrical rotary 2. 1 – 5mm/min 3. Stepless speed change device 4. Worm gear 5. Unknown
Aubertot 2002	1. ϕ = 1mm 2. Flat tip 3. Stainless steel	1. 0 -1N 2. 0.01N 3. 0.5s 4. Unknown	1. 30mm 2. Displacement not measured	1. Not specified 2. 20mm/min
Rolston 1991	1. ϕ = 1.59mm 2. Flat tip	1. 23kg (225N) 2. 5.5g (0.5N) 3. 0.016mm (by depth) 4. SM-50 Interface Inc.	1. 0 – 40mm 2. 0.1mm	1. Stepper motor 2. 8mm/min

2.4 Penetrometer design parameters

2.4.1 Probe and cone

The shape and size of the probe and cone should be carefully considered when trying to mimic forces experienced by the emerging seedlings. The shape of the probe determines the type of soil deformation and frictional resistance at the tip.

During insertion the penetration resistance is created by two principal forces (Bengough and Mullins, 1990; Klute and Page, 1982):

- force to deform the soil by the wedge-action of the cone tip
- soil-to-metal frictional force against the cone and probe surface

Smith (2000) explains that the diameter of the probe must be less than 20 times the diameter of the sample core in order to minimise edge effects. A larger diameter probe would laterally displace more soil pushing against the side of the core and artificially increase the penetration resistance. The change in penetration resistance due to probe diameter is exaggerated for small cone diameters, Whiteley and Dexter (1981) determined that changing the cone diameter from 2mm to 1mm resulted in a 45-55% increase in PR. The probe must therefore be small enough to negate sample container edge effects but large enough to minimise the frictional contribution to the total PR. Rolston et al. (1991) found that a 1.59mm cone was strong enough to penetrate soils in the field whilst Drahorad and Felix-Henningsen (2012) used a larger 3mm diameter probe required for harder in-field soil PR measurements. Aubertot et al. (2002) and Liu et al. (2006) on the other hand used smaller 1mm diameter probes in their laboratory micropenetrometers. Both sets of micropenetrometer were able to detect compaction layer boundaries; however, the edge effects are far more damaging to a reading than a slight additional friction component since there are methods which can measure frictional contribution. Therefore, the probe should be chosen to be as small as possible but still able to resist the buckling load.

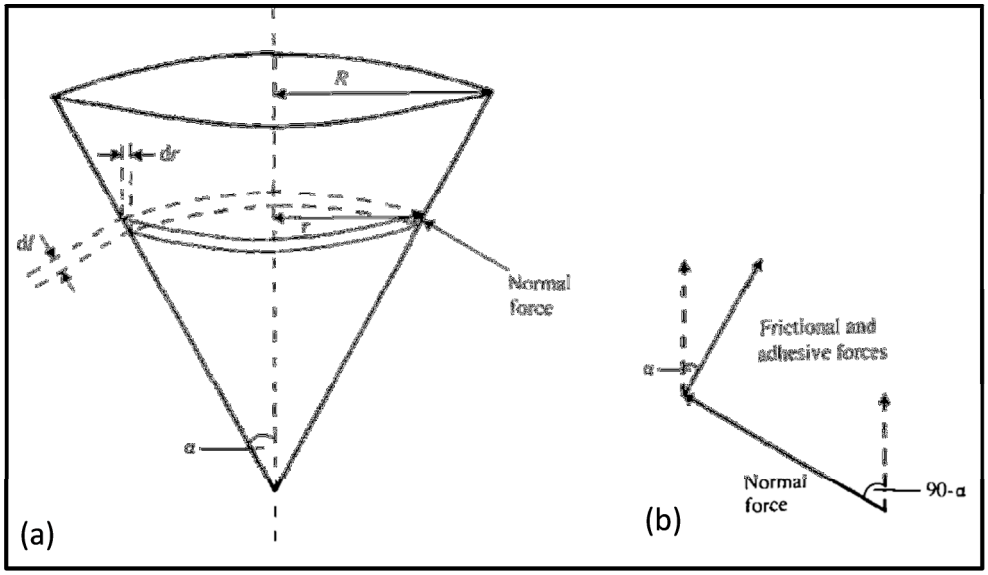

Figure 5 - Diagram of (a) a penetrometer cone and (b) the force acting at a point on the cone surface. Reproduced from Bengough (1992).

Penetrometer resistance, Q, is given by the following equation (Bengough, 1992):

$$Q = \sigma(1 + \cot\alpha \cdot \tan\delta) + C_a cot\alpha \qquad (2\text{-}1)$$

Where σ is the stress normal to the cone surface, α the cone semi-angle, δ the angle of soil-metal friction and C_a is the soil-metal adhesion. The angles and forces acting on the cone are illustrated in Figure 5. For a given cone as the cone angle decreases the cone length increases, increasing the cone surface area and therefore the frictional component of penetration resistance. As the cone angle decreases the mechanical advantage of the cone wedge is surpassed by the force of friction due to surface area. This causes penetration resistance to be at a minimum when the angle is 30° (Smith, 2000; Klute and Page, 1982).

All of the micropenetrometers described in Table 1 have utilised a flat tip probe. From equation (2-1) Aubertot et al. (2002) explains that for a cone semi-angle of 90° the mechanical resistance of the soil is equal to the normal stress experienced at the tip. Putting α=90° means that the friction terms fall away in equation (2-1) and the penetration resistance equals the normal stress ($Q = \sigma$). Rolston et al. (1991) found that in a homogeneous surface a flat tipped probe reached constant force at lower depth than a pointed probe. These results suggest that a flat probe might be more suitable for soil surface measurements. However, equation (2-1) is suggested only to be used to probes with relatively narrow cone angles (Smith, 2000). A review of studies in Bengough (1990)

have shown that narrowly tapered probes (with a tip semi-angle of 5°) and plant roots deform the soil in the same manner, while blunt probes cause a sphere of soil to form in front of the advancing probe. This increases penetration resistance. It is suggested that seedling emergence and hypocotyls growth is similar in action to root growth and therefore a narrow tip probe needs to be considered. Due to the conflict of opinion in the literature, it is warranted that two types of probe tip should be investigated further, a 30^0 cone angle and a flat tip, to see the effect on PR and which type best identifies the compacted crust layer.

2.4.2 Penetration rate

Penetration rate has been found not to have a significant effect on penetration resistance; however, this depends on the soil type and water content of the soil (Smith, 2000). Bengough and Mullins (1990) and Rolston et al. (1991) did several studies in which penetration rate was varied. Results showed that except for very wet and remoulded soils, PR is weakly dependant on penetration rate. Since root and seedling growth rates are very slow, typically 0.17mm/min it is near impossible to reproduce this penetration rate in field or laboratory conditions (Smith, 2000). High penetration rate; however, can cause surface cracking which would affect the accuracy of the measurement (Rolston et al., 1991). Drahorad and Felix-Henningsen (2012) used a penetration speed of 16mm/min to great effect in determining soil crust strength on a micro-scale, while Rolston et al. (1991) suggests using a rate of 8mm/min. A rate within these values is suggested as preferable to avoid excessive surface break up.

2.4.3 Dealing with friction

Friction occurs between the soil and the metal of the probe and increases the measured penetration resistance. Therefore it is important to find methods to estimate the friction and deduct this value from the total measured penetration resistance. Since seedling growth is very slow, typically 1.0 x 10-3 mm/min, it is suggested that friction has minimal effect on the seedling. Studies which investigate the influence of the general soil characteristics such as bulk density, texture and water content are not concerned with the actual PR but rather aim to find differences between soils (Rolston et al., 1991; Bedaiwy, 2008). In the design of these devices the effect of friction is not considered. When looking

to understand the finer structural characteristics of soil crust strength, friction cannot be ignored and must be eliminated as much as possible during or post measurement because Soil-metal frictional forces on the probe of a penetrometer can account for between 40% and 80% of the total PR (Bengough et al., 1991). It is therefore important to try to eliminate friction from the penetrating probe.

Frictional effects can be deducted post measurement as in Aubertot et al. (2002). Aubertot et al. (2002) uses a probe with a constant penetration rate and the frictional element is assumed to be the constant force measured before the probe encounters the crust. The crust force is thus taken as the peak in measurement minus the friction force. This method is a good, simple way to measure friction but is not entirely accurate. Since the probe has already forced its way through the soil creating a cavity; the friction on the probe is reduced.

Armbruster et al. (1990) proposed a measurement of the force from immediately behind the cone tip (Armbruster et al., 1990). In this way the shaft-soil friction was eliminated. This method is very effective; however, it necessitates a complex load cell installation of miniature size. This would be difficult to achieve and increase build costs for only a small gain in accuracy.

Liu et al. (2006) measured the frictional force during withdrawal of the probe and deducted the frictional force from the total resistance using post processing software. This method would underestimate the friction force since the cavity had been created by the probe, however the approximation is considered to be fairly accurate.

Rotating the probe during penetration measurements is another way that greatly reduces frictional effects (Bengough et al., 1991). Greater reduction of frictional force was found at higher rotational rates. Friction is reduced due to rotation of the shaft since the frictional force acts in the direction opposite to the probe velocity vector (Bengough et al., 1991). Increasing rotation increases the horizontal vector component thereby decreasing the vertical vector component. Including probe rotation could be beneficial, however, this would add complexity to the design.

2.4.4 Load cell

The main requirement of the instrument is to record the penetration resistance force of the crust. Thus the core of the instrument is the device used to measure the forces, namely the load cell. Position of the load cell needs to also be carefully considered. In all of the reviewed devices the load cell is located immediately behind the probe. This is a good location for the load cell since it eliminates any additional friction forces introduced by the drive system.

As discussed in section 2.1 the resolution of the load cell is important to be able to capture changes in the soil strength throughout the crust thickness. Schneebeli and Johnson (1998) developed a snow micropenetrometers to explore the thin weak layers within snow formations. The microscopic physical properties of the snow layers were detected. For stronger material such as soil crust the resolution of the load cell need not be as high as the device developed by Schneebeli and Johnson (1998), however, there should be some improvement on the resolution given by devices used solely for comparative studies such as the Rolston et al. (1991) and Bedaiwy (2008) micropenetrometers. The load cell used by Liu et al. (2006) with a resolution of 0.1N (10g) is considered adequate.

There are 5 basic types of load cell: compression, tension, S-type tension-compression, bending and shear (Bahra and Paros, 2010). PR is a purely vertical force and therefore compression and universal tension-compression load cells are applicable to micropenetrometers. Drahorad and Felix-Henningsen (2012) used a purely compressive load cell with very fine resolution which was able to detect subtle changes in force within soil crusts. Whilst the load cell recorded minute changes in the crust strength, no frictional component of the PR could be determined by measuring the tension force during probe withdrawal. The high accuracy and resolution also comes at a high price, this particular load cell costing approximately £800. Although less accurate with coarser resolution, both the Rolston et al. (1991) and the Liu et al. (2006) micropenetrometers used tension-compression S-type load cells. These two machines were still very effective at measuring the soil crust strength with the additional benefit of being able to measure tension forces upon probe withdrawal. Liu et al. (2006) used this advantage by recording this frictional tension force and subtracting it from the total PR to get a more accurate measurement of actual soil strength PR.

2.4.5 Motor and drive selection

In all the micropenetrometers evaluated, constant speed motors have been utilised. Constant speed ability is certainly the main requirement for the micropenetrometer drive system since static cone penetrometers (SCP) are considered best for soil science studies.

2.4.5.1 Electric motors

Electric stepper motors in combination with a linear drive system, comprising of either a rack and pinion gear or lead screw, have been used successfully in micropenetrometer designs. Both the devices developed by Rolston et al. (1991) and Drahorad and Felix-Henningsen (2012) utilise the stepper motor for better performances. The stepper motor offers excellent open-loop position control that does not require complex feedback control systems. Stepping motors are easily controllable by computer or microprocessor. Commands from the micro-controller rotate the shaft in discrete angular steps. The number of steps in one rotation gives the motor its resolution, the more steps the motor is capable of the finer the motion control. This makes the motor suited to drive machine tool slides connected to a lead screw or rack and pinion gear set (Hughes, 1993). The tolerance in achieving the ideal position for one step is the accuracy of the motor. The electric stepper motor is seen to be superior to the continuous drive system utilised by Liu et al. (2006). Continuous drive motors require feedback control and therefore increases the cost of the control system for the instrument. An electric motor in combination with either lead screw or rack and pinion drive would be evaluated in our design.

2.4.5.2 Linear Actuators

Other types of drive system include pneumatic and hydraulic actuators. These offer the benefit of an incorporated linear drive system. These types of drive system are expensive, complex and require additional equipment such as a compressor. Hydraulic actuators offer the greatest accuracy and control of position compared to pneumatic due to the incompressibility of oil.

Hydraulic and pneumatic actuators used in industry to control robots would also be considered for the design (Drahorad and Felix-Henningsen, 2012; Liu et al., 2006).

2.4.5.3 Lead screw drive systems

Backlash is the amount of linear motion between the screw and the nut without turning the screw. This is important for positional accuracy and repeatability. There are devices which have been made to reduce this backlash effect, including the ball lead screw.

Lead screws are used to convert rotation to linear motion. They offer several advantages (Hamrock et al., 2005):

- Precise positioning of an axial movement can be obtained, resulting in less play and backlash than the rack and pinion.
- Frictional effects can be reduced using roller bearing lead screw sometimes called ball lead screw.
- Offer mechanical advantage in lifting weight.

Lead screws can be used as linear actuators: a motor drives the lead screw and the ball nut or linear nut translates rotation to linear motion. The devices are used to move a table or work piece, in the case of the micropenetrometer the lead screw would be used to advance the probe into the soil sample. If the rotating input is driven by a stepper or continuous motor in combination with a precision lead screw, very accurate positioning is possible (Norton, 2011). The design parameters of a lead screw to work out translational motion and required drive torque is detailed in Appendix D.1. Rolston et al. (1991) and Liu et al. (2006) both used the lead screw system to achieve suitable accuracy and resolution of motion. In these two micropenetrometers the advantage of the lead screw compared with a rack and pinion system is apparent due to the fine control achieved. Rack and pinion systems need to have very accurate gears to measure to the same resolution as these lead screws. The lead screw is also an extremely cost effective drive system.

2.4.5.4 Rack and pinion drive systems

Rack and pinion drives use gears to translate rotational motion to linear motion. Teeth on a circular gear are attached to the motor mesh with a flat gear. Fine precision are more difficult to achieve with the rack and pinion system compared to a lead screw, due to the relative motion between the mating gears.

The rack and pinion drive system is considered to be less accurate than a lead screw; however, this is not always the case. Drahorad and Felix-Henningsen (2012) made use of a highly accurate rack and pinion gear produced for precision robotics. This solution offers simplicity and good adaptability since gears could be easily swapped. Cost of this type of gear needs to be considered though; a highly accurate rack and gear drive will cost significantly more than a lead screw system (Rolston et al., 1991; Liu et al., 2006).

2.4.6 Depth measurement

Depth measurement is important for understanding of the crust structure, leading to accurate identification of the boundary between soil strength variations (Liu et al., 2006). For crude measurement simple markings on the probe can be utilised (e.g. in the standard ASAE penetrometer designs). Greater resolution of displacement requires better measurement equipment. The use of stepper or continuous electric drive motors which have encoders that measure the amount of rotation will measure displacement. Here, the accuracy of the measurement is determined by the motor controllability; higher accuracy gained with increased control complexity and cost. Accurate motor positioning can offer excellent accuracy and resolution determining position to within 40μm by using a stepper motor, achieved by Drahorad and Felix-Henningsen (2012). Rolston et al. (1991) used a less precise motor which outputted displacement to an accuracy of 0.1mm; at this resolution crust strength was determined but with less definition of the micro-structural strength variations. Both of these penetrometers directly recorded displacement from the stepper motor while Aubertot et al. (2002) indirectly measured displacement by recording the time of penetration. Since the penetration was at constant speed, position could be calculated. This method is not as accurate because it is difficult to synchronise time with the recorded load. Liu et al. (2006) uses an economic electric continuous motor with no position control built in. Position is instead measured using a displacement transducer. This adds additional equipment and complexity to the design. By measuring depth with the motor position there is less likely to be accumulated error in measurement. Measurement error occurs in the motor drive system and additionally in the transducer itself, whilst displacement measurement using the motor alone would only have motor error. The best system for depth measurement is a compromise between the complexity of the design installation, cost and the total error of the measurement devices.

3 Theory of measuring soil crust strength

There are many parameters that need to be considered when designing a soil penetrometer. The main soil characteristic affecting soil crust strength, the considerations required to measure soil crust strength and to design a penetrometer will be discussed in this section.

3.1 Main characteristics affecting soil strength

- **Soil texture**

Soil texture describes the physical composition of the soil in terms of the percentage of clay, sand and silt. Clay, silt and sand are characterised by a specific particle size According to the British Standard (BS 5930 :1999) classification, the sizes of clay, silt and sand particles are:

Clay: < 0.002mm
Silt: 0.06mm to 0.002mm
Sand: 2mm to 0.06mm

The soil texture influences several important soil characteristics, including water retention and soil structure (Smith, 2000)

- **Water content**

Increasing the water content usually decreases the soil strength (Jury et al., 2004). This is true for all cohesive soils, i.e. soils that contain a significant fraction of clay or silt (Rose, 2004). Higher water content slackens the cohesive forces between particles in the soil since particles are separated during water absorption (Marshall et al., 1996). A study done by March et al. (2013) showed that for three loamy soils the mechanical impedance decreased with increasing water content in an exponential decay relationship (Figure 6).

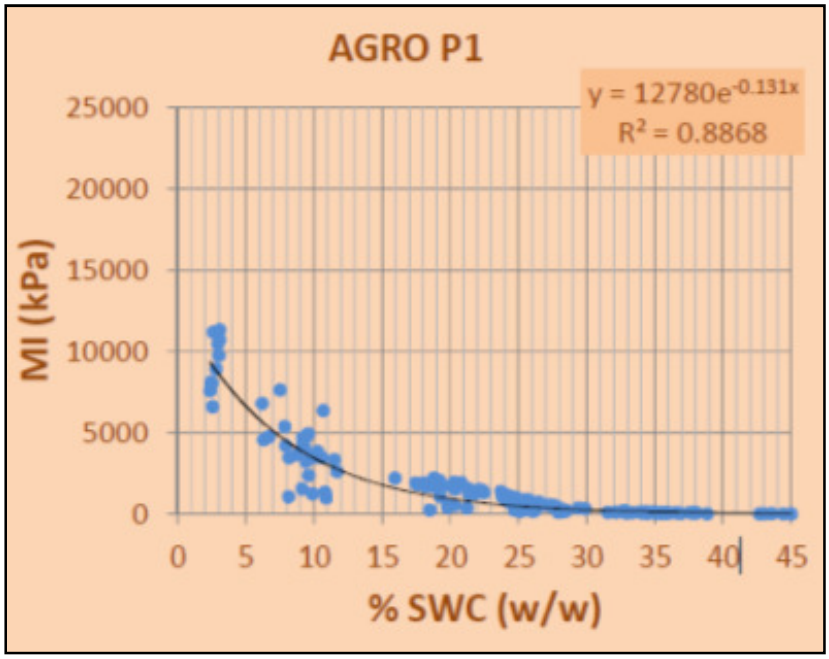

Figure 6 - Results from March et al. (2013) illustrating the exponential decay of mechanical impedance with increasing water content.

- **Bulk density**

In general, increased bulk density increases the soil strength (Smith, 2000). Bulk density affects penetration resistance more in dry soils than wet soils as shown in Figure 4.

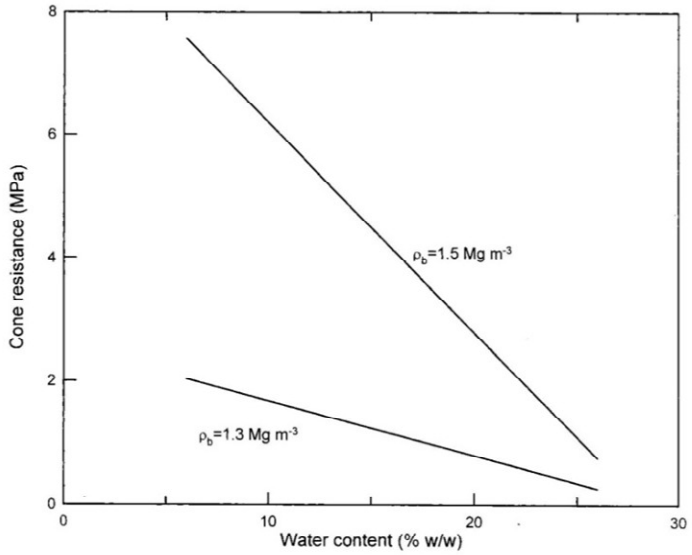

Figure 7 Variation of penetration resistance with water content at different bulk densities. Reproduced from Smith (2000).

- **Soil Structure**

Soil structure is the physical organization of soil particles which bond together to form "clumps" or aggregates (Smith, 2000). Voids form between the aggregates creating pathways for water movement. Soil structure stability influences soil strength. An unstable soil structure means that aggregates are easily disintegrated by impact of rainfall and water infiltration. This break up of aggregates can lead to formation of a crust and blockage of soil pores.

The interaction of the physical properties is complex and soil behaviour cannot be predicted using a single property as an indicator. To determine soil behaviour or soil treatment effects it is important to measure or control these properties independently (Gregorich and Carter, 2008).

A correlation exists between soil strength and root growth and seedling emergence, with hard soils generally preventing seedling emergence and root growth (Bécel et al., 2012; Aubertot et al., 2002; Taylor and Ratliff, 1969). Bécel et al. (2012) showed that increased penetration resistance reduced the root elongation rate in peach trees. In this study, the effect of water content, bulk density and penetration resistance on the root growth of peach trees was tested. It was determined that the penetration had the most statistically significant influence on the root growth. This illustrates the importance of identifying the strength properties of a soil to inform appropriate soil management strategies for maximising crop yield.

3.2 Soil crust

Studies have been performed under laboratory conditions to understand rainfall characteristics that effect soil crust formation and strength. Bedaiwy (2008) showed that silt-loam and clay soils developed crusts under simulated rainfall. In this study crust strength was measured using a penetrometer with a flat tipped probe of 1.59mm. The penetrometer was able to detect the strength of the soil crust, and it was determined that crust penetration resistance increased with rainfall intensity or applied kinetic energy as shown in Figure 8. In addition it was observed that a silt-loam soil produced a crust with greater strength than a clay soil except under low intensity rainfall treatment.

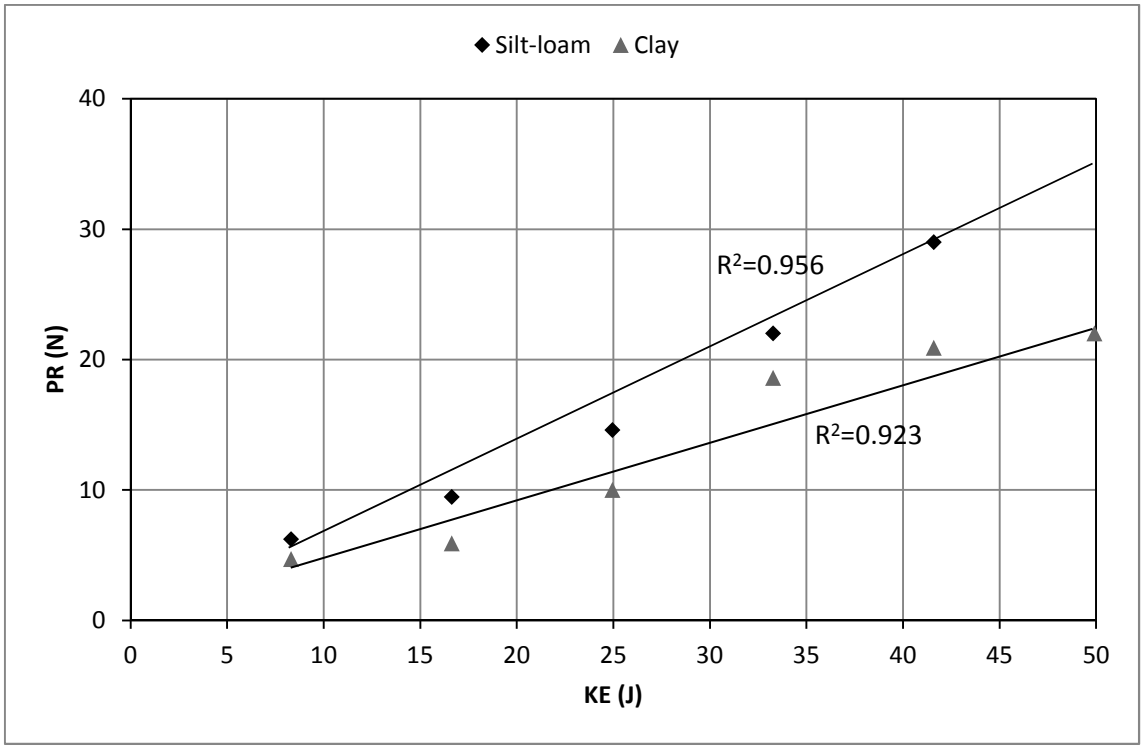

Figure 8 Effect of kinetic energy (KE) of falling water droplets on the penetration resistance (PR) of soil crusts. Reproduced from Bedaiwy (2008).

3.3 Penetration resistance (PR)

Penetration resistance is usually expressed as a function of pressure, i.e. it is the force required to push the cone into the soil divided by the cross-sectional area of the cone. This is known as the cone index or CI of the soil and is usually measured in units of pascal (Pa), kilopascal (kPa) or megapascal (MPa)

There are two main types of penetrometer which differ in the way that the shaft and cone are driven into the soil: static cone penetrometer (SCP) and dynamic cone penetrometer (DCP). Static cone penetrometers are driven into the soil at a slow constant rate to avoid the need to include dynamic effects in the analysis. Inserting the cone at constant velocity also ensures that no acceleration or impact forces are introduced to the measurement and only penetration and frictional forces are measured.

Dynamic cone penetrometers are driven into the soil by a known amount of applied energy using the impact of a hammer or a falling weight. This type of penetrometer is used for highway pavement and roadbed evaluations but has been rarely applied in soil science investigations (Carter and Gregorich, 2008).

The American Society of Agricultural Engineers (ASAE) has developed a standard for static cone penetrometer design (American Society of Agricultural Engineers Standards, 1999) which is commonly used in soil-based activities (Herrick and Jones, 2002). The standard includes a 30° circular stainless steel cone with a driving shaft of smaller diameter to minimize soil friction between the shaft and the soil.

4 Micropenetrometer design

4.1 Design requirements

From the review of existing micropenetrometer designs in chapter 2 it can be seen that certain parameters produce more desirable outcomes. Aspects considered important to make the instrument capable of measuring PR similar to seedling forces and able to detect structural changes in the crust would be taken from the designs reviewed. Possible improvements in the designs would also be incorporated.

The following design requirements for the ascending micropenetrometer were set out based on the literature review:

- A laboratory micropenetrometer, capable of holding a prepared soil sample of 50mm diameter and penetration to a depth of minimum 100mm.
- Ascending action, measuring PR of the soil sample from below, penetrating first the bulk soil and then into the soil crust (Aubertot et al., 2002).
- A method of measuring displacement with 0.1mm resolution (Drahorad and Felix-Henningsen, 2012; Rolston et al., 1991; Liu et al., 2006).
- Frictional effect should be measured independently during withdrawal of the probe. This is seen as a better method compared to the method used by Aubertot et al. (2002) where friction is recorded as the constant force reached after penetration. In reality friction is not constant throughout the measurement.
- Good resolution of force needs to be recorded to capture microstructural strength changes in the crust. A force resolution less than or equal to 0.1N would be sufficient (Liu et al., 2006; Rolston et al., 1991).
- A probe diameter less of 1.6mm. This would eliminate edge effects since the diameter would be more than 20 times less than the sample (Smith, 2000; Rolston et al., 1991).

- Static cone penetrometer capable of a constant penetration rates between 8mm/min and 16mm/min (Drahorad and Felix-Henningsen, 2012; Liu et al., 2006; Rolston et al., 1991).

4.2 Design methodology

With the requirements finalised the design phase of the project could begin. The design, manufacture and testing of the ascending micropenetrometer is broken down into methodical stages aimed at developing an understanding of the mechanics and design parameters. Stages of the project were defined as follows:

- **Preliminary laboratory experiment** (section 4.3- 4.4)

  First an experiment was designed and conducted to develop understanding of the ascending penetration method. The experiment explored certain fundamental design characteristics of the micropenetrometer and built an understanding of soil science practises.

- **Finite Element Analysis (FEA)** (section 4.4)

  A model was developed to explore the failure mechanics of the soil during ascending penetration compared with traditional descending penetration. The model would also be used to help explain findings of the preliminary experiment.

- **Concept designs** (section 5.1)

  Once certain design parameters were validated concept designs for the micropenetrometer were developed, making use of knowledge gained from the preliminary experiment, reviewed components and devices from existing literature.

- **Concept evaluation** (section 5.2)

  A multi-criteria decision making tool was used to evaluate the design concepts.

- **Final design selection** (chapter 6)

  Following design concept choice three possible systems were proposed using various commercially available components. The final configuration chosen and the micropenetrometer manufactured and control software programmed.

- **Testing** (chapter 7)

  The micropenetrometer was first calibrated and then various settings of the micropenetrometer were explored by testing some samples.

4.3 Preliminary experiment

In order to evaluate the expected range of force created by the soil crusts an initial experiment to investigate force application (ascending and descending), probe shape, water content and soil type effects was conducted. The results of the experiment would also form the basis for several of the micropenetrometer design parameters as well as aim to demonstrate the effectiveness of measuring penetration resistance with an ascending probe.

4.3.1 Materials and method

The spring balance is a simple instrument that can be used to measure static applied forces (Bahra and Paros, 2010). The instrument offered a low cost option to manually determine approximate soil crust penetration resistance. Using the spring balances with force ranges between 250g to 5kg six pocket penetrometers were manufactured and a simple experiment set up to investigate the effects of four factors on PR:

- Ascending force application
- 2x Soil types – Duffy's (S1) and Pinchbeck (S2)
- 2x Soil water contents - Air dried soil and fan dried soil
- 2x Probes- A flat tipped and pointed probe

By controlling the factors and investigating their effect in isolation where possible, the results were compared with other studies from literature. The pocket penetrometers (Figure 9) were manufactured by drilling a hole into the spring balance push rod end, and inserting a 1.5mm needle. The needle had two ends, a flat end and a pointed end, with a cone angle of 30 degrees.

Figure 9 - Completed pocket penetrometer and detail of probe with flat tip at base and 30^0 at the top.

Two soils were used for the experiment (Table 2). Both soils were classed as Sandy Silt Loam, however, there were some significant differences in texture. Notably, Pinchbeck (S2) contained a higher sand and fine sand content than Duffy (S1). Twelve samples were packed into 46mm diameter PVC cores to a depth of 50mm and bulk density of 1.2 $g.cm^{-3}$. Two different drying regimes were tested: i) air drying, ii) fan blow drying; details of the drying methods are found in appendix A.1. The two drying regimes generated two different soil water contents, and the effect of water content on the soil crust strength was investigated.

Table 2 - Soils main physical characteristics

Soil Name	**Soil Texture**	**Particle-size distribution**				**Organic matter (%)**	**Initial bulk density ($g.cm^{-3}$)**	**Initial Water Content (%)**
		Sand (%)	**Silt (%)**	**Clay (%)**	**Fine Sand (%)**			
Duffy **S1**	Sandy Silt Loam	35.95	47.55	16.95	35.55	1.171	1.2	14.2
Pinchbeck **S2**	Sandy Silt Loam	40.43	45.42	14.15	39.84	1.331	1.2	15.9

Crusts were formed on the samples by applying simulated rainfall with appropriate characteristics (i.e. duration, intensity, kinetic energy) and subsequent drying. The cores were exposed to a rainfall event of 15min at an intensity of 47mm/hr and kinetic energy content of 12.8 – 18.9$Jm^{-2}mm^{-1}$. Rainfall characteristics were obtained by calibrating an 8.8m rainfall tower fitted with a randomising mesh. Homogenous rainfall characteristics on the rainfall catchment area were ensured by adjusting the rainfall simulator consisting of 73 open drip needles. Then, using a Laser Optical Distrometer (LOD) (Model Parsivel 2), drop size velocity and particle size distribution was measured. Details of the calibration method and results are detailed in appendix A.2. The water content of the samples was measured using the gravimetric method at three depths within the cores (this allowed the identification of the water content profile): surface, middle and bottom of the samples. Two replicate measurements were considered for each soil and the average water content at the three depths and two drying regimes was calculated and compared. Six soil crust penetration measurements were obtained from each sample, three using the flat probe and three using the pointed probe. Ascending penetration measurements were taken and recorded by video camera so that the maximum force reached could easily be obtained during video playback.

Once the samples had been prepared and subjected to the relative drying regime, PR measurements were performed on all samples. The equipment (Figure 10) and procedure for study are detailed below.

The following steps were used to test the soil crust strength on each of the 12 soil cores:

1. Soil cores were clamped into stand and hold in place for penetration measurement.

2. For ascending force measurements the probe of the penetrometer was inserted from underneath the soil sample into the crust. The pocket penetrometer was pushed upwards evenly, keeping it perpendicular to the soil surface, and the measurement monitored using the Nikon D3100 video camera.

3. The maximum force at the soil crust was recorded after watching the video recording in slow motion. When the applied force was not sufficient for the needle to break through the crust, step one and two were repeated using the next spring balance with greater rated force range.

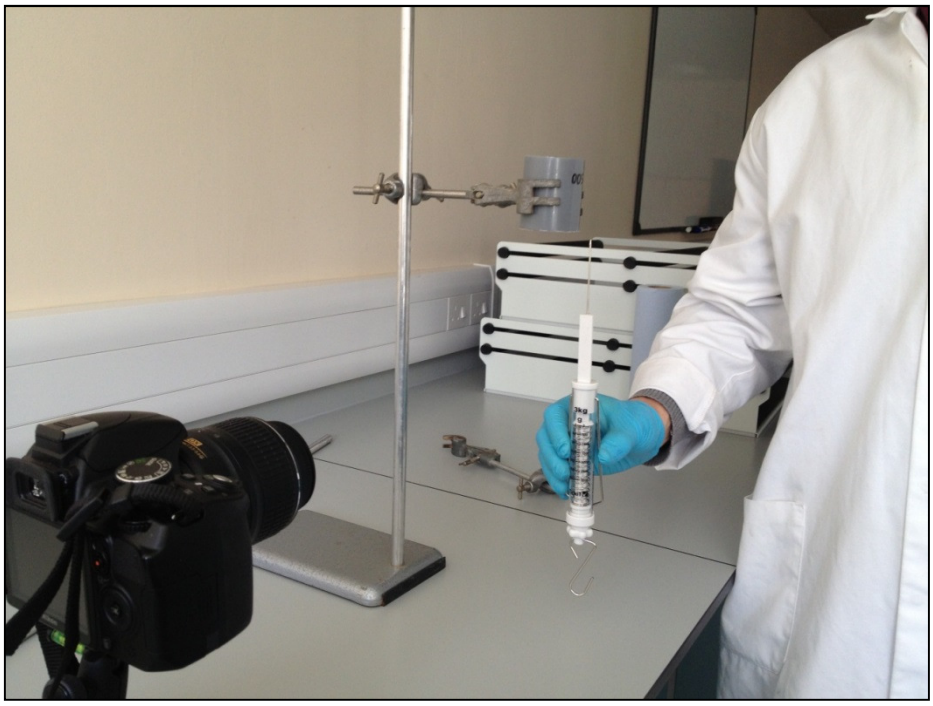

Figure 10 - Photograph of equipment used in PR measurements

The same procedure was repeated with the pointed tip probe and then the flat tip probe ensuring that each measurement taken on in a position of undisturbed crust area. Three replicate measurements were taken on each soil core. All measurements were taken as close to centre of core as possible. A triangular probe pattern around the core centre was used to minimise the container edge effects.

4.3.2 Data analyses and results

All data analyses were performed using R (R Development Core Team, 2010) and Microsoft Excel 2010. Several statistical methods were used to compare results.

Notch boxplots were used to compare penetration resistance (PR) data. Notch boxplots are a good method to graphically compare data sets using the confidence intervals of the medians. The range of the confidence interval for the medians of the data is represented by the length of notch in the boxplot. When the notches of two data sets do not overlap then it can be said that the medians are statistically different to a confidence level of 95% (Chambers, 1983). Notch boxplots also include the following information: minimum value (end of the lower whisker), 25^{th} percentile (bottom of the box), 75^{th} percentile (top of the box) and the maximum value (end of the upper whisker). Data considered as outliers are

represented by separated points on the plot. The 95% confidence interval of the median was calculated using the formula from:

$$median \pm 1.57 \cdot \frac{IQR}{\sqrt{n}} \quad \textbf{(4-1)}$$

where *IQR* is the interquartile range (difference between the 75th and 25th quartiles) and *n* the number of observations (Chambers et al., 1983).

4.3.2.1 Probe tip effect on penetration resistance

Since both probe types in this study have the same cross-sectional area, penetration resistance can be compared in grams force. There were significant differences observed between the effects of the flat probe compared to the pointed probe. The pointed probe penetrated the surface with little damage to the soil crust, while the flat probe lifted the crust and broke it into several fragments. Figure 11 shows clearly the effect of the shape of the probe on the fracture of the crust. Both soils showed fracture in a similar manner to Figure 11 in samples from both drying regimes.

Figure 11 - Photograph of S2 samples after flat probe (left) and pointed probe (right) penetration

Figure 12 compares the penetration resistance of the two soils within the same drying regime. These figures combine the effect of texture of the different soils and the water content on the penetration resistance. The results show a significant difference between penetration resistances obtained using the two different tip types, but show no clear differences between penetration resistances of the two soil types. The pointed needle type

recorded significantly higher PR than the flat needle in both the fan drying regime (Figure 12 a) and air drying regime (Figure 12 b). This is true for both soil types although the differences are more marked in S1 and in the fan drying regime (Figure 13).

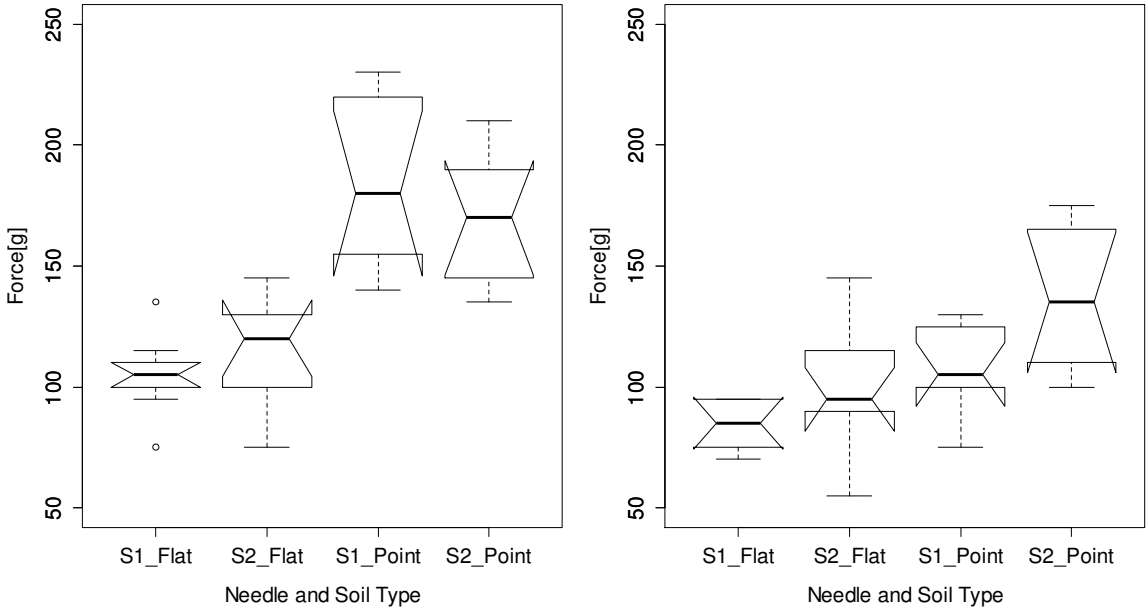

(a) **(b)**

Figure 12 – Notch boxplot for soil type (S1 and S2) and needle type (pointed and flat) in the fan drying regime (a) and air drying regime (b).

4.3.2.2 Water content effect on penetration resistance (PR)

Table 3 reports the effects of the drying regimes on the water content of the two soils and the resulting penetration forces recorded by the two cone tip types with further detail presented in appendix A.3. The results show that the drying regime had little influence on the tendency of S2 to dry out, since the difference in water content between the drying regimes was very small i.e. 0.44%. The drying regime did, however, affect water content of S1 far more; resulting in a decrease in water content of 2.47% compared to 0.46% in S2.

Table 3 – Effect of soil type and drying regime (fan and air) on soil water content and penetration resistance of two needle types (flat and pointed).

	Water Content [%] (location within sample)	Force (Averaged Maximum) [g]	
		Flat Tip	Pointed Tip
Soil 1 (S1)			
Air Dried	14.70 (surface) 16.20 (middle) 17.35 (bottom)	84	108
Fan Dried	11.56 (surface) 14.63 (middle) 14.62 (bottom)	104	183
Soil 2 (S2)			
Air Dried	18.29 (surface) 18.45 (middle) 19.42 (bottom)	98	138
Fan Dried	17.91 (surface) 18.16 (middle) 18.76 (bottom)	114	168

In order to show that the samples needed to be moist to obtain a measurement of the penetrative resistance of the crust, a fully dry sample was tested. The sample was impossible to penetrate, even with the highest rated spring balance (5kg force).

Figure 13a shows the effect of the drying regime and needle type on the measured penetrative resistance in S1. It is evident that the notched box plots for the same tip used in different drying regimes do not overlap and therefore the water content on penetration resistance is statistically significant for soil S1. Figure 13b shows the effect of the drying regime and needle type on the measured penetrative resistance in S2. It indicates that the penetration resistance measured by the two tips tends to be higher in the fan drying regime

compared to the air dried. The notches of the flat tip and the pointed tip for both air and fan drying regimes do not overlap; resulting in statistically significant differences in the forces recorded by the flat tip compared to the forces recorded by the pointed tip.

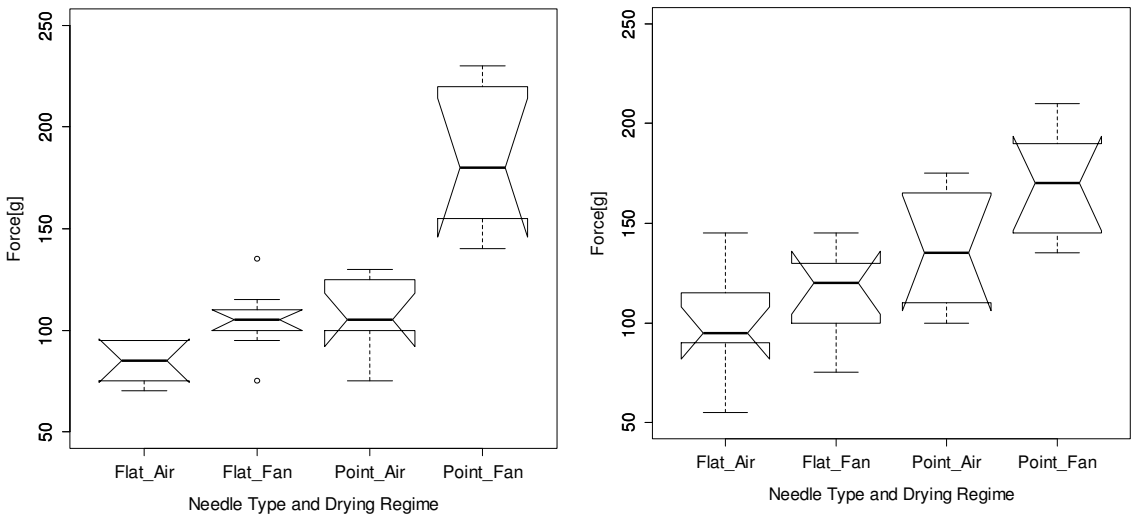

(a) **(b)**

Figure 13 – Comparison of drying regime (fan and air) and needle type (pointed and flat) within S1 (a) and S2 (b).

4.3.2.3 Textural effect on penetration resistance

Comparison of water contents in S1 and S2 (Table 3) shows that the air drying regime for soil S1 produced a surface water content of 14.70% while the fan drying regime produced a surface water content of 17.92%. The average water content (throughout the depth profile) of the air drying regime in S1 was 16.08% while for the fan drying regime in S2 the average was 18.28%. These conditions produced the most similar water contents in the two soils of different texture. The resulting PR from these conditions is compared in Figure 14 to investigate the influence of texture on structural strength and penetration resistance. Results show that for both tip types S2 produced statistically significant higher penetration resistance.

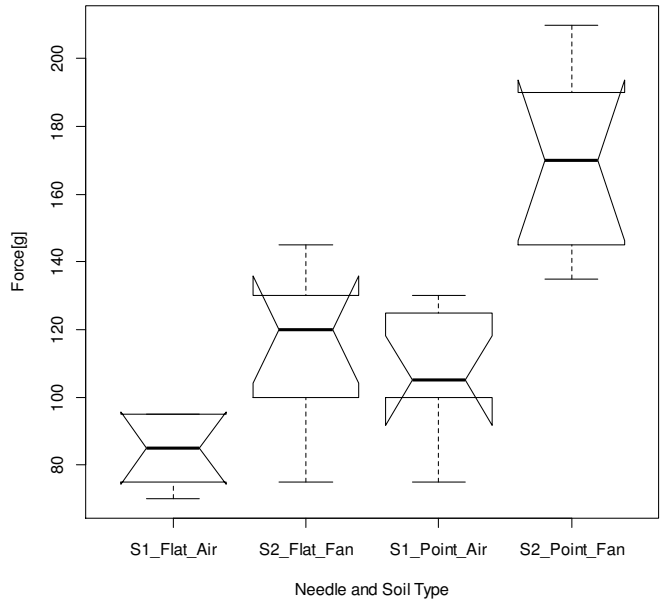

Figure 14 - Comparison of penetration resistance in different soils (S1 and S2) with similar water contents (Air dried S1 and Fan dried S2)

4.3.3 Discussion

Several factors influence the penetration resistance of soil. Among the factors that influence penetration are soil texture, soil-metal friction (between soil and penetrometer) and the soil deformation mechanism. The factors are inter-dependant and influence each other so care must be taken when comparing results. To determine effect of the drying regime on penetration resistance, results from samples with the same texture should be compared. When evaluating the effect of soil texture on penetration resistance, samples of different texture but similar water content should be compared. Using the results from the experiment the following discussion will explore the interactions between soil texture, water content and deformation mechanism on penetration resistance. These observations would determine some micropenetrometer design parameters and identify soil conditions to be used during PR measurements.

Figure 15 explains the interaction of the different factors that affect the PR of soil crusts. Soil texture is the main contributor; it determines the ability of the soil to form a crust. Texture determines the water retention characteristics of the soil, influencing how quickly the soil dries out; this drying is a main contributor to crust hardening (Baumhardt and Schwartz, 2005). Soil texture determines the adhesion and cohesion forces within the soil

matrix. These forces give the soil its structural strength. The particle shape, particle size and cohesion forces also determine the soil-metal friction contribution to PR. The drying regime affects the final water content of the soil crust and the underlying soil; lower water content is associated with an increase in PR. Frictional and deformation mechanism directly influence the penetration resistance; the shape and size of the probe changing the direction, magnitude and friction component of PR.

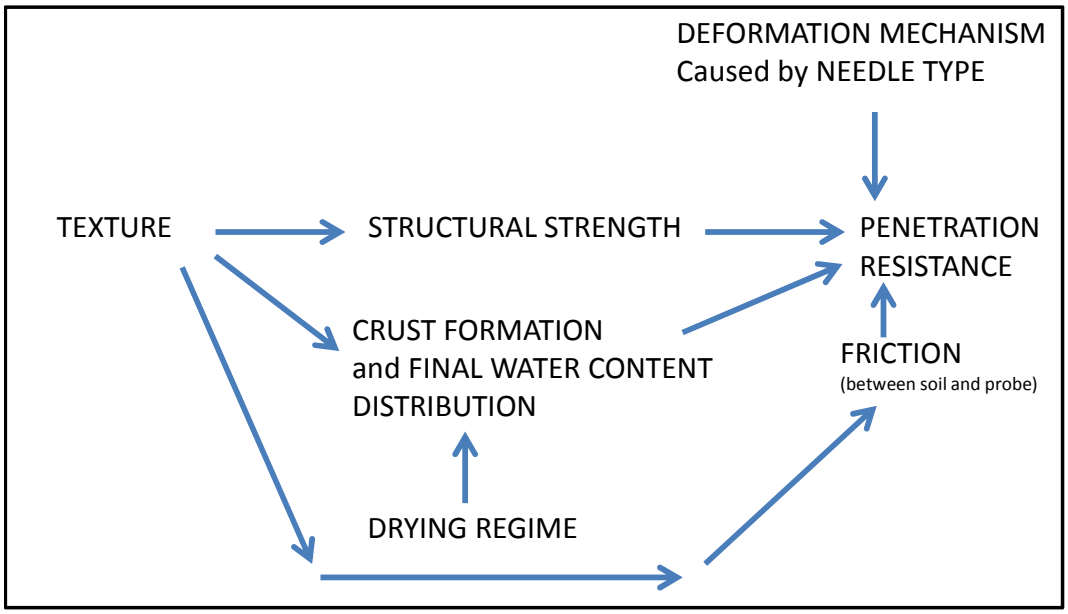

Figure 15 - Flow diagram showing the interaction of different parameters on penetration resistance

4.3.3.1 Force range

Results from Table 3 show that the force range during ascending penetration using the 1.5mm probe was 84 – 168g or 0.8 – 2.3 N. This is a good indication of the expected forces during measurement with the micropenetrometer using a 1.5mm diameter probe, in soil with water content between 12 and 19%. Uncertainty of these measurements are perceived to be quite high due to the quality of the spring device, the difficulty in controlling the penetration speed during manual insertion and the way in which the magnitude was recorded using video playback. Therefore an element of risk would need to be applied to these forces to include a safety factor that the results of the micropenetrometer forces would lie within the 0.8 – 2.3 N range. A conservative safety factor would be to multiply the force by 2 times; resulting in a force range of 0.3 – 5.0 N (Juvinall and Marshek, 2000). Thus the results of the experiment reveal that a load cell of

suitable accuracy within the 0.3 – 5 N range would be ideal for the micropenetrometer. The repeats within each sample varied by approximately 10g or 0.1 N and thus the resolution of the load cell would need to be close to this value.

4.3.3.2 Tip shape and deformation mechanism influence on penetration resistance

There are two factors which the tip or cone angle affects during penetration, soil-metal friction and the soil deformation mechanism.

Smith (2000) explains that the frictional component becomes predominant in smaller diameter probes. This is true since a small reduction in cone angle results in a larger proportional increase in surface area compared to large diameter cones. Therefore compared to the flat tip, the pointed probe is certainly measuring PR with a greater more soil-metal friction component. In all soil conditions the pointed probe recorded higher penetration forces (Table 3). The result is particularly highlighted in the soils with lower water content. Figure 12 illustrates the significantly higher PR measured by the pointed probe; resulting in forces ranging between 140g -225g for the pointed probe compared to 85g – 137g of the flat probe.

The shape of the penetrometer cone tip determines the deformation of soil during penetration. A flat cone tip compacts the soil in front of the tip causing vertical deformation of the soil. On the other hand, a pointed tip with a smaller cone angle tends to deform the soil laterally (Smith, 2000). During insertion the pointed tip is forcing the soil sideways which compresses the soil in horizontal direction. Since the soil is confined laterally by the adjacent soil, forces normal to the probe tip are created and this increases soil-probe friction and therefore the measured penetration resistance. The flat probe pushes the soil vertically upwards. Since the soil is unconfined at the surface, the soil is able to deform more easily compared to the lateral deformation. The surface of the soil is put into tension which the soil cannot resist due to low cohesive forces and therefore the surface breaks into fragments. This fact is clearly illustrated in the photograph of the soil surfaces after penetration (Figure 11). Here, the crust is cracked and lifted in which is similar in action to the emergence of seedlings while the pointed probe simply creates a neat hole.

The results illustrate very clearly that the shape influences the PR. The pointed probe is better at measuring the differences between crusts formed in the soils of varying texture (Figure 14) and water content (Figure 13). The flat probe; however, is better at deforming the soil in a way similar to seedling (Figure 11) and the forces obtained 80g – 175g are closer to the forces seedling can exert (Bouaziz et al., 1990). Further testing using a micropenetrometer of greater accuracy was warranted to find the most suitable probe shape.

4.3.3.3 Water content influence on penetration resistance

PR can be determined using bulk mechanical properties of the soil (Bengough, 1992). However, certain properties of the soil need to be known, such as the angle of soil metal friction and the coefficient of soil metal adhesion. These properties are not easy to determine, therefore several studies have been performed to correlate PR to other more easily determined soil properties such as water content and soil texture via regression equations (Ayers and Perumpral, 1982; Ayers and Bowen, 1987; Dexter et al., 2007; Hernanz et al., 2000; Vaz et al., 2011; Whalley et al., 2007).

In the pocket penetrometer experiment the PR of the same textured soil at two water contents was compared. Higher PR was recorded in samples with lower water content within both S1 and S2 soils (Figure 13). This result is in line with previous studies (March et al., 2013; Bedaiwy, 2008). However, PR was compared between only two different water contents and therefore the possibility of other factors influencing these results cannot be excluded. Difference in the average of the surface water content was large for S1 at 3.13% and the box plots in Figure 13a reveals a statistically significant difference in PR between the flat probe and pointed probe. The difference in average water content at the surface was only 0.38% for S1 which still resulted in measureable differences in penetration resistance but not as significant. Further evidence to suggest that the water content is influencing the PR is that in both soils of different texture the samples with the lower water content recorded higher PR (Figure 13). This was true for both the flat and pointed probe. In the S1 soil with average water content of 16.08% PR ranged between 84g-108g compared to the fan dried S1 of average water content 13.61% with PR from 104g – 183g (Table 3); resulting in very clear increase in PR with decreasing water content for the pointed probe (Figure 13). These results confirm that PR differences can be detected

within soils of water content ranging between 13 and 19% but lower water content of 13% will result in larger differences in PR between different soil crusts. Soil samples for the micropenetrometer should aim to have approximately 13% water content.

4.3.3.4 Textural influence on penetration resistance

In order to fully understand the influence of texture on the structural strength and penetration resistance the water contents of the two soils should be similar. It can then be said that the effect of the water content can be eliminated.

Soil strength has been shown to be influenced by soil texture (Gerard, 1965; Smith et al., 1997). Smith (1997) compared PR in 29 South African soils of varying textures, water contents and bulk densities. Smith (1997) found that clay content and organic matter strongly influence PR. Organic matter content was found to increase the soil strength and therefore PR in samples in wet soils (soils with greater than 5% water content) and decrease soil strength in samples with dry soils (soils with less than 5% water content) (Causarano, 1993). Gerard (1965) showed that PR of remoulded samples, at varying water contents, increased with increasing silt and clay contents. By contrast other studies have correlated an increase in sand content to an increase in PR and an increase in clay content to a decrease in PR (Spivey Jr. et al., 1986). Spivey Jr. el al. (1986) compared 17 samples of varying soil texture. To simulate field conditions, where soil is compacted by rainfall and gravitational forces, samples were compacted by water consolidation. Samples were first slowly saturated by submerging them in water and then lowering the water table allowing for consolidation. The samples were then dried for 24hrs and then the water content was equilibrated to a tension of -100kPa.The samples in our study were prepared by simulated rainfall and then allowed to drain, therefore sample conditions can be considered similar to those in Spivey Jr. el al. (1986) and the results compared.

In our study the two soils are of the same texture class, sandy silt loam (Table 2), however, S2 soil has a larger sand and fine sand content. S2 presented higher PR of 114g and 168g for the flat and pointed probe respectively compared to S1 with PR of 84g and 108g despite that fact that S2 was wetter at an average water content of 18.28% compared to 16.08% of S1 (Figure 14 and Table 3). Therefore the structural strength given by the texture of the soil has had more of an influence on penetration resistance than water content. The increase in PR of S2 is consistent with the results found in Spivey Jr. el al.

(1986) and is attributed to the fact S2 has higher sand content (40%) and lower clay content (14%) compared to S1 which has 35% sand and 17% clay content. The organic matter content was higher in S2 (1.331 %) than S1 (1.171 %) and the water content higher than 5% in both soils, therefore lower PR was expected in S1; results are in agreement with Causarano, (1993). Again when investigating different textural crusts the pointed probe produced greater differences in PR (Figure 14).

4.3.3.5 Limitations of ascending penetration experiment

Measuring PR using ascending penetration is unusual. The results in many respects are incomparable with other penetration studies and the method does not conform to the ASAE Standards for measuring PR.

In the experiment with the pocket penetrometer the frictional forces could not be assessed, however, they are considered significant. The method to measure friction in itself presents some limitations. Since the probe creates a cavity in the soil sample, during withdrawal of the probe the friction would be reduced compared to during insertion.

There was no control sample measurement taken during this experiment to compare the crust measurements to a sample with no crust. Thus there is no certainty that the maximum PR recorded is actually caused by the crust or the underlying bulk soil. The depth at which the maximum force occurs is unknown and therefore a micropenetrometer which records position accurately as well as force would be advantageous.

The method of application of force and recording of force gives a wide range of results. This means that only very general trends can be observed.

4.3.4 Conclusions

Influences of drying regime, soil texture and needle type have been observed to affect crust penetration resistance. The trends observed in our experiment, for the most part, agreed with the literature. The study has proven that even with a crude instrument and measurement technique differences in penetration resistance of the crust can be detected. Results confirm the effectiveness of ascending measurement and an ascending penetrometer should be designed and built to study PR of soil crusts. The

micropenetrometer needs to be able to record both position and force in order to fully understand where the maximum forces are occurring within the sample.

Frictional effects play a large role in the measured penetration resistance; therefore the ascending micropenetrometer should measure friction.

The flat tip experienced less frictional effect compared to the pointed tip, however, greater differences in penetration force were shown using the pointed probe. The flat tip causes vertical deformation, fragmenting the soil surface while the pointed tip pierces the surface, deforming the soil laterally, causing sideways compression, and increasing friction. The shape of the probe should be investigated further in the ascending penetrometer of increased accuracy and resolution.

The fan drying regime produced more obvious differences in penetration resistance between needle types. Therefore in order to produce good results, the crust should be produced using a more extreme drying regime (applying large amounts of energy to the surface of the sample. The water content of the samples should be approximately 13% for testing of sandy silt loam soils similar to those used in the experiment The ideal water content could be different for various soil textures, therefore it is important to test a range of water contents to find ideal soil characteristics for highlighting soil strength variations.

For all measurements taken, the measured force range falls between 0.8 N and 2.3 N. Applying a safety factor of 2 would result in a force range of 0.3 -5 N. A load cell capable of measuring this range to a resolution of 0.1 N would be suitable for the micropenetrometer.

4.4 Modelling soil behaviour

Simply explained, soils rely on two properties for their strength; cohesion and friction. The particles in the soil determine these two properties. Finer particles such as clay and silt are cohesive, while sand particles are frictional (Faber et al., 1976). Soil under the influence of stresses behaves, for the most part, as an elastic-plastic material (Fielke, 1999). This means that under initial stresses the soil will deform under load but return to the original shape when unloaded until the stress reaches a yield stress and permanent plastic deformation occurs. Several failure models for soils have been developed, some of them very complex and involve many parameters. For most engineering purposes only the key features of soil

behaviour are of importance and therefore often simple models can be used to illustrate the mechanics of soil (Huang et al., 2004). One such simple model, Drucker-Prager model, assumes elastic plastic material behaviour and includes material hardening under compression.

Descending soil penetration by a rigid body penetrometer has been modelled in studies using FEA and ABAQUS 6.10 modelling software (Huang et al., 2004; Mouazen, 2002; Naderi-Boldaji et al., 2013; Tekeste et al., 2007). ABAQUS 6.10 is a finite element analysis tool which is capable of modelling Drucker-Prager hardening and was used to first perform a case study based on the Tekeste et al. (2007) study and then to model ascending and descending penetration of a crust zone similar to the pocket penetrometer experiment. Tekeste et al. (2007) modelled descending penetration using a 2D axisymmetric model in order to determine the location of the hardpan in a sandy loam soil. Tekeste et al. (2007) considers a compacted soil layer in the middle of the sample while in our study the compacted layer will be the soil crust at the surface.

4.4.1 Definition of the FEA problem.

To investigate the failure mode and stress distributions in the soil during ascending and descending penetration a simplified model of the soil with a crust zone was created.

ABAQUS/Explicit was used as this solver is good for dynamic simulations. The explicit technique is used to solve complex dynamic problems where the implicit solver is inefficient. The explicit solver is better suited to complex contact problems with large deformations in reduced computational time (Susila and Hryciw, 2003).

Soil properties of the crust and underlying bulk soil were estimated using previous studies, since tri-axial tests could not be performed and the purpose of the model was simply to visualise the soil deformation and compare resistance force between force application methods and probe shapes.

The crust is not a discrete layer of denser, higher strength soil but rather a non-uniform layer of variable density (Roth, 1997). The strength and density decreases from most dense at the surface until convergence with the density of the underlying bulk soil. Therefore, for the model the crust layer was modelled in two layers, with strength decreasing with depth.

Two layers were chosen to represent the crust since increasing the number of layer would make the problem too complex and greatly increase computing time.

The FEA modelled the soil with a hard crust layer from 0 – 2.5mm depth a softer crust layer from 2.5 – 5mm and a soft bulk soil layer from 5mm to 50mm. Drucker-Prager strength properties for the layers with are given in Table 4.

Table 4 – Soil layer material properties used in FEA model

Soil Layer Depth	**Bulk Density ρ (g.cm)^3**	**Elastic modulus (kPa)**
Crust Layer1 0 -2.5mm	1.71	364
Crust Layer 2 2.5-5.0mm	1.54	222
Bulk Soil 5mm– 50mm	1.20	134

Common input values for the remaining parameters were used for all soil layers (see Table 5).

These parameters have been approximated using the information from Fielke (1999), Mouazen (2002), Tekeste et al. (2007) Nareri-Boldaji et al. (2013). For the Drucker-Prager hardening properties values from Tekeste et al. (2007) at compaction III were chosen due to the similar bulk density and elastic modulus compared with our soil samples (see appendix B.1 for calculation of parameters).

Table 5 - Soil properties for the Drucker-Prager model

Parameter	**Value**
ν, Poisson's ratio	0.3
β, Internal friction angle, Drucker-Prager (degree)	38
ψ, Dilation angle (degree)	38
μ, Soil-metal friction	0.5
K, Flow stress ratio	1

4.4.2 Results and discussion

Unfortunately the case study of modelling the conditions described by Tekeste et al. (2007) produced results that were out by a factor of ten (appendix B.6). The produced output PR curves did; however, have a very similar shape so it was assumed that the error was caused by an incorrect soil parameter inputted into the model. After much investigation the reason for the error could not be determined and so the FEA study results cannot be presented with confidence. Therefore the results and explanation of method are only detailed in appendix B. Even though the results are not conclusive and magnitudes of PR under-estimated, there were some good general observations which help to clarify the results of the pocket penetrometer experiment which are worth discussing here.

Modelling of large deformations proved extremely difficult due to simulation instability. Excessive distortion of the finite grid elements meant that often the simulation could not be computed. To overcome the excessive distortion Tekeste et al. (2007) used an inbuilt adaptive re-meshing algorithm called Arbitrary Lagrangian-Eulerian (ALE) method. When ALE was attempted on our soil model there was little success. Eventually a method of manual re-meshing was adopted. The method is described in Roberts (2012) and involved dividing the penetration sequence into smaller discrete steps. Once a small penetration depth was completed the deformed mesh of the soil body was converted into a new geometric shape. The new shape was then repartitioned and meshed to allow for a further penetration step. This method proved very successful and should be used in future large deformation studies of soil penetration.

The FEA model illustrated that the flat probe produces compaction and higher stresses in front of the advancing probe. With improved accuracy the FEA model can be used to detect changes in crust strength and distinguish the interface between layers of compaction.

With development of an effective model the simulation could be expanded to test a variety of probe shapes in order to find one which best highlights soil strength variations. The advantage of the FEA model would be the ability to test several shapes in a short amount of time. Ultimately a growing seedling could be modelled to determine the actual seedling forces experienced.

5 Concepts

Traditionally micropenetrometers are configured to measure from the soil surface down into the soil. In the ascending micropenetrometer, the vertical translation of the probe and application of force through the soil is similar to traditional devices, only the direction of force application changes. Therefore the same drive mechanism and assembly configuration used by traditional micropenetrometers could be adapted for the ascending measurement.

The main types of power drive system considered were:

- Electric motor
- Hydraulic actuator
- Pneumatic actuator

These power drive systems could be used to create vertical translation using the following drive trains:

- Rack and pinion gearing
- Lead screw or power screw
- Direct drive from Hydraulic or Pneumatic actuator

5.1 Concept generation

Using these basic building blocks, five concepts were proposed based on already available penetrometers and the findings from design parameters discussed in section 2.4. Some minor modifications to the five designs were also considered as options. In total 11 configurations were defined and put forward for evaluation using a multi-criteria decision making tool. Concept designs were drawn using the 3D CAD package Solidworks.

Concept 1

The device utilises a rack and pinion gear and electric motor to force the probe into the sample which is fixed to the top of the micropenetrometer frame. The load cell is located underneath the probe.

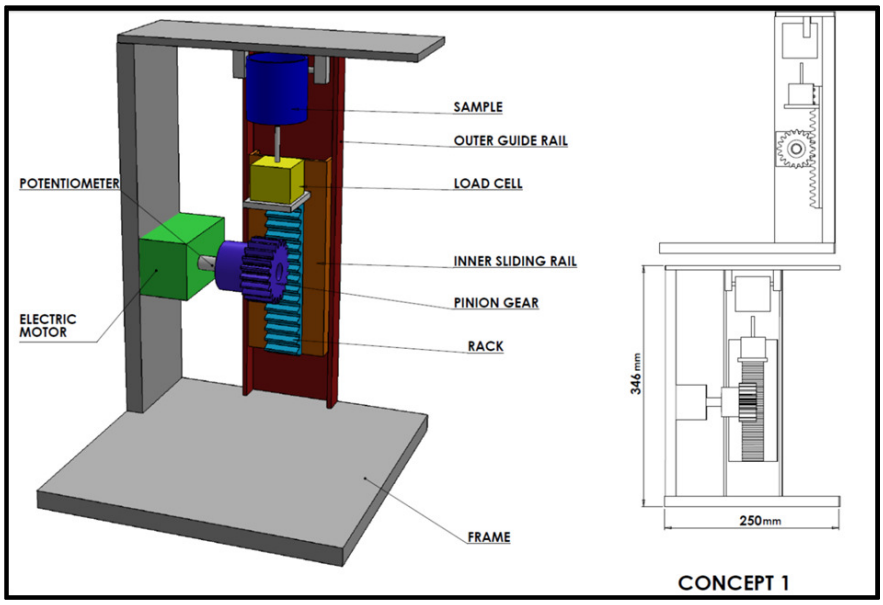

Concept 2

Concept 2 uses an hydraulic actuator to drive the sample. The hydraulic actuator system is used in many triaxial load machines testing machines. The sample is driven down onto a fixed probe and load cell at the base of the micropenetrometer.

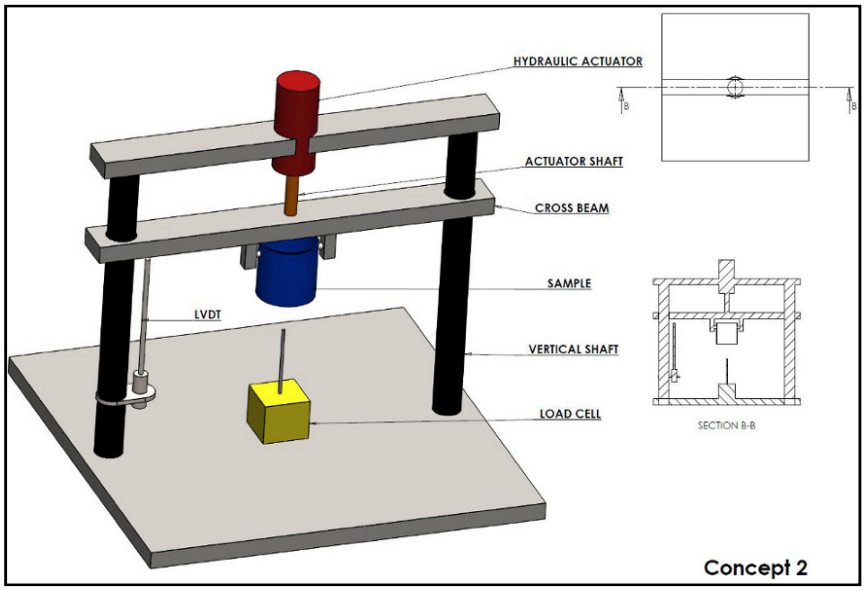

Concept 3

A lead screw system is at the core of concept 3. Lead screws or power screws are used extensively in axial load machines. The lead screw could directly drive the load cell and probe (similar to concept 1).

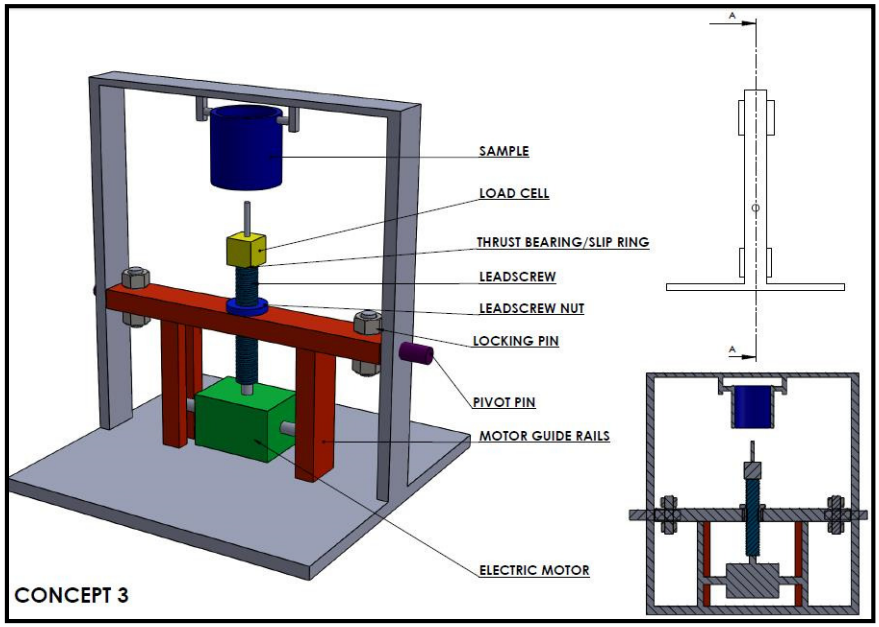

Concept 4

This is a variation of concept 3; the motor remain stationary. A pair of gears drives the load cell and probe into the fixed sample at the top of the micropenetrometer.

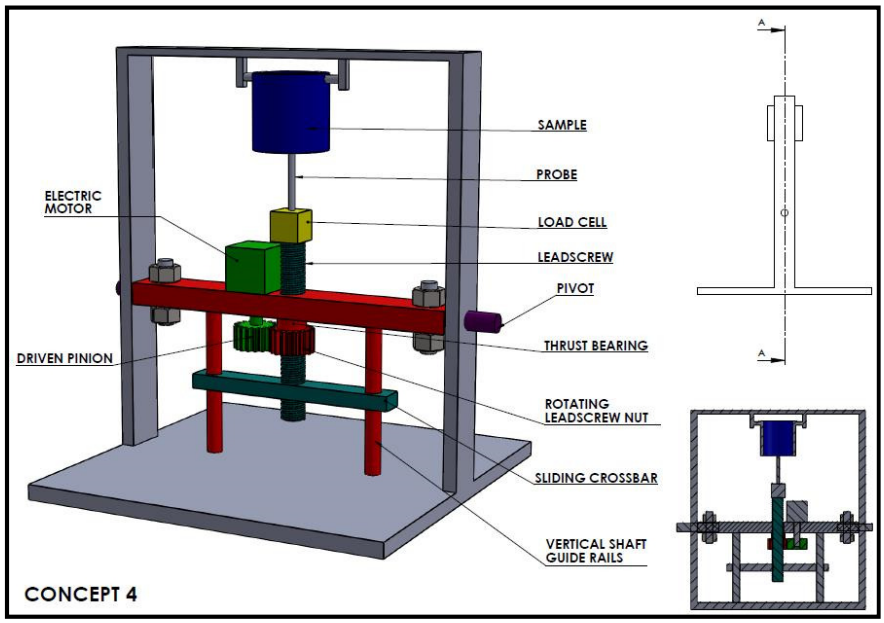

Concept 5

Two lead screws are driven by the motor using a drive belt system. The lead screws drive a vertical cross beam which moves the sample up and down. This concept is based purely on traditional axial load devices such as the INSTRON universal testing machine. The load cell and probe are fixed at the base (similar to concept 2)

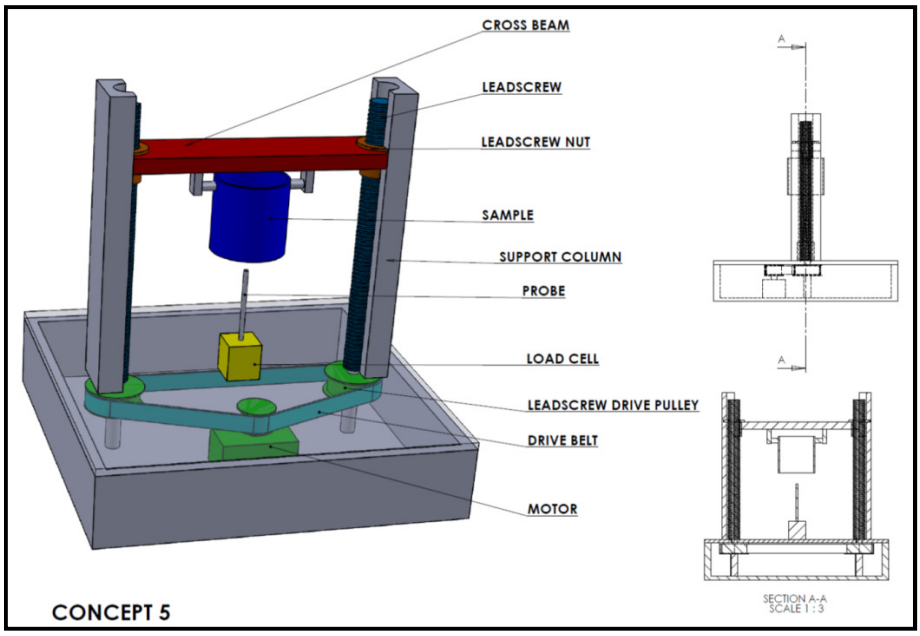

5.2 Concept Evaluation (TOPSIS)

In order to evaluate the design concepts, a multi-criteria decision making tool was used: Technique for Order Preference by Similarity to Ideal Solution (TOPSIS). The TOPSIS method was used to:

- Obtain an expert opinion about design considerations.
- Identify a final design concept objectively, by ensuring qualitative and quantitative evaluation of each concept relative to each other.

The outcomes from this analysis were crucial to select the components to be used in the ascending micropenetrometer final design.

TOPSIS was developed in 1981 by Hwang CL(1981). This method is a multi-criteria decision making tool and an excellent means to find the optimal design solution for

problems with multiple design criteria. The technique asks experts to objectively score the design concepts and is fairly simple in computation.

In this method two artificial alternatives are hypothesised:

1. Ideal solution: the solution which has the best values for all attributes considered
2. Negative ideal solution: the solution which has the worst attribute values

TOPSIS selects the solution that is closest to the ideal solution and farthest from the negative ideal solution.

Figure 16 presents the full procedure for TOPSIS method. A full explanation of TOPSIS with formulae is described in appendix C1.

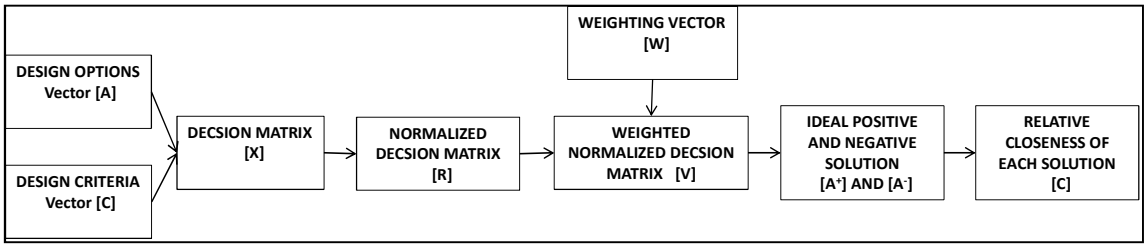

Figure 16 - TOPSIS procedure flow diagram. Adapted from (Kolios et al., 2010)

For the purposes of this study a survey was compiled and distributed to 27 experts. Survey participants were divided into three groups depending on their area of expertise. 13 Engineering experts, 12 Soil Science experts and two Manufacturing experts completed the survey.

5.2.1 Design Criteria

Very few researchers evaluate the relationships between the criteria (Ginevicius, 2011). In most cases the criteria are very much interrelated and this should not be ignored. The accuracy of the expert's evaluation of the criteria largely depends on the number of criteria. When the number is large it becomes difficult for the experts to mentally do comparisons of the criteria. For this reason the number of criteria was limited to eight.

The design criteria were defined after consultation with Soil Science and Engineering experts.

1. Accuracy - Ability of device to measure force and displacement precisely
2. Repeatability – Ability of device to repeat the exact same measurement consistently
3. Durability – Robustness of device, strength and resistance to environmental factors such as rust and dirt
4. Manufacture and Integration – Ease of manufacture and integration of components into assembly
5. Adjustment and Control – Ease of adjustment and control of components within assembly
6. Ease of use - Ability of end user to perform measurements
7. Adaptability – Ability to change and adapt configuration
8. Low Cost – Relative price of device

Once the criteria were chosen a survey questionnaire was prepared using the marketing software Qualtrics. The questionnaire was sent out to experts to fill out electronically (see appendix C2 for survey document).

5.2.2 Weighting Vector

Part A of the survey requested experts to assign an importance score to each criterion. The results would determine various weighting vectors applying a relative importance to each criterion. In total three opinion weighting vectors were determined i) Engineering, ii) Manufacturing and iii) Soil Science. The scores for each criterion (within each group) were averaged to give a relative weight to each criterion.

A baseline weight and a weighted weight vector were also used for extra comparison. The baseline vector gave equal weight to each of the criteria. The weighted weight vector attempted to assign more importance to the opinion of experts whose expertise were judged to be most valuable. In this case engineering experts were judged to have the most relevant expertise to score the concepts since these experts have extensive knowledge of design and engineering projects. Manufacturing experts score were weighted next highest at 30%, followed by Soil Science experts at 20% and Phd Students (engineering) at 10%. The final weighting vectors are given in Table 6.

Table 6 - Weighting Vectors

	Accuracy	Repeatability	Durability	Manufacture and Integration	Adjustment and control	Ease of Use	Adaptability	Low Cost
Engineering	**9.5**	**9.3**	**6.2**	**5.4**	**7.2**	**6.5**	**6.5**	**5.7**
Manufacturing	**9.0**	**9.5**	**6.5**	**7.5**	**7.5**	**7.5**	**3.0**	**5.0**
Soil Science	**9.3**	**9.6**	**8.8**	**6.4**	**7.5**	**8.3**	**6.9**	**6.4**
Weighted	**9.2**	**9.5**	**6.8**	**6.2**	**7.4**	**6.9**	**5.8**	**5.4**
Baseline	**1.0**	**1.0**	**1.0**	**1.0**	**1.0**	**1.0**	**1.0**	**1.0**

A sensitivity study was performed to evaluate the variability of the weighted vectors (Table 7). The weighting given to each group was increased by 5% and the percentage change in the vectors determined. Results indicate that the apart from the Ease of Use Criterion, which varied by up to 3.3%, the vector obtained does not depend on the weighting of the group of experts.

Table 7 - Sensitivity study of the obtained vectors

	Accuracy	Repeatability	Durability	Manufacture	Adjustment	Ease of Use	Adaptability	Low Cost
Weighted Vector (Engineering 40%, Manufacturing 30%, Soil Science 20%, PhD Students 10%)	9.2	9.5	6.8	6.2	7.4	6.9	5.8	5.4
Sensitivity Analysis								
Vector increasing Engineering weight by 5%	9.3	9.5	6.7	6.2	7.4	6.7	5.9	5.4
% Change	0.5	0.7	-1.2	0.7	-0.6	-2.9	2.4	1.5
Vector increasing Soil Science weight by 5%	9.1	9.4	6.7	6.1	7.3	6.7	5.8	5.4
% Change	-1.0	-0.6	-1.8	-0.2	-1.8	-3.3	0.6	0.6
Vector increasing Manufacturing weight by 5%	9.2	9.5	6.7	6.2	7.3	6.7	5.8	5.4
% Change	-0.4	0.0	-1.6	0.9	-1.1	-2.7	0.1	0.9

5.2.1 Decision Matrix

Part B of the survey asked experts to score the concepts relative to each other. A score was given for the ability of each concept to meet each design criteria. The scores were averaged from all participants' scores to form the decision matrix. Using this logic the decision matrix is unbiased towards any one group or opinion. Opinion judgement was incorporated using the weighting vector. The final decision matrix is detailed in Figure 17.

Total Averaged Scores

5 MAIN Concepts	Criteria	1 Accuracy	2 Repeatability	3 Durability	4 Manufacture and Integration	5 Adjustment and Control	6 Ease of Use	7 Adaptability	8 Low Cost
Concepts	n=								
m=									
1 Concept 1		6	6	6	7	6	7	6	7
2 Concept 2		7	7	7	8	6	8	6	7
3 Concept 3		7	7	8	7	7	7	6	6
4 Concept 4		7	7	7	6	7	6	6	6
5 Concept 5		6	6	6	6	6	7	6	6

Figure 17 - Averaged decision matrix

5.2.2 Results

Statistical analysis performed on the survey results was based on Thiel (2008) where the number of participants was low ($n<30$). Thiel, 2008 proposes some statistical analysis of the calculated means from the relative importance of the criteria scoring. In this way the reliability of using the means as the weights vectors in the TOPSIS method was assessed before going ahead. Descriptive statistics were used to evaluate the data. Variance, Standard deviation, rate of change, asymmetry rate or skewness and concentration rate were used and the results analysed. The samples where hypothesised to follow a normal distribution. A student t-test was used to find the 95% and 90% confidence intervals of the mean. Results are presented in Table 8.

Table 8 - Values of descriptive statistical measure for criteria scores

Criterion	Mean $\bar{x}$	Variance $s(x)^2$	Standard Deviation $s(x)$	Dispersion $Vs(x)$
Accuracy	9.4	0.69	0.83	8%
Reliability	9.4	0.62	0.79	8%
Durability	7.4	2.90	1.70	23%
Manufacture & Integration	6.0	3.63	1.91	32%
Adjustment & Control	7.4	1.57	1.25	17%
Ease of use	7.3	3.63	1.91	26%
Adaptability	6.4	4.02	2.01	31%
Low Cost	6.0	3.52	1.88	31%

The results of the TOPSIS analysis are presented in Table 9. After evaluation of the main five concepts for all weight vectors, concept 3 was deemed the best concept (closest to 1). When the modifications were considered, all weight vectors, except the baseline vector, produced Concept 1 with modification 2 as the best solution. It should be noted, however, that Concept 2 also scored very well (above 0.6 for all weight vectors). Three experts indicated in the survey that having the load cell fixed at the base of the frame would help eliminate extra signal noise produced by the rotation of the actuator.

Table 9 - TOPSIS Concept score results, green highlights concept closest to positive ideal and red highlights concept closest to negative ideal.

	Weights Vector	Soil Science	Engineering	Manufacturing	Weighted Vector	Baseline
		Relative Closeness to Ideal (1.00)				
Concept 1		0.297	0.274	0.278	0.279	0.311
Concept 2		0.664	0.630	0.655	0.641	0.672
Concept 3		0.792	0.802	0.778	0.797	0.746
Concept 4		0.462	0.489	0.449	0.473	0.423
Concept 5		0.091	0.090	0.086	0.087	0.098
		Incl. Modifications				
		Relative Closeness to Ideal (1.00)				
Concept 1		0.314	0.281	0.279	0.285	0.339
Concept 2		0.544	0.500	0.531	0.515	0.557
Concept 3		0.668	0.648	0.656	0.655	0.656
Concept 4		0.409	0.403	0.389	0.401	0.393
Concept 5		0.168	0.155	0.141	0.151	0.188
Concept 1. MOD 1		0.615	0.627	0.623	0.626	0.595
Concept 1. MOD 2		0.727	0.751	0.747	0.748	0.688
Concept 2. MOD 1		0.442	0.431	0.389	0.419	0.465
Concept 4. MOD 1		0.705	0.686	0.682	0.693	0.693
Concept 4. MOD 2		0.712	0.724	0.717	0.724	0.670
Concept 5. MOD 1		0.213	0.230	0.235	0.228	0.216

5.2.3 Discussion

Results show that criteria 1 and 2 (i.e. accuracy and reliability) have the smallest standard deviation (approximately 0.8) and smallest dispersion (8%), which suggests that all of the participants agreed unanimously on their value (Table 8). Criterion 5 (adjustment & control) also has a relatively low standard deviation of 1.2 and dispersion of 17%. The other criteria have relatively large values of standard deviation with a maximum of 2 for adaptability, however, the dispersion about the mean is still moderate at approximately 30%. Thus, statistical analysis of the weighting of criteria indicates agreement between the experts in evaluating the importance of the criterion. The sensitivity analysis (Table 7) confirms a general homogeneity of the results, therefore the mean values of the criteria scores are suitable for the TOPSIS study. The only criterion which perhaps gives some doubt is adaptability with a deviation of over 2 across the experts' responses. Therefore, the values used in the TOPSIS study were not modified to account for statistical variance.

TOPSIS results clearly indicated that the concepts that should be considered for the design are Concept 3, Concept 2 and Concept 1 with modification 1. Concept 3 received the highest scores in the TOPSIS study (Table 9); however, elements from the other concepts would be considered for the final design.

Concept 1 modification 1 scored the highest of the modified concepts (Table 9), however, concept 1 without modification scored very low (second lowest of all main concepts) and therefore the result is unreliable. The number of participants that scored the modified concepts was considerably less than those that scored the main concepts (14 compared to 5). For these reasons concept 1 modification 1 was rejected for consideration of the final design.

Having the load cell located in a fixed position would eliminate the much of the load noise produced by the rotating motor drive. For this reason, and the fact that it scored a close second behind concept 3, concept 2 would be considered for the final design. From the decision matrix shown in Figure 17) concept 2 scored 7; equal to concept 3 for accuracy and repeatability but lower for adjustment and control (6 compared to 7). Utilising an electric motor similar to concept 3 would improve the adjustment and control of concept 2, whilst keeping the accuracy of the configuration.

5.2.4 Conclusions

The final micropenetrometer design was based on the configurations of concept 2 and concept 3. A lead screw and electric stepper motor would be used to drive the system. A slight modification to concept 3 was implemented in order to keep the load cell fixed. Fixing the load cell is considered highly advantageous since this would exclude noise and eliminate the need for post processing of the load signal. An electronic stepper motor and a good tolerance lead screw (as utilised in concept 3) would give smooth motor control and precision motion. The lead screw also has increased durability compared to gearing and rack and pinion options. An appropriate lead screw and stepper motor with accurate load cell would be sourced from available manufacturers for the final design proposal.

6 Final Design Selection

6.1 Final design configuration

Using the results of the TOPSIS study final component selection and integration into a manufacturable design was completed; resulting in three possible final instrument design systems presented in section 5.3. Commercial components were reviewed and selected based on their price and ability to achieve the technical requirements.

6.1.1 Load Cell

The technical requirements for the load cell were as follows:

- Based on the experiment, the expected force range was 0.3N – 5N. To increase the micropenetrometer ability to measure larger samples in future studies, an expanded load range capability would be advantageous. Thus a range of 0.3 – 10N was deemed good for larger samples (twice as large) Juvinall and Marshek (2000) stated that when materials and loads are well defined, a reasonable safety factor of two can be applied to design calculations. An additional safety factor of 2 was applied to this final force, meaning the load cell would need to be able to measure up to 20N.
- Required accuracy of the load cell was based on literature and previous micropenetrometer devices (Liu et al., 2006; Drahorad and Felix-Henningsen, 2012). An accuracy of approximately 0.01 N was considered adequate to detect microstructural changes in strength, as described in Liu (2006). This accuracy would need to be achievable throughout the 0 – 20N range of the load cell.

A review of available load cells (Table 10) revealed several that would yield the desired requirements. The Richmond Industries 900 Series load cell was selected as the final choice.

This load cell had many advantages:

- 20N force range
- Excellent minimum accuracy of 0.012 N throughout range
- S-type load cell, providing good durability

- Easy installation: the load cell could be mounted into the frame using a simple M6 bolt. No other mechanical considerations or mounting plates required.
- 500% Mechanical force overload protection.
- Direct USB connection to the PC via an analogue to digital module. Module manufactured by supplier and offered excellent resolution of 10Hz or 120 000 steps, far more than required. The module also included signal filtering and noise cancellation for improved signal.
- Price: both the USB module and the load cell together would cost £330 excl. VAT.

Table 10 - Load Cell Specifications Comparison

Comparison of Load Cells	OMEGA PN: LCL-454G	OMEGA PN: LCMFD-10N	OMEGA PN: LCMKD-20N	HONEYWELL PN: FSS1500NSB	RICHMOND INDUSTRIES PN: 900 Series – 20N ✓
Type	Thin Beam	Compression/Tension	Compression – Push Button	Compression – Push Button	Compression/Tension
Range	0 – 454g	0 – 20N	0 – 20N	0 – 1.5kg 0 – 15N	0 – 20N
Advantages	Inexpensive Potentially tension/compression	Durable Accuracy	Accuracy Price	Inexpensive	Ease of Installation Accuracy Tension/Compression
Disadvantages	Difficult Installation Very fragile	Expensive	Compression only	Push button Low accuracy/repeatability Compression only	None
Non-linearity	N/A	N/A	N/A	1.5% FSO 0.2255N	0.03 % FSO 0.006 N
Repeatability	N/A	0.2% FSO 0.04N	N/A	0.7% FSO 0.105N	N/A
Total Accuracy	0.25% FSO 1.14g or 0.012N	0.15% FSO 0.03N or 3.06g	0.25% FSO 0.05N or 5.10g	1.5% FSO 0.225N or 22.9g	0.06 % FSO 0.012N or 1.22g
Cost	£50	£510	£375	£43	£160

6.1.2 Frame

Weight and portability was deemed not important to the design criteria. However, durability and reliability was valued highly, therefore, corrosion needed to be avoided. Aluminium 6082T6 section was selected as the most economical and durable, corrosion resistant material to manufacture the instrument frame. Due to the very low loads expected, 1.2Kg maximum, the smallest available box section (25.4 mm x 25.4mm x 16SWG) was chosen. Deflection of the frame was calculated to be minimal.

Clamp design

The clamp is an important component of the frame design. It needed to hold the sample securely to motion error during measurements. The clamp was therefore designed to hold the sample around its entire circumference (Figure 18a). The initial design did not ensure that the sample was located at the same position for every measurement. To ensure the sample started at a fixed location a base plate was incorporated (Figure 18b).

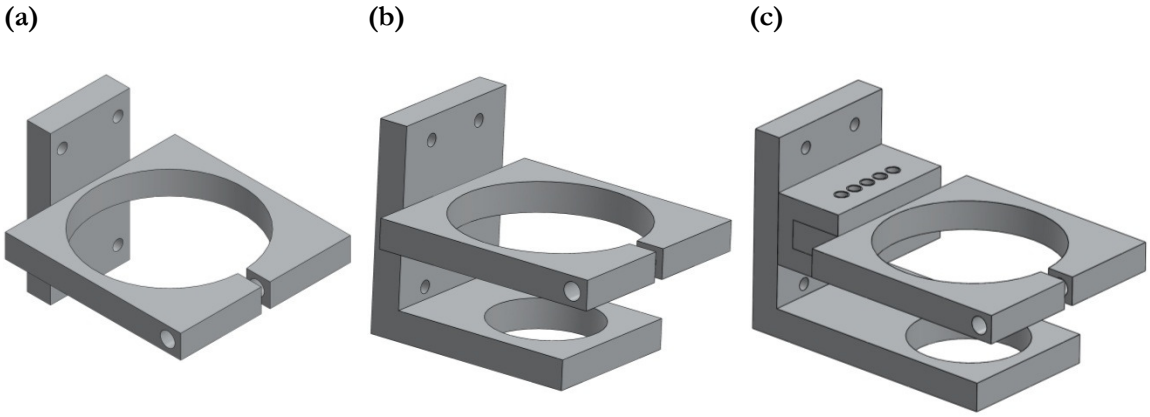

Figure 18 – Design progression of the sample clamp. (a) Simple clamp with circular grip to hold sample firmly. (b) Base plate introduced to ensure starting datum position of sample. (c) Final clamp design including slotted key mount allowing repositioning of sample before penetration measurement.

Since the clamp and probe in the final design would be fixed, only a single point in the sample could be penetrated. With the probe located at the centre of the sample, the centre of the sample was the only penetration point (Figure 19a). Having a single possible penetration point in the sample amplifies the risk of having an inaccurate measurement, since the centre of the sample could contain a crack in the soil or localised hard spot. To increase the possible penetration points, the probe would be offset from the centre, thus creating an annulus, around the centre but not including the centre, of possible penetration points(Figure 19b). The final clamp design (Figure 19c) includes a slotted key mount which allows the circular clamp to be moved sideways and fixed in multiple positions. This configuration creates the possibility of penetrating the centre of the sample as well as several annuli around the centre (Figure 19). Due to the damage that is caused to the crust surface during penetration measurements the number of penetrations per sample was limited to a maximum of two.

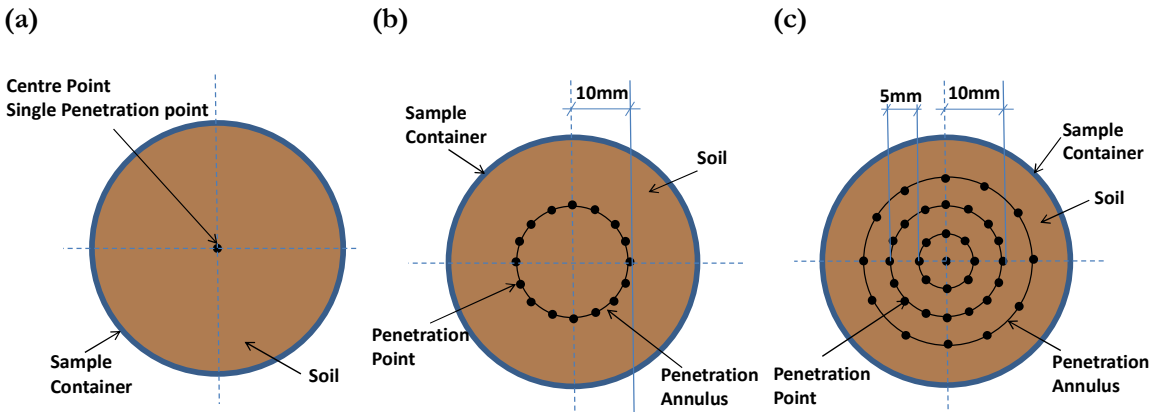

Figure 19 – Possible penetration patterns available for the clamp designs from

(a) Clamp and probe fixed at centre point. (b) Probe fixed at offset position from sample centre point. (c) Final design, multiple penetration annuli possible.

6.1.3 Motor

Application requirements should be assessed when selecting an electric motor (Alciatore and Histand, 2003):

- Will the motor start and will it accelerate fast enough? Starting torque of the motor needs to be high enough to overcome the applied static loads.
- What is the maximum speed a motor can reach? The corresponding torque at the maximum required speed must be high enough to overcome loads.
- Is accurate position or speed required? For accurate positioning at discrete locations and incremental motion a stepper motor is well suited. Stepper motor can also operate over a wide range of speeds and open loop control is simpler, eliminates the need for a position sensor.
- Are there any size and weight restrictions? Direct current (DC) stepper and servo motors offer good torque at small size.

The motor would need to be able to apply 20N of vertical force whilst being well within the maximum torque capability. This would ensure that the stepper motor would not lose pulse count and therefore position control would remain accurate. To calculate the required torque of the motor the efficiency of the lead screw, motor and load inertia, the maximum speed/acceleration and maximum loads were required. The total torque requirement was calculated using three methods, two theoretical calculations and a using

commercial software package for motorised stages (COOLWORKS), and produced similar results. For safety the largest of these values was used as the maximum resultant torque (0.133Nm). Full calculation methods are described in appendix D.2. Table 11 tabulates the obtained motor requirements.

Table 11 - Motor technical requirements for the micropenetrometer.

Requirement	Value
Maximum Load	20(N) / 2 (kg)
Maximum Speed	100 (mm/min)
Maximum Acceleration	9600 (mm/min^2)
Motor Resolution (best)	0.001 (mm)
Minimum Torque	0.133 (Nm)

6.1.4 Electronic components

Data measurements need to be captured and stored so that the force measurements can be reviewed and displayed. The data logger system needs to integrate with the load cell and displacement transducer. The signal from the load cell will most likely be analogue and will need to be converted by an analogue to digital converter (ADC) (Liu et al., 2006).

6.1.5 Analogue to Digital Converter

The output signal from the load cell and displacement transducer will be in the form of a continuous analogue voltage signal. This signal will need to be converted to a digital signal that can be measured and displayed by the controller or PC. In order to accurately measure the continuous output signal from the components the data must be sampled at a discrete time interval which is small enough to give a good representation of the original signal (Kularatna et al., 2003). An analogue signal with frequency f_a must be sampled at a rate of $f_s > 2f_a$ to avoid loss of information (Kularatna et al., 2003). For a penetration rate of 12mm/min and a measurement resolution of 0.005mm the frequency of sampling is 4Hz. Therefore the ADC needs to be capable of a sampling frequency of 10Hz. It is important when selecting the ADC to check the dynamic specifications of the device. The effective frequency is a parameter which incorporates the signal-to-noise-plus distortion errors. Most commercial ADC's will offer effective noise cancellation through signal filtering, this should be checked when deciding which device to use.

6.2 System Options

Selection of the drive and control systems depended largely on price. There was a plethora of components available that could achieve the desired accuracy and control of the micropenetrometer. For this reason three possible systems were proposed, full details are shown in Appendix D.3. All three systems would meet the technical specifications and be within the build budget of £3000.

6.2.1 System 1 – "Rolls Royce" Most Expensive

The most expensive system proposed boasted a highly configurable, fast and accurate control system from National Instruments (NI). The NI Compact RIO control system is fully "stand-alone", meaning no PC connection would be required to run the micropenetrometer load cell and drive devices. Included in the Campact RIO control system is a stepper motor controller, capable of micro-stepping the stepper motor, a load cell excitation and data acquisition module. Further modules could also be added to this system if additional measurement devices are required at a later stage, to measure for example water content, temperature or displacement using an LVDT. The NI controller would control a standard stepper motor which drives a lead-screw incorporated in a mechanical linear stage manufactured by IGUS.

6.2.2 System 2 – Intermediate

This system utilises an integrated motorised linear stage manufactured by Reliance Precision Ltd. The linear stage incorporates a "Cool Muscle" motor with an integrated lead screw, motor and controller in one unit. The motor offers very fine controllability, accuracy and resolution through the use of micro-stepping. Software to control the motor is provided, alternatively LabView could be used. To control the motorised stage the unit is connected to a Personal Computer (PC) via a Universal Serial Bus (USB) cable. The load cell would be powered and controlled via USB ADC amplifier from Richmond Industries and connected to the PC in another USB slot. The Richmond industries PC-USB in-line ADC load cell amplifier was chosen for the micropenetrometer as it offered the correct technical requirements described in section 5.1.4. Additionally this amplifier connected to the (PC) via USB the same as the Reliance Cool Muscle motorised stage; thus minimising incompatibility of the two devices.

6.2.3 System 3 – Economical

This system uses base components; standard stepper motor with USB motor drive and a controller. The motor would drive an "off the shelf" lead screw linear actuator from IGUS. The system would need to be programmed using MATLAB or controller software such as Arduino language. The load cell would be controlled using the manufacturer USB module. It was understood that this configuration would take the most amount of time to build and program. The Arduino or similar controller would have some limitations in fine motor control. The resolution would most likely be less than both the "Rolls Royce" and Intermediate systems due to the lack of fine micro-stepping capability.

6.3 Final System Design

Advantages of the Intermediate System led to it being chosen for the final design presented in Figure 20. Price, accuracy and ease of manufacture were the main characteristics for selection. Comparison of the three systems (Table 12) highlights that the Intermediate System offered the easiest manufacture including time for manufacture, high accuracy, control ability and reasonable cost. Compared to commercially available micropenetrometers the intermediate system offers a significant cost savings. The micropenetrometer (TA.XTPlus) used by March et al. (2013) for example costs £12684.

System Description	Cost	Accuracy	Time	Ease of Use	Controlability	Adaptability
"Rolls Royce" (Expensive) Version Expensive Control Mechanical Actuator Standard Stepper Motor	£2900 - £3000	Medium Accuracy	Intermediate	High Fully automated Would only require PC to download data or change the sequence of motion	High Stand Alone Unit No PC Required for controlling motor or data logging	High 2 Free slots for expansion can add other units, for accurate displacement measurement
Intermediate Version Integrated Linear Actuator Cool Muscle Motor Fully Integrated Controller, Encoder for Highly Accurate Positioning and Linear Actuator	£1800 - £2000	High Accuracy	Shortest	Medium - High Would require 2 x USB channels Program launch from PC	Medium - High Require PC control LABVIEW Interface	Low Motor and configuration unchangable
Economical Version Standard Control System Drives bought and programmed from fundamental prinicples.	£900 - £1100	Medium Accuracy	Longest	Medium - Low Program for PC would be written and basic GUI	Medium LABVIEW or Matlab GUI Interface	Medium Low cost to add or change components

Table 12 - Comparison of systems

Full component technical specifications are given in Appendix D.4. Pertinent specifications of the device are summarised below:

- **Drive system** – Reliance Cool Muscle motorised stage.
  - 5kg - Maximum vertical load
  - Torque (dynamic) – 0.38Nm. This would allow the motor run at 40% maximum load for the worst sample load case.
  - Accuracy of 0.0006mm/mm or 0.12mm over full 200mm guide length.
  - Variable resolution and speed settings. 500 pulses per revolution to 50000 pulses per revolution. Speed settings increased from 10 pulses per second in 10 pulses per second intervals. Resulting large range of speeds.

- The motorised stage is easily programmable and configurable. An encoder allows micro-stepping of the stepper motor, resulting in very fine control of the motor rotation. Memory is in-built into the motor allowing storage of program sequences. This means that the codes during operation of the motor are reduced.
- Offers torque protection and displacement protection mechanisms.

- **Load Cell** – Richmond Industries 900 Series
  - Maximum measurable load 20N (compression and tension)
  - 500% Overload protection
  - Accuracy 0.06% or 0.012N
  - USB Module Analogue to Digital Converter – The module offers superior sampling rate of up to 1000Hz more than sufficient for the required 10Hz sampling rate desired. This module also includes full noise cancelling filters. When purchased with the load cell the load cell and module are pre-calibrated and certified for accuracy.

All these specifications were well within the requirements allowing for larger samples to be used in future experiments adding to the systems flexibility. Final specifications of the micropenetrometer are detailed in Table 13.

Table 13 - Mechanical and electronic specifications of the micropenetrometer

Parameter	Mechanical		Electronic	
Force	Maximum Load	20N or 2kg	Load Cell	Richmond Industries PN: 900-020N2U
	Resolution	0.00001N	Interface	USB
	Accuracy	±0.006N or 0.6g	Data format	Excel Spreadsheet
	Maximum Sample Weight	600g	Control Software	LabView 2013 and DSC Toolkit 3.0.0
Displacement	Maximum Penetration	170mm	Motor	Reliance Cool Muscle Motorised Stage RCMS17L-M02-C-1-12
	Maximum Speed	300mm/min	Interface	USB
	Resolution	0.001mm		
	Accuracy	0.0006mm/mm	Control Software	LabView 2013 and CoolWorks Lite
	Maximum Motor Torque	0.129Nm 45% Peak Motor Torque		

Using all the selected system components, the configuration and materials the final design was completed. Drawings of the frame and integrated components were created using Solidworks 2011 (full details in Appendix D.4). Included for the workshop to manufacture were the instrument frame to house the components, the sample clamp to support the sample and the probe collar, needed to house the probe and attach it to the load cell. The manufactured ascending micropenetrometer and layout diagram is illustrated in Figure 20.

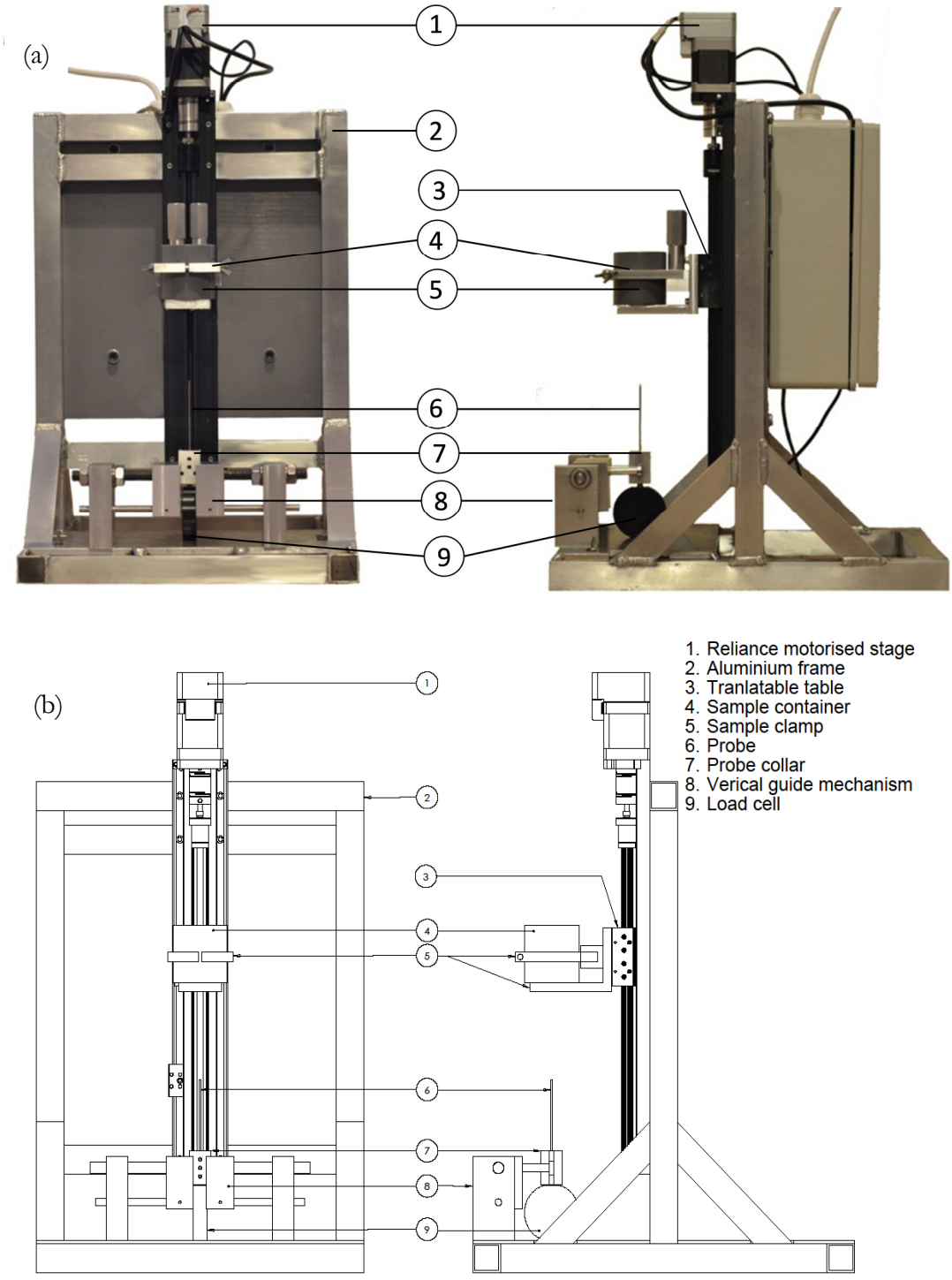

Figure 20 - Layout (a) photograph and (b) diagram of the Ascending Micropenetrometer

6.3.1 Data acquisition and programming

The fundamental requirement of the micropenetrometer was to accurately measure the penetration force on the probe from the load cell, and, at the same instant, to record the displacement of the probe within the sample. In this manner a good description of the PR throughout the penetration can be achieved. It is therefore important that the two signals be "tied" together and recorded at an instant in time as close to each other as possible. Since the load cell and the motor use separate software to drive and record the respective instruments, a program was needed to control both components simultaneously. There are several programming software packages available which could achieve this. Software that was considered suitable for the program development were Microsoft Visual Basic, C++ and National Instruments LabView. The first two packages are text based programming languages, with Visual Basic offering a simpler visual interface. LabView, however, is a visual based programming language allowing the user to drag and drop blocs of code and "stitch" these together to carry out the desired function.

LabView was chosen to be the most suitable for the micropenetrometer, because it offered several advantages in instrument programming. LabView was developed specifically for data acquisition and management making it easy to configure and communicate with components. The visual nature of the program language also makes it very easy to learn and understand data flow; complex code can be implemented quickly since code is built using building blocks. Visual programming does; however, make it difficult to debug the program due to the inherent parallel processing.

6.3.2 Micropenetrometer sample sequencing

All programming for the micropenetrometer was performed using LabView 2013. The program needed to ensure that the sample sequence and timing of the measurements was accurate. It was also essential that the program incorporated some protection mechanisms to safeguard the expensive load cell and motorised stage. Additional requirements:

- Variable speed of penetration measurement, enabling the end user to explore the effects of penetration speed on the crust PR profile.
- Variable penetration depth, allowing the end user to test PR in various sizes of sample.

- Output of penetration depth and PR at the same instant in time. These data would be saved in an Excel CSV file for later analysis. Saving of the sampling parameters and sample ID would need to be added to the file.
- Safety to prevent the motor pushing the sample too far and onto the load cell, protecting the motor and load cell from overload.
- Safety to stop the program and motor if the load cell reached its maximum load of 20N.
- Limit the maximum torque of the motor to 40% allowing a maximum load of 20N. This would add redundant protection of the motor and load cell.

It was important to know that the absolute position of the motor is correct at the time the sampling starts, since no additional hardware such as a linear displacement transducer was being used to determine the position. The motor would first execute an origin search to zero the motor position. This would be done by forcing the motor to the physical limit of the sliding stage. Then the motor would execute the sampling sequence, recording position relative to the origin. This method ensures that the motor is reset for each sample, and the position control is not out of synchronisation if the motor was by chance overloaded in the previous measurement.

Sampling sequence would start 10mm above the probe, wait 2sec and then start the penetration through the entire sample. The load cell and position data acquisition would start once the sampling sequence has begun. Once the probe had penetrated the sample, the motor would stop and wait to allow for a period of zero load in the data. The zero load period would allow for easy post-processing of the data since there would be a clear distinction between the PR and friction measurements.

After the wait the motor would extract the probe by 10mm while continuing to record position and load. This extraction measurement would serve to determine the friction component on the PR (Liu et al., 2006).

Depth of penetration and speed would be stipulated by the end user and these sent to the motor at program execution.

7 Micropenetrometer testing

7.1 System setup

Calibration of the load cell resulted in excellent linearity. Force measured by the load cell compared with calibrated weights produced a calibration curve with 100% linear correlation. The conversion equation from measured load to actual load is given in equation (7-1). Full calibration results can be found in appendix E.

$$\text{Actual force} = (\text{Load Cell Force}) \times 1.0031 + 0.0005 \quad (7\text{-}1)$$

To prove that the micropenetrometer was sensitive enough to detect strength variations in soil samples and to find the ideal settings for the micropenetrometer, effects of certain settings were investigated. Different motor resolution, speed and probe shapes were tested to find the settings most likely to produce results good at detecting soil crusts. A simple flour dough experiment was conducted. This type of test has been used in structural strength distribution analysis of soft soils (Liu et al., 2006). The flour was mixed and kneaded with water to create dough with 40% water content. The dough was then inserted into the sample container to a depth of 50mm and allowed to dry for 30min. Flour made of fine consistent particles is a good way to make a homogeneous material for strength testing. With the top surface exposed to air drying a "crust" is formed. A series of penetration tests, at settings given in Table 14, were then performed to determine whether or not the micropenetrometer could detect the crust zone and which settings were best at doing so. Measurement readings were taken at intervals of 0.05mm which is sufficient to capture variations within small crust zones of 1 – 3mm (Liu et al., 2006; Rolston et al., 1991). A test for direct comparison with the Liu et al. (2006) study was also conducted by inverting the dough sample and driving the probe into the material from above, creating a penetration test equivalent to traditional descending penetrometers.

Table 14 - Test settings for the micropenetrometer dough experiment

Motor Resolution (Pulses per revolution)	Linear Resolution (mm)	Speed (mm/min) Flat Probe	Speed (mm/min) Pointed 30^0 Probe
500	0.005	6	6
		12	12
		24	24
2000	0.001	6	6
		12	12
		24	24
5000	0.0004	6	6
		12	12
		24	24

7.2 Test results

Direct comparison of probe shapes was achieved by plotting the PR curves of the flat probe and pointed probe at penetration rate of 12mm/min (Figure 21a). Results indicate that the pointed probe measures consistently higher PR throughout the sample with a peak in PR at 50.2mm of 0.224N. The flat probe produced a peak at 51.5mm of 0.162N. Although the pointed probe produce a higher PR the inflection at the start of the crust zone was not as sharp as the flat probe PR curve. In fact it is extremely difficult to notice an inflection point on the pointed probe, while on the flat probe penetration curve the micropenetrometer clearly hits a harder crust zone at 48.5mm (Figure 21b).

(a)

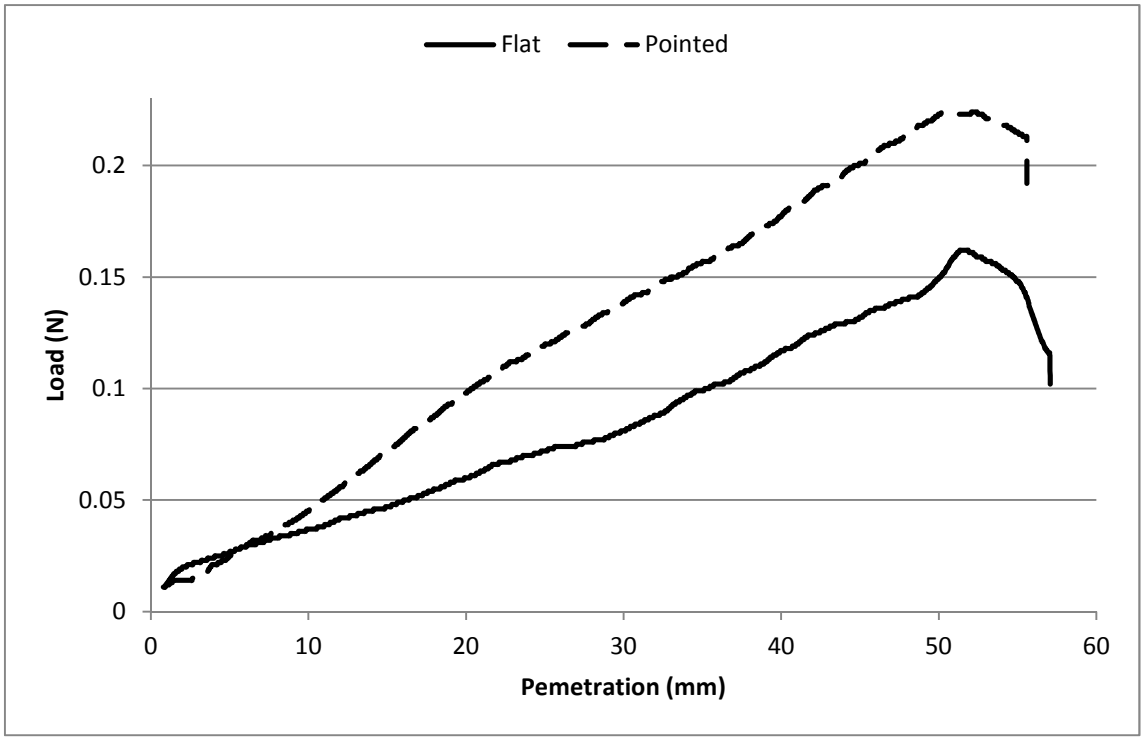

(b)

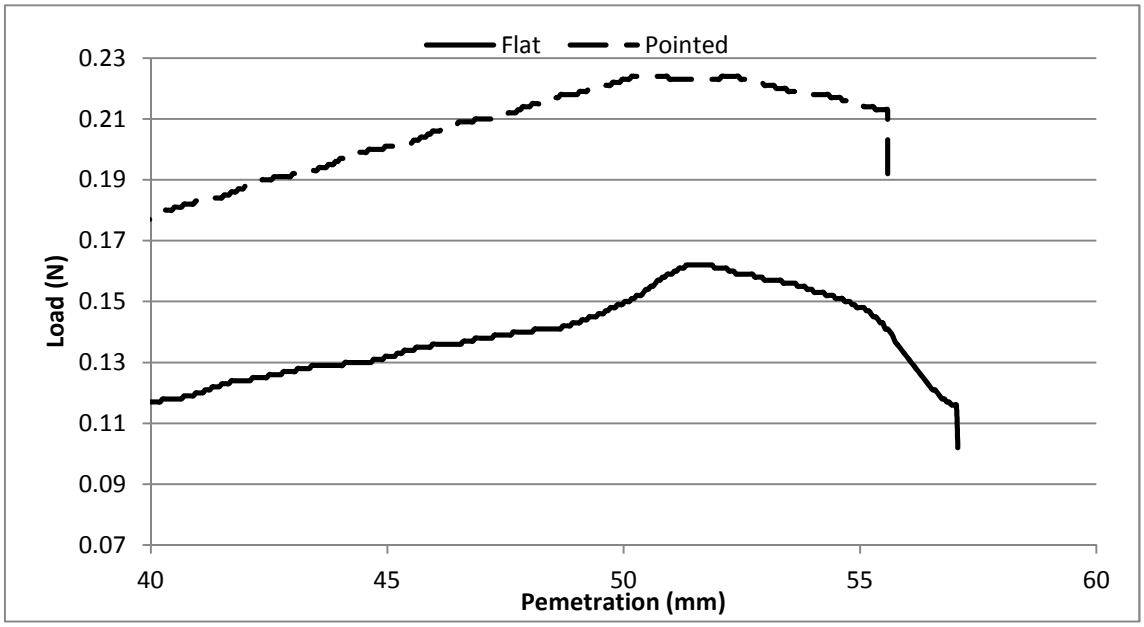

Figure 21 - PR during dough test for flat and pointed shape probes at 12mm/min (a) full penetration; (b) detail of penetration in the crust zone.

(a)

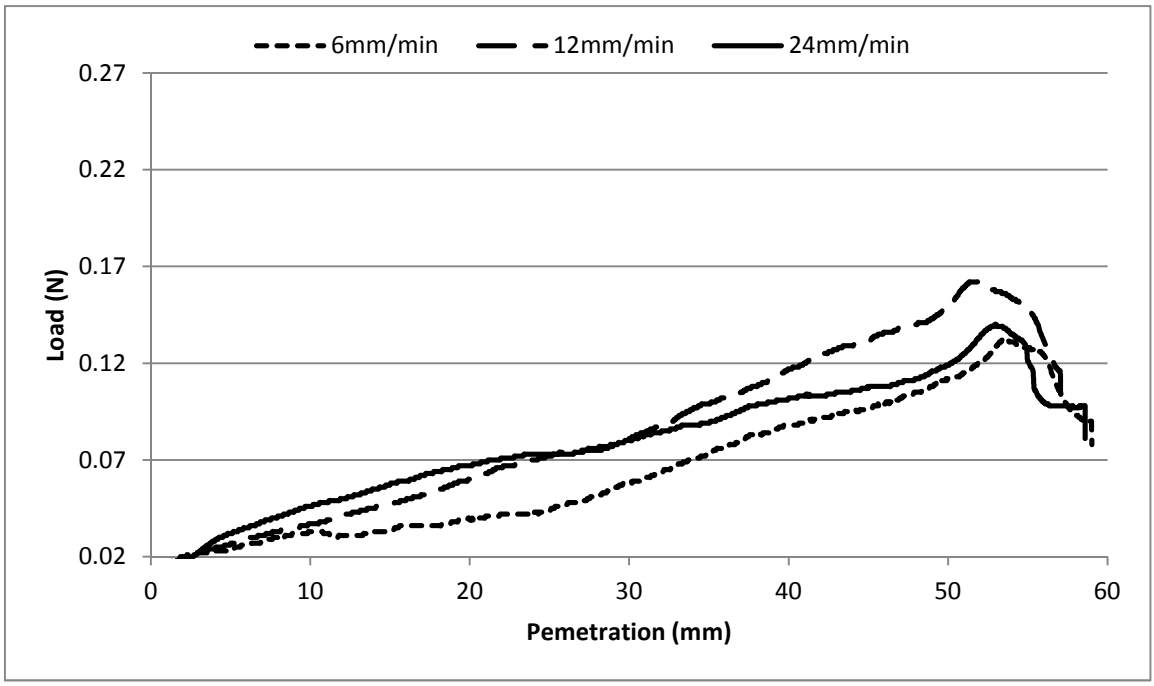

(b)

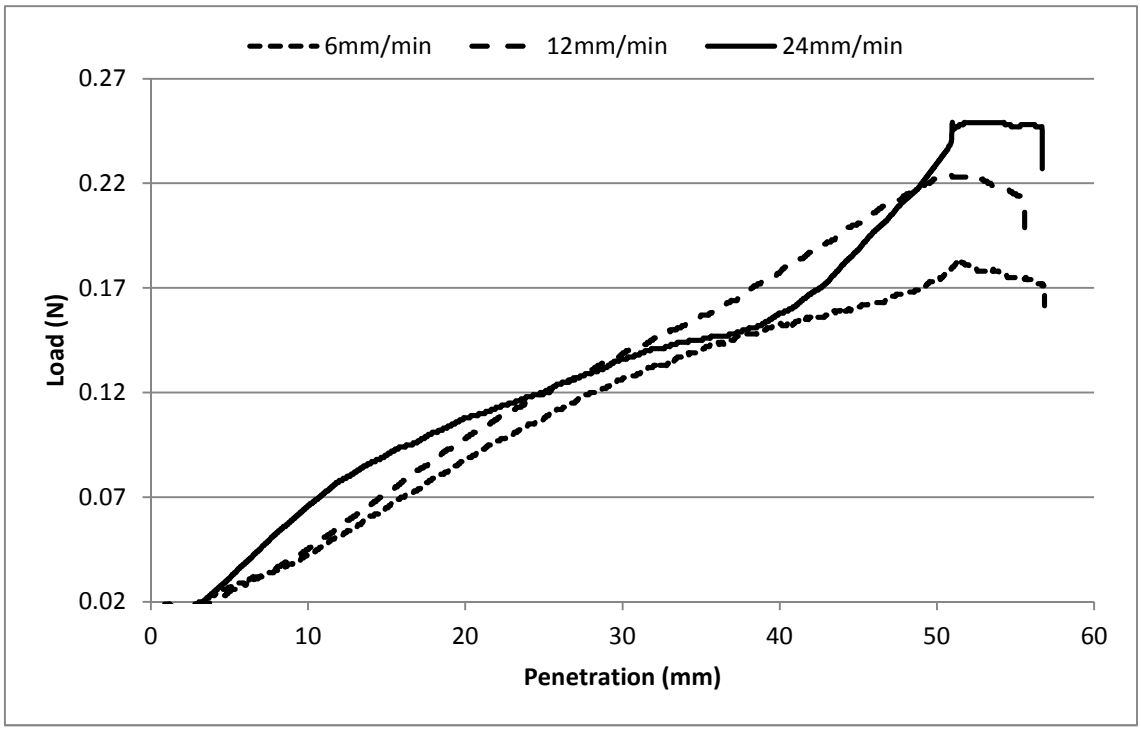

Figure 22 - PR results at different penetration rates with (a) flat probe and (b) pointed probe

Speed settings resulted in PR curves of very similar shape for both the flat (Figure 22a) and pointed (Figure 22b) probe. Generally PR has slightly increased in-line with increasing penetration rate.

Since the Cool Muscle Motorised Stage is capable of multiple position resolutions three resolution settings were tested to see if this affected the accuracy and repeatability of the PR measurements. A single dough sample was penetrated twice at each setting of 500, 2000 and 5000 position steps (or pulses) per revolution (Figure 23). The results indicate that the repeatability increases with increasing resolution. At 5000 pulses per revolution (0.0004mm linear resolution) the two repeat measurements are almost identical (Figure 23c). Looking at the 500 pulses/revolution (Figure 23a) the PR curves have different shapes and PR values while the 2000pulses/revolution curve (Figure 23b) shows similar shape curves which start off identical but diverge at 35mm producing different peak values.

(a)

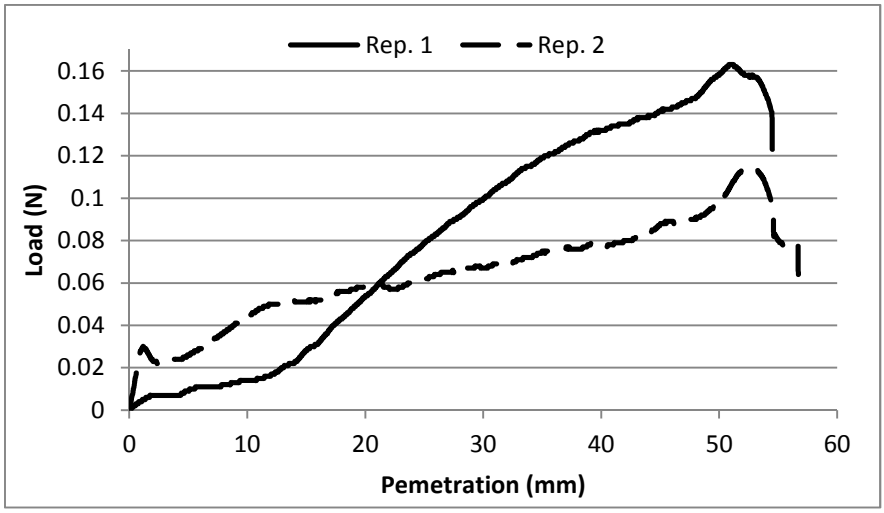

(b)

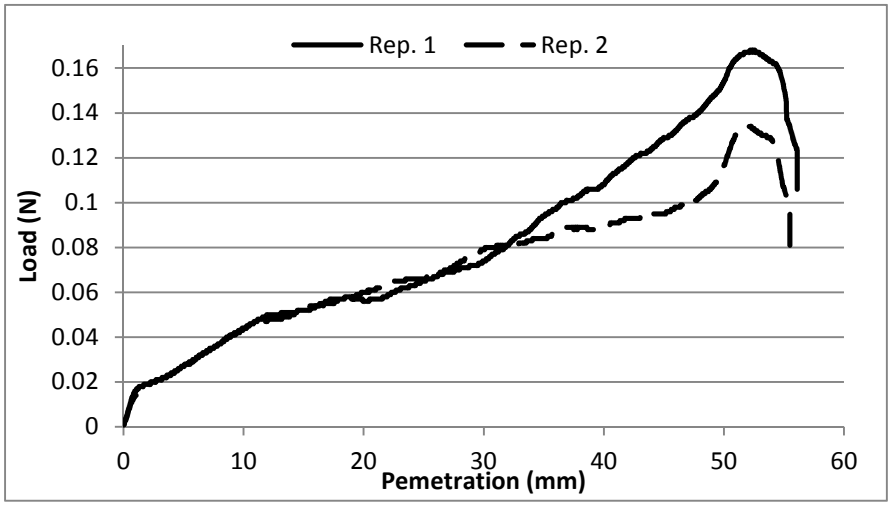

(c)

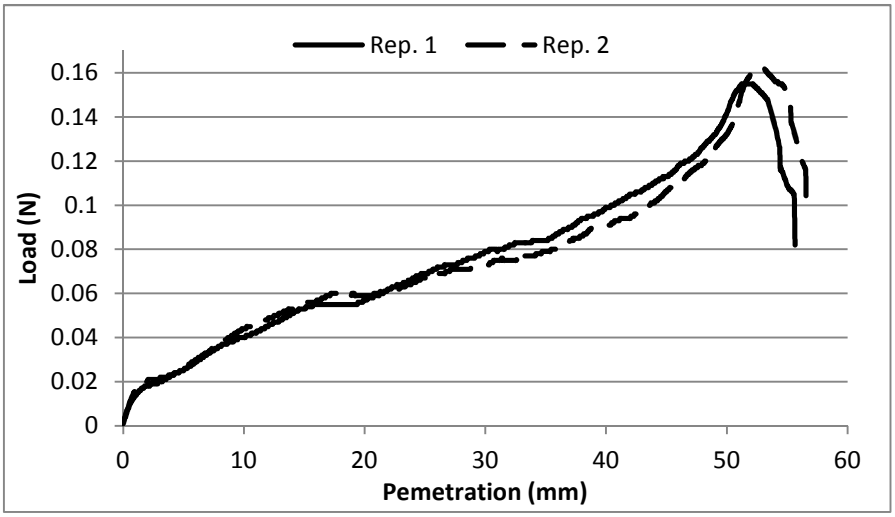

Figure 23 - PR results at resolution (a) 500pulses/revolution, (b) 2000pulses/revolution and (c) 5000pulses/revolution

In order to compare the micropenetrometer results with existing penetrometer studies the sample was flipped so that the crust surface faced downwards and penetration performed at 12mm/min for both flat and pointed probes. This setup created a traditional descending penetrometer very similar to the Liu et al. (2006) device. Figure 24 shows that the PR is again greatest in the crust zone (within 3mm of surface) with a peak in PR of 0.16N for the flat probe and 0.13N for the pointed probe with the pointed probe producing the peak slightly earlier than the flat probe; at 1.2mm compared to 1.5mm.

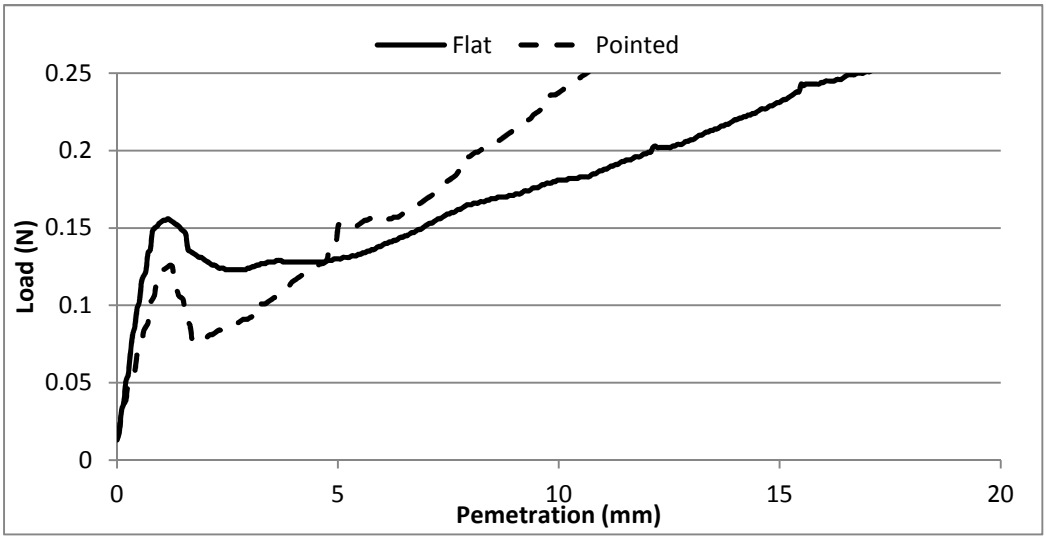

Figure 24 – PR results for descending penetration at 12mm/min

7.3 Testing discussion

As with the pocket penetrometer experiment (Section 4.3) the pointed probe produces higher PR values. What the micropenetrometer shows; however, is that the flat probe has detected the harder crust zone of the dough more clearly than the 30^0 pointed probe since the inflection point at the crust zone and peak in the PR more pronounced (Figure 21b). This was not expected since in the pocket penetrometer experiment the pointed probe was better at detecting differences between PR in varying soil conditions and so it was thought that pointed probe would be more sensitive to changes in strength within the crust zone. Results indicate that due to the slow, smooth and more controlled nature of the penetration from the instrument the flat probe is more sensitive to strength variations. At a fine level of control it is therefore best to limit friction by increasing the cone angle and using a flat probe. The flat probe detects a crust of 1.5mm thick which given that the sample had only 30min drying time is a reasonable result; a thin crust was expected.

Speed settings did not affect PR to extremes; in the range of 6mm/min to 24mm/min the resulting PR curves are similar in shape. PR increases with increased speed, the exception being the 12mm/min penetration of the flat probe which produced the highest PR of the three speeds tested. Previous study by Rolston et al. (1991) proved that speed should have little effect on PR so this result is in-line with theory. The increase in load was attributed to an increase in friction due to higher speed. To prove this, friction was measured during 10mm withdrawal of the probe after penetration through the crust. Plotting the friction during withdrawal shows that the friction reaches a steady state between 2mm and 4mm for the flat probe and between 6mm and 10mm for the pointed probe (Figure 25).

A frictional force, for each PR curve, was calculated by averaging all PR readings between these two positions. The resulting averaged frictional force was then deducted from the PR to produce Figure 26. Both the flat and pointed probe curves correlated much more closely confirming that friction is the main contributing factor for differences in PR at higher penetration rates. What is not expected is that after friction has been subtracted, the resulting PR curve from the flat probe has a negative load throughout penetration (Figure 26a). The reason for this highlights a disadvantage of measuring friction during withdrawal; during penetration particles adhere to the probe and collect on the tip. Then during withdrawal the clump of particles is pulled back into the sample, exacerbating the frictional force. The pointed probe does not produce a fully negative PR curve (Figure 26b). This is because the flat surface of the flat tipped probe collects more particles during penetration and thus produces a more exaggerated frictional force compared to the pointed probe.

An interesting observation is that during the first stages (0-0.5mm) of probe withdrawal the load is still positive and not a negative frictional force. This load is present due to the particles of dough which have adhered to the probe during penetration.

The large frictional component of the PR measurement highlights the need to implement ways to reduce friction during sampling. Due to the small diameter of the shaft a large amount of friction can be attributed to the friction between the shaft and the soil, or skin friction. To reduce skin friction a probe with a slightly relieved shaft (the shaft made of smaller diameter compared to the probe cone/tip) should be used.

(a)

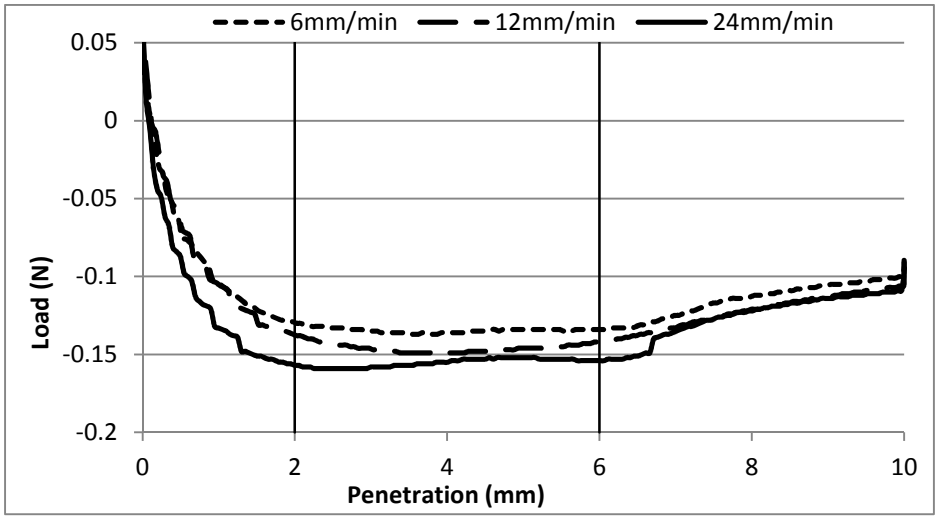

(b)

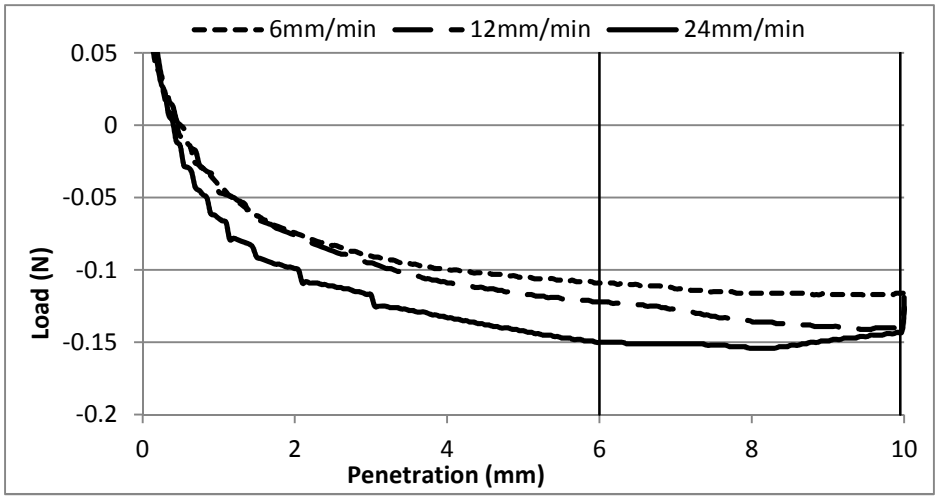

Figure 25 – Frictional load during probe withdrawal for (a) flat and (b) pointed probe. Vertical lines represent region for average friction value calculation

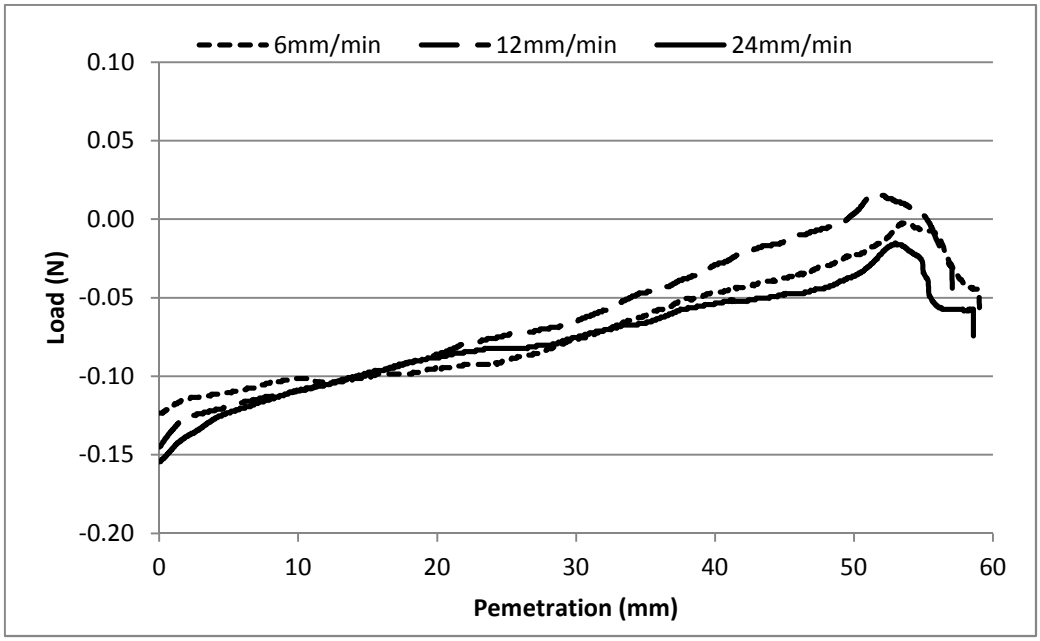

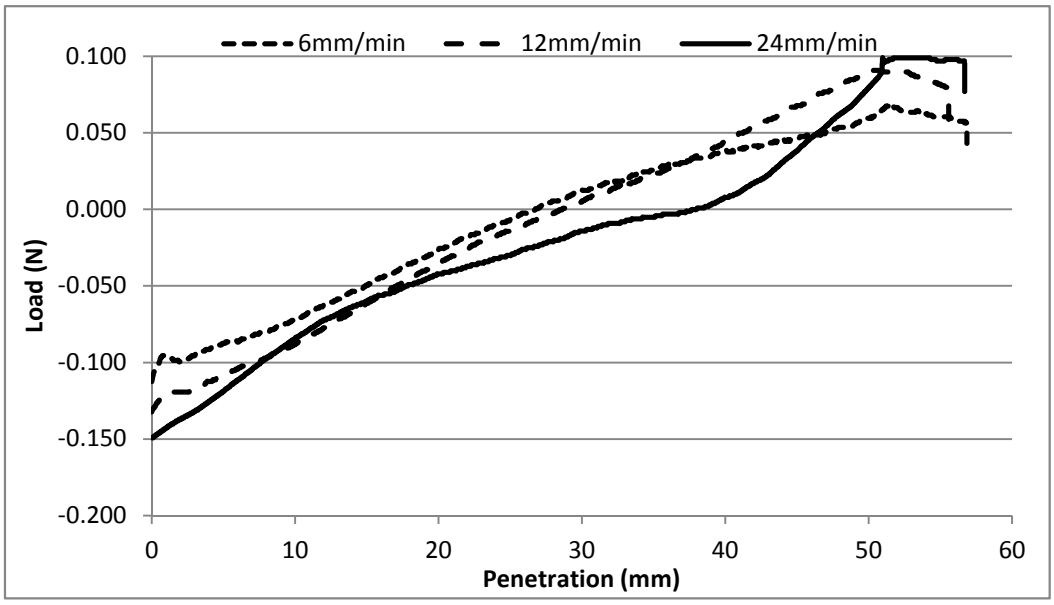

Figure 26 – PR results for (a) flat probe and (b) pointed probe after average frictional value deducted.

Resolution setting results clearly indicate that a resolution of 5000pulses/revolution or linear resolution of 0.0004mm produces the best repeatability between measurements (Figure 23c). This is due to the increased smoothness of the motor operation. At 500pulses/revolution each step of the motor results in a linear motion of 0.005mm which

is causes too great a position increase making repeatability difficult because strength variations within small zones are not captured. Figure 27 presents an exaggerated illustration of the difference between fine 5000pulses/revolution and coarse 500pulses/revolution. Course resolution results in a large position step between each discrete pulse of the motor. At pulse 1 the 500pulses/revolution probe reading 1 is taken as 0.05mm and a low load recorded as the probe is in the low load zone. Pulse 2 records the load at position 0.10mm and a high load. The 5000pulses/revolution probe; however, due to the smaller position change per pulse compared to the coarse probe, the position is still 0.05mm at pulse 2 recording a low load and at pulse 3 the position reading is 0.10mm but the load is still low. So, the coarse probe records a high load and the fine probe records a more accurate low load at position 0.10mm. Strength variation is minimal in the bulk of the dough sample underneath the crust, meaning a coarse resolution will capture the strength similar to the fine resolution. It is near the crust where the change in strength with position varies quickly and this makes fine resolution necessary. This is why the 500pulse/revolution and 2000pulse/revolution measurements start out with good correlation but diverge within the crust zone (Figure 23a and Figure 23b). The 5000pulses/revolution is fine enough to capture the variation well and thus we see good correlation between the repeat measurements in Figure 23c.

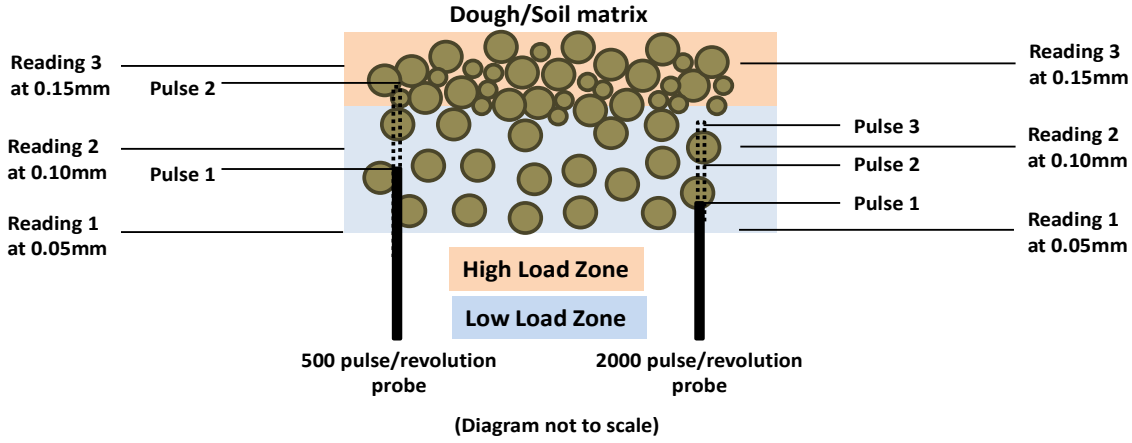

Figure 27 – Diagram illustrating the effect of motor resolution on PR load readings

The descending penetration test produced results which could be directly compared with Liu et al. (2006). Comparing the two curves reveals that the curves are very similar in nature. Liu et al. (2006) found that the dough produced a peak PR of 0.75N within a crust zone of 1mm, while the manufactured micropenetrometer measured only 0.25N peak PR within a crust zone of 1.5mm. There are several factors that could be sighted for the differences in the results. Although both dough samples were made with 40% water content there is no mention of the type of flour used in the Liu et al. (2006) study. The flour used in our test was plain flour and could be of finer grain than that of Liu et al. (2006). Drying conditions could also cause the discrepancy; ambient temperature was low and humidity high during the drying of the dough used in our test. The fact that the tests exhibit the same response curve, albeit not in magnitude, is taken as confirmation that the manufactured micropenetrometer is working effectively.

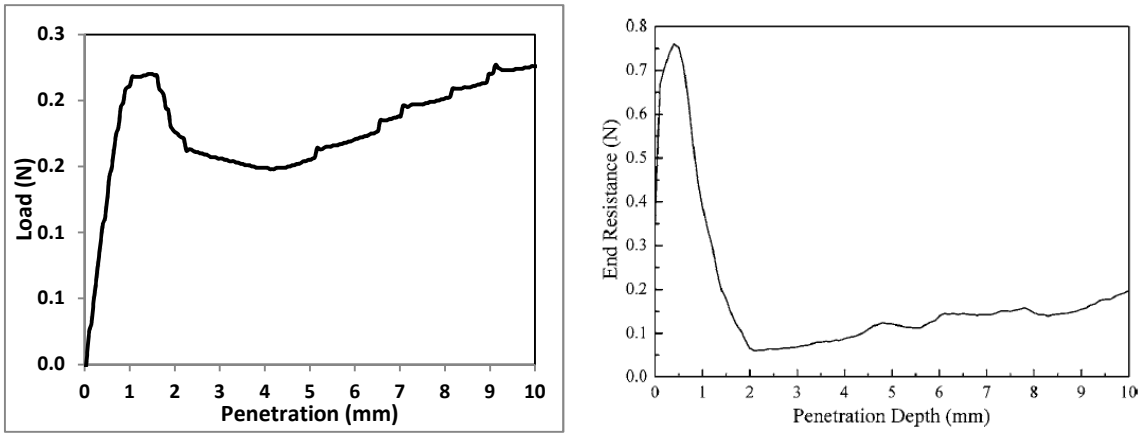

Figure 28 – Comparison between obtained PR curve with the micropenetrometer test and Liu et al. (2006) results for descending penetration. Reproduced from Liu et al. (2006)

7.4 Testing conclusions

The dough test has proved that the micropenetrometer is sensitive enough to detect very small variations in material strength. At a linear resolution of 0.0004mm or 5000pulses/revolution the micropenetrometer also produces excellent repeatability between measurements. The "crust" zone of the dough was successfully identified by both the flat and pointed probe; however, the flat probe is more sensitive to changes in PR strength and should be used in future soil testing using the micropenetrometer.

Frictional effects on the probe are very high contributing to almost 100% of the total load in the case of the pointed probe and over 100% in the flat probe results. This fact is attributed to the nature of the dough; being sticky, and is not expected with soil samples. Care should be taken, however, to minimise friction further in future soil testing. One way to ensure more accurate friction measurement would be to clean the probe before friction measurement, ensuring adhered particles are not adding false frictional load.

Finally, the penetration rate of 12mm/min is considered to be ideal for PR tests. The results of the ascending penetrometer prove that the instrument is well suited for soil penetration studies and should be successful in identifying differences in soil crust strength between samples of varying preparation or material.

8 Conclusions

The project set out to validate the value of creating a micropenetrometer for measuring soil crust strength by mimicking seedling growth rather than conventional downward penetration. During development of the micropenetrometer the study sought to answer the following questions:

1. What are the required design specifications of a micropenetrometer to achieve effective soil crust strength measurements?
2. Is ascending penetration a useful method for measuring soil crust strength and does it require development of a micropenetrometer?
3. What is a good design for an ascending micropenetrometer sensitive enough to capture micro-structural strength variations within thin soil crust regions?
4. Is TOPSIS and effective multi-criteria decision making tool for evaluating design concepts?

Validation of ascending penetration method was confirmed during preliminary experiments using a manufactured pocket penetrometer. Conclusions from the experiment were as follows:

- Ascending penetration is a valid method which could be used to compare crusts of different strength. Using the hand held pocket penetrometer two soil textures at two water contents were tested and compared. The results confirmed that the ascending penetration method was as effective as conventional descending penetration methods. Trends in soil strength were identified in-line with existing theory. Penetration decreased with increasing water content and increased with increasing sand content. These results proved that an ascending micropenetrometer with increased resolution and accuracy would be helpful in more precisely comparing soil crusts and evaluating micro-structural strength variations within small crust regions.
- Penetration forces obtained varied between 84g and 168g. This force range was found to be above what seedling can physically exert (30g for wheat seedlings); however, the force was 50% less exaggerated compared to conventional methods

with produce forces ten times greater than seedling forces. The range was used to identify suitable load cells for use in the ascending micropenetrometer.

- A 30^0 pointed probe was more effective than a flat probe at highlighting differences in soil strength between soil samples. The flat probe; however, fractured the crust surface in a manner more similar to how a seedling would penetrate the soil. These results identified the need to further investigate the probe shape.

A finite element analysis (FEA) of the dynamic soil penetration was explored using ABAQUS 6.10 with the objective of identifying differences of deformation mechanism between ascending and descending penetration as well as various probe shapes. The FEA proved complex and results were somewhat inconclusive; however, some points were identified:

- The ABAQUS in-built Drucker-Prager deformation model can be used to model large soil deformations; however, soil properties need to be clearly defined and these can be difficult to obtain without significant soil testing.
- The ABAQUS adaptive remeshing technique used in isolation is not a very effective method for solving complex large deformations. Instead a sequential approach using manual remeshing of the soil matrix in combination with adaptive remeshing is more promising. Manual remeshing of the soil matrix after small deformation increments should be used for large deformation modelling.
- By further developing the model a tool could be developed to explore different probe shapes and their effectiveness at identifying strengths variations. Ultimately a comparison between a growing seedling forcing its way through the soil and probe penetration could be achieved.

A literature review was carried out to determine what specifications are required for a micropenetrometer capable of measuring soil crust strength. The review identified the following conclusions:

- Several conventional micropenetrometers did not accurately measure position to a high enough resolution. Accurate position measurement to at least 0.1mm accuracy was imperative for an effective ascending micropenetrometer. Higher resolution of position would prove advantageous. Position measurement in

combination with force measurement to 0.01N or 1g accuracy would produce excellent results and allow for understanding of strength variations within the crust region.

- Several ways to measure probe-soil frictional effects were compared. Measuring friction during probe withdrawal is the most effective.
- Three main drive trains were identified as effective for micropenetrometer design. Electric motor in combination with either a lead screw or rack and pinion gear or hydraulic drive would be the best options.

Concept selection was achieved using a multi-criteria decision making tool, TOPSIS. Results proved that this is an effective method to achieve confidence in a chosen design solution. It should be noted; however, that it is important to be pragmatic and consider other design improvements that could be made. A design should be adaptive and evolve to include novel ideas to improve the device. This ethos led to the modification of the final design concept to incorporate a fixed load cell, eliminating potential signal noise produced from motor vibrations.

A review of available components and technology identified three effective final design solutions for the micropenetrometer. Further evaluation identified the following:

- Using cost, time to manufacture and ease of manufacture as criteria an effective and highly accurate ascending micropenetrometer could be manufactured.
- The resulting micropenetrometer could be manufactured for £2050, well within the available budget of £3000. This cost included unexpected repair costs and eight weeks of development time lost due to repair turnaround time. This proves that an effective micropenetrometer can be produced for approximately 30% of a commercially available conventional micropenetrometer.

Upon final micropenetrometer manufacture final testing of the device revealed:

- A simple dough test whereby the micropenetrometer penetrates flour dough is an effective and rapid testing method for finding optimal penetration parameters.
- Penetration speed and resolution settings which allow for best results in detecting strength variations were found using this method. With a penetration rate of

12mm/min and step increments of 0.0004mm the ascending micropenetrometer could detect a crust of approximately 1mm on a dried dough sample.

- The dough test results prove that the micropenetrometer will be effective in future soil science studies, capable of detecting very small strength variations within crust regions. Due to the accurate position resolution, the micropenetrometer can also be used to explore exactly where within a sample strength variations occur.

Due to the ascending action of the penetration the emergence of the probe is similar to growing seedlings and so studies can be made to quantitatively determine whether or not seedlings will be able to emerge through different types of soil crust. The micropenetrometer could be used to determine the strength characteristics of the soil which would ultimately lead to developing a method which could be used to advise farmers whether or not their soils need treatment for ensured seedling emergence. Different soil treatment regimes should be investigated to determine an effective method to make soil conditions suited for seedling emergence and therefore improve crop yields. A decision diagram is presented in Figure 29 as a possible model for ensuring good seedling emergence in agriculture. The micropenetrometer would be used to determine crust strength characteristics and whether or not the strength is low enough to allow good seedling emergence.

Other uses for the micropenetrometer could include characterisation of the soil or the effect of water content and bulk density on PR. Comparisons to current studies could be made to further validate the effectiveness of the ascending micropenetrometer compared to traditional devices. Understanding the effects of soil properties like bulk density, water content and organic matter could lead to empirical characterisation of soils. One could develop a method that predicts the PR curve of a soil given the pertinent soil properties or vice versa. This would allow farmers to know when to plant or what crops might emerge better given the soil they have available.

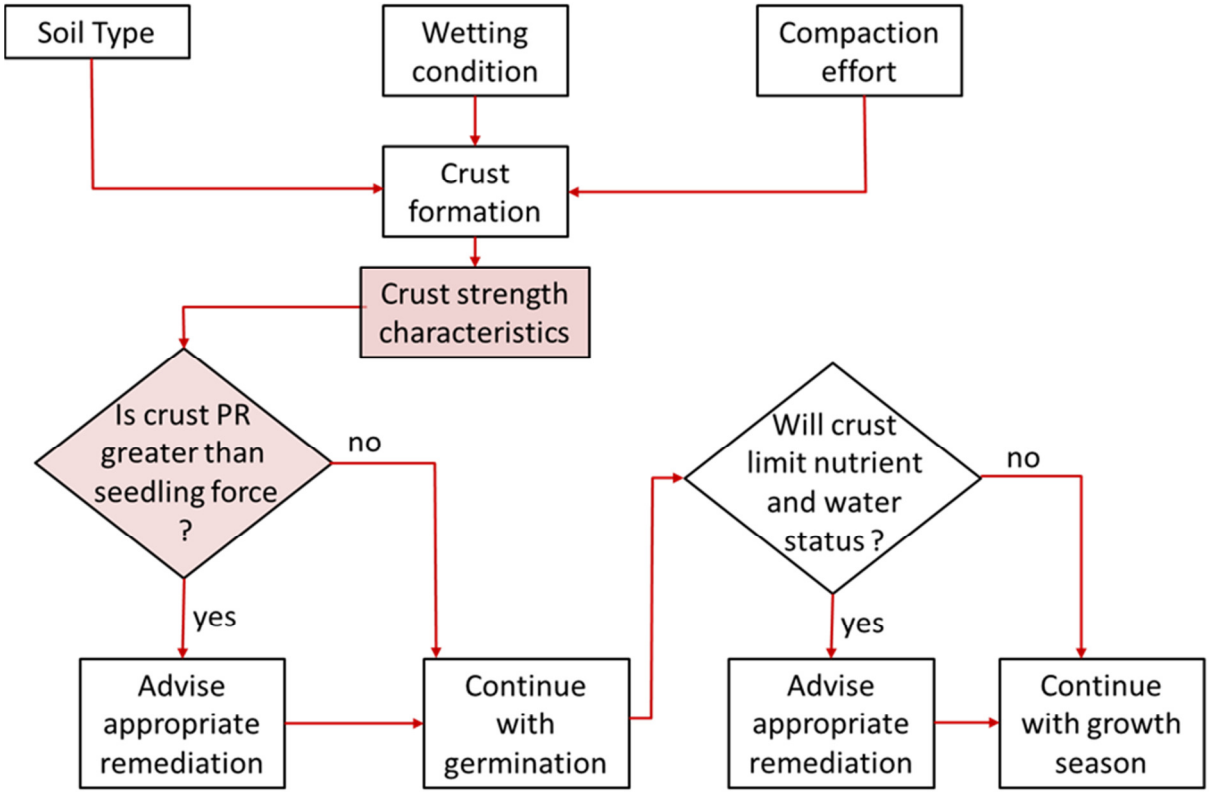

Figure 29 - Decision flow diagram for ensuring seedling emergence. The red blocks indicate areas where the ascending micropenetrometer would be used.

9 Future Work

During operation of the micropenetrometer some improvements have been identified. These ideas could form the basis for future work to improve the functionality and accuracy of the instrument.

9.1 Programming

The uncertainty of position readings is determined by two factors; component specification and the ability of the LabView program to read the load cell and motor at the same time. Due to the nature of the LabView program first the load is obtained and then the position is read. To determine the error produced by the delay between readings, time taken to make each reading was measured in LabView. The resulting 6ms delay will produce a position error of 0.0012mm at a penetration rate of 12mm/min. The position error due to the motor specifications is 0.0006mm/mm so for a typical 50mm sample the position error is 0.03mm giving a total possible position error of 0.0312mm between readings. This error is considered acceptable but there could be improvements made to the sequencing within the LabView program to try get more synchronous readings of load and position.

During operation it was discovered that sometimes a false reading is returned from the load cell and motor. This false reading is probably caused due to the sequencing of the programming. A way to filter out the false readings within the LabView program or investigation into stopping the readings from happening should be developed.

9.2 Micropenetrometer design

Currently the loads onto the load cell are kept vertical by "pinching" the probe collar between two normal roller bearings. Better horizontal load restriction would be achieved by using a V slot with V-bearings instead of the square groove for the normal bearings. This would create less allowable movement between the bearings and the guide groove. Figure 30 illustrates how the V-bearing will restrict motion in both horizontal directions whilst the normal bearing only restricts a single direction.

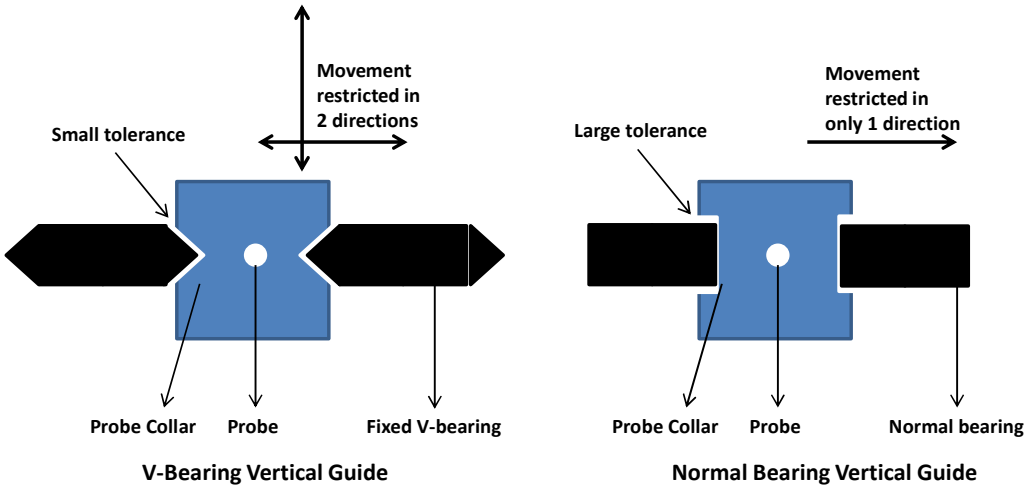

Figure 30 - Diagram illustration differences between V-bearing and normal bearing guide

Probe shape and design is an area that needs further investigation. It is suggested that a relieved shaft would produce advantages of reducing frictional effects on the shaft. The frictional component of the penetration measurement would then be due to the cone only and not the shaft.

9.3 Results interpretation

The penetration tests result in a PR curve of depth versus load. Multiple soil samples of different soils will produce a large amount of data. These data need to be characterised in order to compare the resultant curves. Important areas within the curve have been identified such as the inflection point at the start of the crust zone, the peak of the curve and the drop-off after penetration including the friction measurement. To compare the curves a method needs to be developed so that the differences in the soil types or treatments can be quantitatively measured.

REFERENCES

ABAQUS (2010), "ABAQUS User's Manual Version 6.10.1", *ABAQUS Inc. Providence, RI,* .

Alciatore, D. G. and Histand, M. B. (2003), *Introduction to mechatronics and measurement systems,* 2nd ed, McGraw-Hill, Boston ; London.

Altintas, Y. (2000), *Manufacturing automation : metal cutting mechanics, machine tool vibrations and CNC design / Yusuf Altintas,* Cambridge : Cambridge University Press, 2000.

Armbruster, K., Hertwig, A. and Kutzbach, H. (1990), "An improved design of cone penetrometer", *Journal of Agricultural Engineering Research,* vol. 46, pp. 219-222.

Atkinson, J. (2007), *The mechanics of soils and foundations,* Taylor & Francis.

Aubertot, J. N., Dürr, C., Richard, G., Souty, N. and Duval, Y. (2002), "Are penetrometer measurements useful in predicting emergence of sugar beet (Beta vulgaris L.) seedlings through a crust?", *Plant and Soil,* vol. 241, no. 2, pp. 177-186.

Ayers, P. D. and Bowen, H. D. (1987), "PREDICTING SOIL DENSITY USING CONE PENETRATION RESISTANCE AND MOISTURE PROFILES.", *Transactions of the American Society of Agricultural Engineers,* vol. 30, no. 5, pp. 1331-1336.

Ayers, P. D. and Perumpral, J. V. (1982), "MOISTURE AND DENSITY EFFECT ON CONE INDEX.", *TRANS AM SOC AGRIC ENG (GEN ED),* vol. V 25, no. N 5, pp. 1169-1172.

Bahra, C. S. and Paros, J. (2010), "Chapter 12 - Measurement of Force", in *Instrumentation Reference Book (Fourth Edition),* Butterworth-Heinemann, Boston, pp. 127-133.

Batey, T. (2009), "Soil compaction and soil management–a review", *Soil Use and Management,* vol. 25, no. 4, pp. 335-345.

Baumhardt, R. L. and Schwartz, R. C. (2005), "CRUSTS | Structural", in Editor-in-Chief: Daniel Hillel (ed.) *Encyclopedia of Soils in the Environment,* Elsevier, Oxford, pp. 347-356.

Bécel, C., Vercambre, G. and Pagès, L. (2012), "Soil penetration resistance, a suitable soil property to account for variations in root elongation and branching", *Plant and Soil,* vol. 353, no. 1-2, pp. 169-180.

Bedaiwy, M. N. A. (2008), "Mechanical and hydraulic resistance relations in crust-topped soils", *Catena,* vol. 72, no. 2, pp. 270-281.

Bengough, A. (1992), "Penetrometer resistance equation: Its derivation and the effect of soil adhesion", *Journal of Agricultural Engineering Research,* vol. 53, pp. 163-168.

Bengough, A. and Mullins, C. (1990), "Mechanical impedance to root growth: a review of experimental techniques and root growth responses", *Journal of Soil Science,* vol. 41, no. 3, pp. 341-358.

Bengough, A., Mullins, C., Wilson, G. and Wallace, J. (1991), "The design, construction and use of a rotating-tip penetrometer", *Journal of Agricultural Engineering Research,* vol. 48, pp. 223-227.

Bouaziz, A., Souty, N. and Hicks, D. (1990), "Emergence force exerted by wheat seedlings", *Soil and Tillage Research,* vol. 17, no. 3-4, pp. 211-219.

Causarano, H. (1993), "Factors affecting the tensile strength of soil aggregates", *Soil and Tillage Research,* vol. 28, no. 1, pp. 15-25.

Chambers, J., Cleveland, W., Kleiner, B. and Tukey, P. (1983), "Graphical methods for data analysis. The Wadsworth & Brooks/Cole statistics/probability series", .

Chambers, J. M. (1983), *Graphical methods for data analysis / J.M. Chambers... [et al.],* Pacific Grove : Wadsworth Publishing Co, 1983.

Crawley, M. J. (2012), *The R book,* Wiley.

Cullen, A. and Frey, H. (1999), "Probabilistic techniques in exposure assessment: a handbook for dealing with variability and uncertainty in risk analysis", .

Davies, D. B., Eagle, D. J. and Finney, J. B. (1993), *Soil management.* Farming Press Books.

Dexter, A. R., Czyz, E. A. and Gate, O. P. (2007), "A method for prediction of soil penetration resistance", *Soil and Tillage Research,* vol. 93, no. 2, pp. 412-419.

Doran, J. W. and Parkin, T. B. (1994), "Defining and assessing soil quality", in Doran, J. W., Coleman, D. C., Bezdicek, D. F., et al (eds.) *Defining Soil Quality for a Sustainable Environment,* SSSA Spec. Pub. No. 35 ed, Soil Science Society of America, Argon, Madison, WI, pp. 3 - 21.

Drahorad, S. and Felix-Henningsen, P. (2012), "An electronic micropenetrometer (EMP) for field measurements of biological soil crust stability", *Journal of Plant Nutrition and Soil Science,* .

Faber, J., Johnson, B. and Mead, F. (1976), *Foundation design simply explained,* Oxford University Press.

Fielke, J. M. (1999), "Finite element modelling of the interaction of the cutting edge of tillage implements with soil", *Journal of Agricultural Engineering Research,* vol. 74, no. 1, pp. 91-101.

Fornis, R. L., Vermeulen, H. R. and Nieuwenhuis, J. D. (2005), "Kinetic energy-rainfall intensity relationship for Central Cebu, Philippines for soil erosion studies", *Journal of Hydrology,* vol. 300, no. 1-4, pp. 20-32.

Gerard, C. J. (1965), "The Influence of Soil Moisture, Soil Texture, Drying Conditions, and Exchangeable Cations on Soil Strength", *Soil Science Society of America Journal,* vol. 29, pp. 641-645.

Ginevicius, R. (2011), "A new determining method for the criteria weights in multicriteria evaluation", *International Journal of Information Technology and Decision Making,* vol. 10, no. 6, pp. 1067-1095.

Goyal, M. R., Nelson, G. L., Carpenter, T. G., Drew, L. O. and Taylor, G. S. (1979), "STRESSES GENERATED IN SOIL CRUST BY EMERGING DICOT SEEDLINGS.", *Paper - American Society of Agricultural Engineers, .*

Gregorich, E. G. and Carter, M. R. (2008), *Soil sampling and methods of analysis,* Canadian Society of Soil Science.

Hamrock, B. J., Schmid, S. R. and Jacobson, B. O. (2005), *Fundamentals of machine elements,* 2nd ed, McGraw-Hill, New York.

Hernanz, J. L., Peixoto, H., Cerisola, C. and Sánchez-Girón, V. (2000), "An empirical model to predict soil bulk density profiles in field conditions using penetration resistance, moisture content and soil depth", *Journal of Terramechanics,* vol. 37, no. 4, pp. 167-184.

Herrick, J. E. and Jones, T. L. (2002), "A dynamic cone penetrometer for measuring soil penetration resistance", *Soil Science Society of America Journal,* vol. 66, no. 4, pp. 1320-1324.

Huang, W., Sheng, D., Sloan, S. W. and Yu, H. S. (2004), "Finite element analysis of cone penetration in cohesionless soil", *Computers and Geotechnics,* vol. 31, no. 7, pp. 517-528.

Hughes, A. (1993), *Electric motors and drives: fundamentals, types and applications,* 2nd ed, Butterworth-Heineman, Oxford.

Hwang CL, Y. K. (1981), "Multiple attribute decision making: methods and applications.", *Springer, New York, .*

Jury, W. A., Horton, R., Gardner, W. R., Gardner, W. H. and Baver, L. D. (2004), *Soil physics / William A. Jury, Robert Horton,* Hoboken, N.J. : Wiley, 2004; 6th ed.

Juvinall, R. C. and Marshek, K. M. (2000), *Fundamentals of machine component design,* New York : Wiley, 2000; 3rd ed.

Klute, A. and Page, A. L. (1982), *Methods of soil analysis,* Madison, Wis : American Society of Agronomy : Soil Science Society of America, 1982-1986; 2nd ed.

Kularatna, N., Institution of Electrical Engineers and Knovel, (2003), *Digital and analogue instrumentation*, Institution of Electrical Engineers, London.

Liu, Z., Shi, B. and Sheng, D. (2006), "A micropenetrometer for detecting structural strength inside soft soils", *Geotechnical Testing Journal,* vol. 29, no. 6, pp. 443.

March, R. M., Verdú, A. M. C. and Mas, M. T. (2013), "Mechanical impedance of soil crusts and water content in loamy soils", *EGU General Assembly 2013,* Vol. Vol. 15, EGU2013-2332, 2013, .

Marshall, T. J., Holmes, J. W. and Rose, C. W. (1996), *Soil physics,* Cambridge University Press.

Monsanto Company (2013), *Alleviate Soil Crusting with a Rotary Hoe*, available at: http://www.aganytime.com/Documents/ArticlePDFs/Alleviate%20Soil%20Crusting%20with%20a%20Rotary%20Hoe%20-%20agALERT.pdf (accessed 09/01/2014).

Mouazen, A. M. (2002), "Mechanical behaviour of the upper layers of a sandy loam soil under shear loading", *Journal of Terramechanics,* vol. 39, no. 3, pp. 115-126.

Naderi-Boldaji, M., Alimardani, R., Hemmat, A., Sharifi, A., Keyhani, A., Tekeste, M. Z. and Keller, T. (2013), "3D finite element simulation of a single-tip horizontal penetrometer–soil interaction. Part I: Development of the model and evaluation of the model parameters", *Soil and Tillage Research,* vol. 134, pp. 153-162.

Norton, R. L. (2011), *Machine design: an integrated approach,* 4th ed, Prentice Hall, Boston.

Powlson, D., Gregory, P., Whalley, W., Quinton, J., Hopkins, D., Whitmore, A., Hirsch, P. and Goulding, K. (2011), "Soil management in relation to sustainable agriculture and ecosystem services", *Food Policy,* vol. 36, pp. S72-S87.

R Development Core Team, (2010), *R: A language and environment for statistical computing.*, 3.0.0 ed., R Foundation for Statistical Computing, Vienna, Austria.

Raper, R. L. and Erbach, D. C. (1990), "Effect of variable linear elastic parameters on finite element prediction of soil compaction", *Transactions of the American Society of Agricultural Engineers,* vol. 33, no. 3, pp. 731-736.

Roberts, L. M. (2012), "Use of Manual Adaptive Remeshing in the Mechanical Modeling of an Intraneural Ganglion Cyst.", *MSc Thesis, Michigan Technological University,* .

Rolston, D., Louie, D. and Bedaiwy, M. (1991), "Micropenetrometer for in situ measurement of soil surface strength", *Soil Science Society of America Journal,* vol. 55, no. 2, pp. 481-485.

Rose, C. W. (2004), *An introduction to the environmental physics of soil, water, and watersheds / Calvin W. Rose,* Cambridge : Cambridge University Press, 2004.

Roth, C. H. (1997), "Bulk density of surface crusts: Depth functions and relationships to texture", *Catena,* vol. 29, no. 3-4, pp. 223-237.

Smith, K. A. (2000), *Soil and Environmental Analysis: Physical Methods, Revised, and Expanded,* CRC.

Smith, C. W., Johnston, M. A. and Lorentz, S. (1997), "The effect of soil compaction and soil physical properties on the mechanical resistance of South African forestry soils", *Geoderma,* vol. 78, no. 1-2, pp. 93-111.

Spivey Jr., L. D., Busscher, W. J. and Campbell, R. B. (1986), "The effect of texture on strength of southeastern coastal plain soils", *Soil and Tillage Research,* vol. 6, no. 4, pp. 351-363.

Sumner, M. E. and Stewart, B. A. (1992), *Soil crusting : chemical and physical processes,* Lewis Publishers, 1992.

Susila, E. and Hryciw, R. D. (2003), "Large displacement FEM modelling of the cone penetration test (CPT) in normally consolidated sand", *International Journal for Numerical and Analytical Methods in Geomechanics,* vol. 27, no. 7, pp. 585-602.

Taylor, H. M. and Ratliff, L. F. (1969), "Root elongation rates of cotton and peanuts as a function of soil strength and soil water content", *Soil Science,* vol. 108, no. 2, pp. 113-119.

Tekeste, M. Z., Raper, R. L., Tollner, E. W. and Way, T. R. (2007), "Finite element analysis of cone penetration in soil for prediction of hardpan location", *Transactions of the ASABE,* vol. 50, no. 1, pp. 23-31.

Thiel, T. (2008), "Determination of the relative importance of criteria when the number of people judging is a small sample", *Technological and Economic Development of Economy,* vol. 14, no. 4, pp. 566-577.

THK CO., L. (2011), *Features of the Ball Screw - Technical Document*, available at: https://tech.thk.com/en/products/pdf/en_b15_006.pdf (accessed November 2013).

Van Dijk, A. I. J. M., Bruijnzeel, L. A. and Rosewell, C. J. (2002), "Rainfall intensity-kinetic energy relationships: A critical literature appraisal", *Journal of Hydrology,* vol. 261, no. 1-4, pp. 1-23.

Vaz, C. M. P., Manieri, J. M., de Maria, I. C. and Tuller, M. (2011), "Modeling and correction of soil penetration resistance for varying soil water content", *Geoderma,* vol. 166, no. 1, pp. 92-101.

Whalley, W. R., To, J., Kay, B. D. and Whitmore, A. P. (2007), "Prediction of the penetrometer resistance of soils with models with few parameters", *Geoderma,* vol. 137, no. 3-4, pp. 370-377.

Whiteley, G. and Dexter, A. (1981), "The dependence of soil penetrometer pressure on penetrometer size", *Journal of Agricultural Engineering Research,* vol. 26, no. 6, pp. 467-476.

APPENDICES

Appendix A - Pocket penetrometer experiment

A.1 Drying regimes

It was hypothesised that the fan blow dried samples would produce a good crust by applying energy to the top surface of the soil while allowing the deeper soil layers to remain moist. For best results a high amounts of energy would need to be applied to the surface in order to prevent capillary action. For the air dried soil, the samples were left to dry at ambient temperature for 24 h and for a further 24hr in a dry cupboard at 40 ^{o}C. Samples exposed to the fan drying regime were placed in front of a standard household fan which blew air continuously over the samples for a period of 48hr.

A.2 Rainfall Intensity Calibration

The characteristics required to fully define a rainfall event are:

- Drop size distribution and median drop size (D_{50})
- Kinetic energy of the falling droplets
- Rainfall intensity
- Drop velocity

The rainfall tower was calibrated to produce the 10-year return period rainfall event for the Bedford area. For 15min rainfall duration the 10 year return period rainfall intensity corresponded to 49mmh^{-1}. The aim was to achieve a uniform intensity of 49mmh^{-1}on the catchment area at the base of the tower so that all samples received the same characterised rainfall.

The values for the rainfall duration and return period have been selected based on the following considerations:

- Previous experiments conducted by Dr. Armenise observed that a 15min duration rainfall event is often sufficient for the formation of a structural crust. The crust produced was developed enough to be detected by 3D X-Ray scans of the soil core and therefore appropriate for the purposes of the study.

- A 10 year return period storm corresponds to a rainfall event that is probable in urban areas of England and Wales.

To generate information about the homogeneity of produced rainfall, the rainfall tower catchment area was covered with 30 catch cups of 72mm mm diameter producing a spatial catchment array of 6 x 5 positions (Figure 31). Exposure time of cups to rainfall was 15 min. The catchment area was also divided into five regions: top, bottom, left, right and middle (Figure 31).

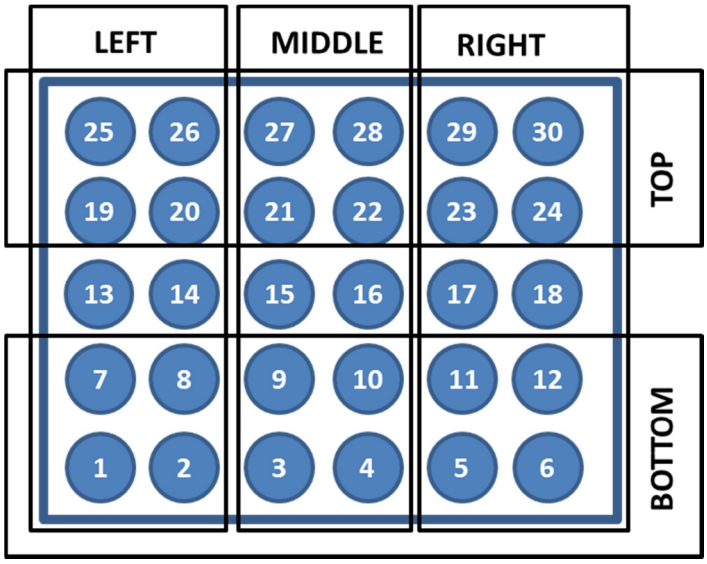

Figure 31 - Spatial arrangement of catch cups on catchment area and associated regions

A.2.1 Rainfall intensity calibration results

In total three rainfall intensity calibration measurements were carried out, adjusting rainfall tower parameters to achieve a more uniform rainfall intensity distribution over the catchment. Results for the calibration measurements are shown in Table 15 where average, minimum, maximum and range of intensity for the catchment area are given. Ideally the range should be as small as possible and the average intensity as close to the desired 49mmhr^{-1} as possible. Table 15 shows that the Calibration 3 produced more desirable characteristics for the rainfall intensity. Results also show that this rainfall event was repeatable since Repeat Calibration 3 gave similar results.

	Average [mmhr^{-1}]	Minimum [mmhr^{-1}]	Maximum [mmhr^{-1}]	Range [mmhr^{-1}]
Calibration 1	66.4	43.3	91.5	48.2
Calibration 2	56.2	35.7	69.7	33.9
Calibration 3	49.1	34.8	60.6	25.8
Repeat Calibration 3	46.8	34.7	59.0	24.3

Table 15 – Catchment Rainfall Intensity Characteristics [mmhr^{-1}] of the Rainfall Tower Calibration Measurements

42.4	44.4	44.8	43.2	41.2	34.8
47.7	56.4	54.8	49.3	47.0	49.0
47.4	51.6	60.6	57.2	53.3	51.2
44.3	49.1	54.7	56.5	52.9	51.8
44.9	47.3	52.2	47.5	46.0	48.0

Figure 32 - Spatial Distribution of Rainfall Intensity (mmhr-1) on Catchment Area Calibration 3

A second replication of the rainfall produced with the Calibration 3was run to ensure that the rainfall event was uniform in time and well characterised. This produced an average rainfall intensity of 47mmhr^{-1} which was taken as the overall rainfall intensity for the catchment area.

A.2.2 Application of simulated rainfall

The average rainfall intensity of the two replicates was calculated for each of the 30 different positions. Similarly, the coefficient of variation (CV%) between the replicates was computed for each position . Subsequently, two constrains were applied to the dataset: average intensity range between 47 and 55mmhr^{-1}; CV% less than 11%. The constraints reduced the number of optimal positions to 13 (Figure 33).

NA	NA	NA	NA	NA	NA
NA	53	51	50	48	50
NA	51	NA	NA	54	53
NA	49	53	54	52	55
NA	NA	NA	NA	NA	NA

Figure 33 - Spatial Distribution of Rainfall Intensity (mmhr-1) at Optimal Positions (purple cells)

The soil cores were placed on the catchment area in the optimal positions previously identified. 10 positions were used in total: position 8 to 12 and 20 to 24 (Figure 33). The 20 cores were therefore split in two batches. Each batch of 10 samples received a 15min duration simulated rainfall event. The soil water content in the samples was brought to field capacity by allowing the cores to drain for 48 h. The top of the cores were covered with plastic foil in order to avoid loss of water via evaporation.

A.2.3 Kinetic energy

Van Dijk et al. (2002) reviewed 19 studies of the relationship between rainfall drop sizes, intensity and kinetic energies from 24 locations around the world. The results showed that kinetic energy ranged from 11.6 to 35.9J m $^{-2}$ mm $^{-1}$, with maximum values averaging around 28.3J m $^{-2}$ mm $^{-1}$ and minimum values of about 13.5J m $^{-2}$ mm $^{-1}$. It was also found that high-intensity storms typical of rainfall simulator studies (> 40 mm h^{-1}) result in average kinetic energies of 23 to 24 J m $^{-2}$ mm $^{-1}$. Values of applied kinetic energy should be as close to this average as possible.

The generic equation for kinetic energy is given by the following formula:

$$KE_G = \frac{1}{2}mv^2 \quad \textbf{(A-1)}$$

Where m is the mass and v is the velocity of the applied mass.

There are two forms of rainfall kinetic energy that can be related to rainfall intensity (Fornis et al., 2005):

- Rate of kinetic energy expenditure (KEr = J m^{-2} h^{-1}): is the kinetic energy per unit area per unit time;

- Kinetic energy content (KE = J m^{-2} mm^{-1}): is the kinetic energy per unit area per unit depth.

These are related by the following expression:

$$KE = \frac{KE_R}{I} \quad \textbf{(A-2)}$$

Where I is the rainfall intensity in mm h^{-1}.

In order to estimate the spatial variability of the rainfall KE and drop size distribution in the rainfall tower catchment area, the LOD was moved during the experiment to five different positions: top, middle, bottom, left and right were used. Three measurements were taken in each position and each measurement had a 1 minute duration. For the simulated rainfall in this experiment the average intensity applied to the catchment area was found to be 47mmhr^{-1}.

Results from the LOD and rainfall intensity measurement indicate that the kinetic energy content is between 18.9 and 12.8J m^{-2} mm^{-1} (Figure 34) which was slightly less than the average desired, however, it was above the minimum obtained by van Dijk et al. (2002) and was therefore considered acceptable.

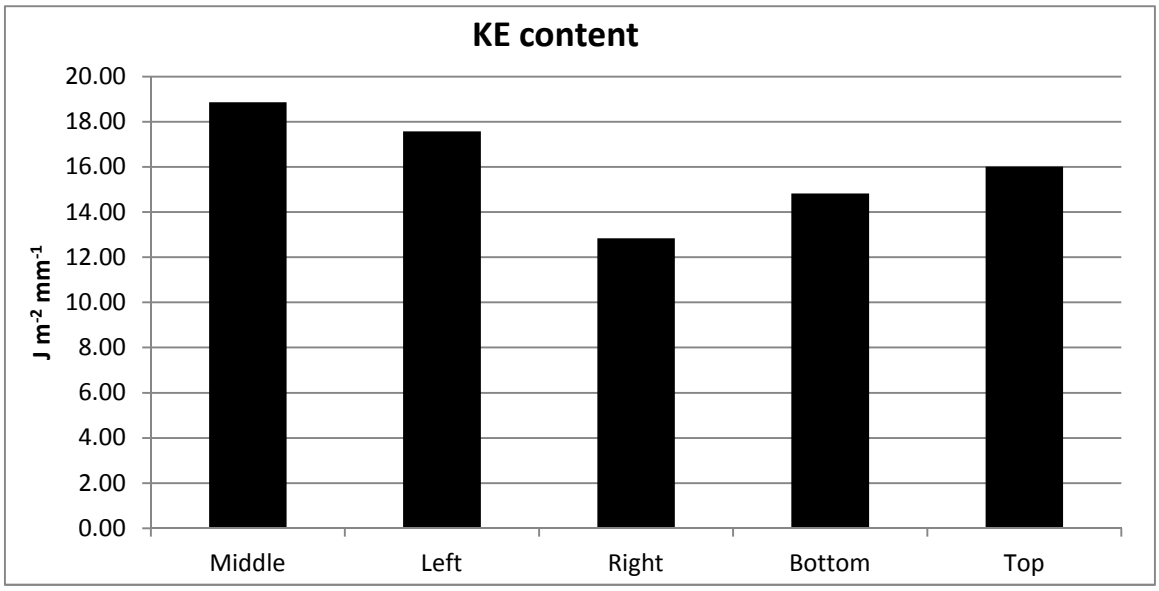

Figure 34 - KE content of the simulated rainfall

The spatial distribution of rainfall intensity obtained from the catch cups was compared to the spatial distribution of KE content obtained using the LOD. To do this the catchment area was divided into regions similar in orientation to the LOD positions (top, middle, bottom, left and right). The average intensity per region was then calculated and plotted against the KE content.

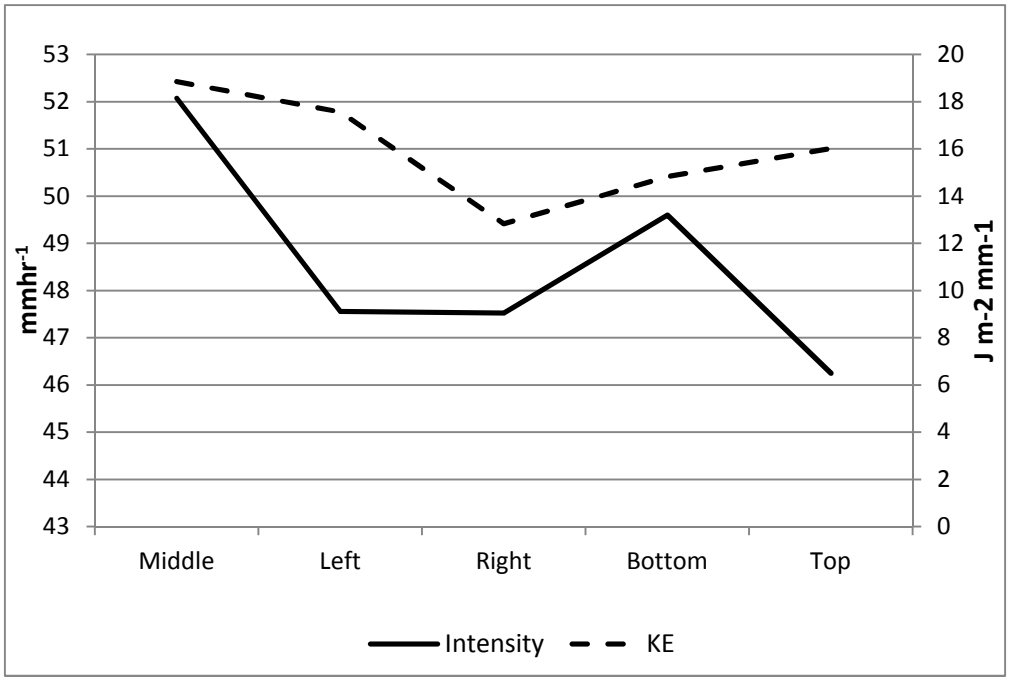

Figure 35 - Comparative results of rainfall intensity and KE content per catchment region

A.2.4 Drop size distribution (DSD)

In order to test what kind of distribution had the best fit to the analytical data produced by the rainfall simulator; a skewness-kurtosis assessment was performed (Cullen and Frey, 1999). The Cullen and Frey graph produced in R using the *fistdistplus* package and *descdist* function displays which type of distribution the data is likely to fit.

The gamma distribution is given by the following equation:

$$f(x) = \frac{\lambda^{r-1} x^{r-1} e^{-\lambda x}}{\Gamma(r)} \quad \textbf{(A-3)}$$

Where λ and r are called the rate and shape parameters.

These parameters determine the shape and position of the curve. Given a set of data, the *fitdist* command in R can estimate the parameters of the gamma curve which would result in the best fit to the empirical data. The command is part of the *fitdistplus* package in R used for distribution fitting. The method that *fistdist* uses to find the parameters follow the Maximum Likelihood method which is a form of regression analysis. Iteratively, *fitdist* finds the parameters of the gamma function which maximises the likelihood function, where the likelihood function is the probability of obtaining the particular data set given the chosen gamma function.

Goodness-of-fit tests were performed to further validate that the random sample comes from a Gamma distribution.

The chi-square goodness of fit test compares the difference between the observed frequency for bin i (O_i) and the expected frequency for bin i (E_i) from the histogram having k bins. The chi-square test is defined for the hypothesis:

H0: the data follow a specified distribution

HA: the data do not follow the specified distribution.

The test statistic is calculated as follow:

$$X_0^2 = \sum_{i=1}^{k} \frac{(O_i - E_i)^2}{E_i} \quad \textbf{(A-4)}$$

The test statistic is compared to the chi-squared distribution with k-p-1 degrees of freedom, where p is the number of parameters in the hypothesized distribution and k the number of observations. If the statistic is higher than the tabled value, HA is accepted and H0 rejected, i.e. the hypothesized distribution does not fit the data well.

The Kolmogorov-Smirnov test is a comparison between the empirical cumulative distribution function and the theoretical CDF (Crawley, 2012). This test is preferred when the sample size is low as with the data from the drop size distribution. In this test the test statistic D is compared to that obtained from tables, for a given significance level α. If the D statistic is found to be greater than the critical value from tables the H0 is rejected.

The results from Cullen and Frey's graph indicate that the gamma distribution is indeed the best fit for the data set (Figure 36). Following this result a gamma probability density function was fitted to the data set.

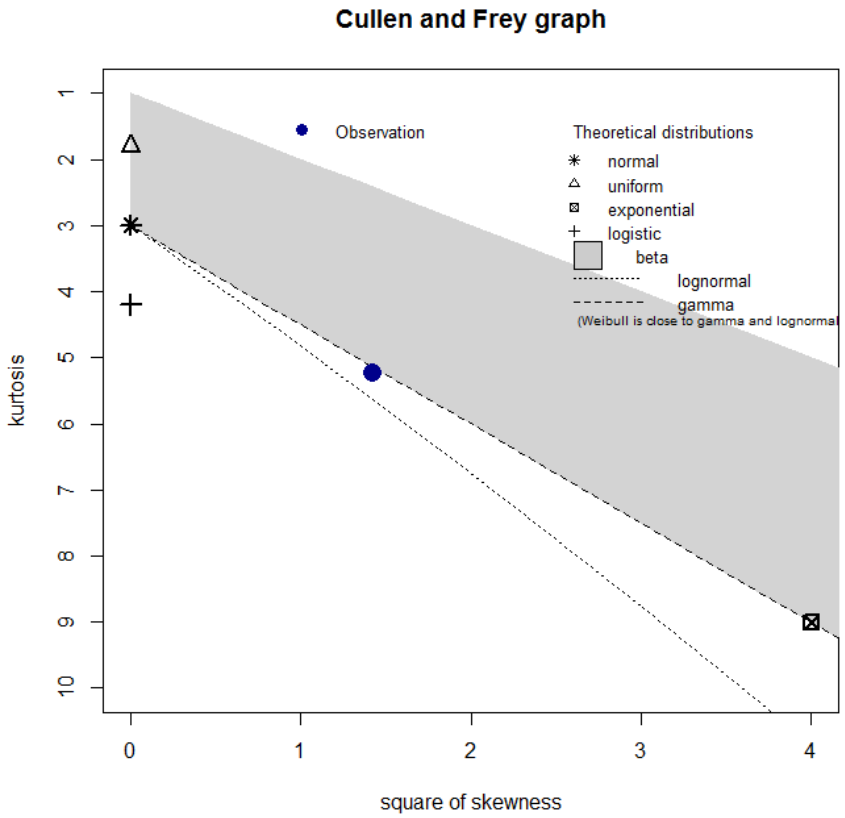

Figure 36 – Cullen and Frey graph illustrating which distribution best fit the data

Using R, the gamma distribution parameters which best fit the data were calculated. The shape (r) and rate (λ) parameters obtained were 9.87 and 16.62 respectively. Using these values, the gamma probability density curve was plotted and superimposed to the histogram plot of the empirical data (Figure 37). Figure 37 shows good agreement between the empirical and fitted distribution.

A.2.5 Chi-square test

At a level of significance $\alpha = 0.05$, and 6 degrees of freedom, the tabled chi-squared statistic is equal to 12.59. The X_0^2 computed from the data set was equal to 16.39. Since the test statistic exceeded the tabled value, the null hypothesis (H0) is rejected and therefore data do not follow a gamma distribution.

A.2.6 Kolmogorov-Smirnov test

The D obtained from the drop size distribution data was 0.448 which was greater than the critical D for significance level $\alpha = 0.05$ of 0.352, therefore the data null hypothesis is rejected and the data does not follow a gamma distribution.

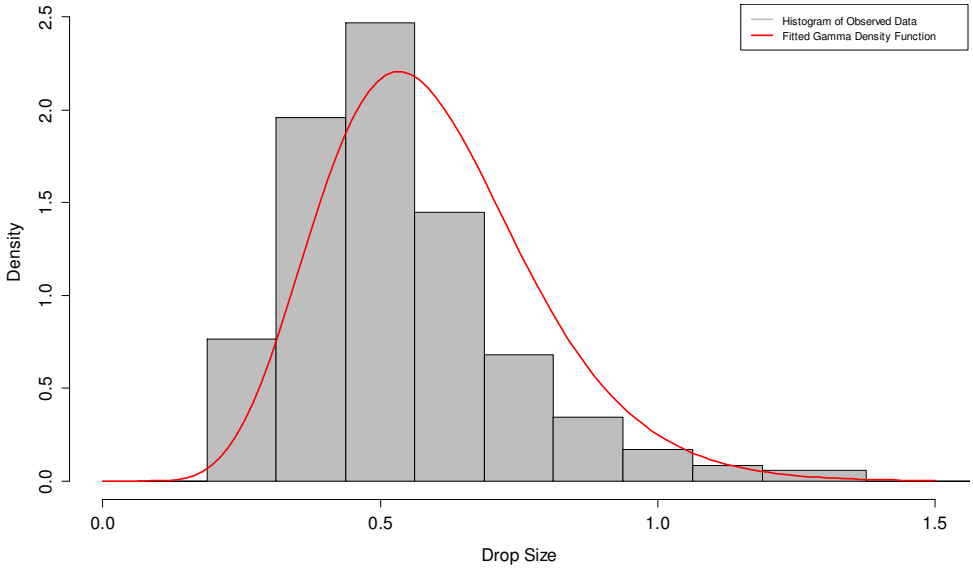

Figure 37 - Density plot of simulated rainfall drop size distribution

The results suggest that the rainfall event created cannot be considered gamma distributed. There is, however, other evidence to suggest that the rainfall event is suitable for comparison with a natural rainfall event. These included the median drop size, the kinetic energy and rain fall intensity.

The median drop size (D_{50}) was computed using the raindrop size distribution. Figure 38 illustrates the median drop size (D_{50}) vs. intensity relationship of natural rainfall obtained in several studies. This figure suggests that drop sizes of approximately 2mm may be appropriate for the simulated rainfall intensity of this experiment.

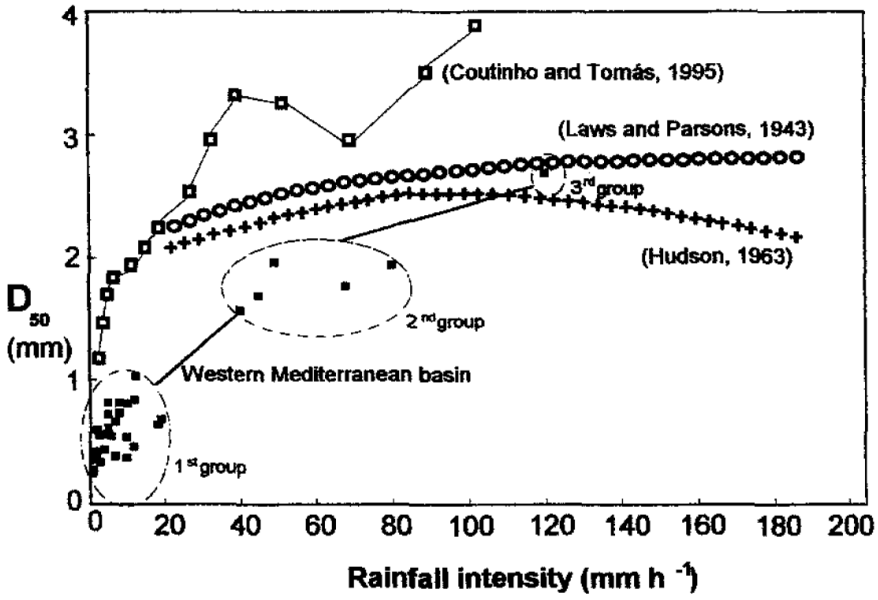

Figure 38 - Relationship between rainfall intensity and D50 (from Cerda 1997)

Figure 39 shows the median drop size obtained in the 5 different positions. Results indicated that the median across all regions was 1.53mm, thus within the desired range at the rainfall intensity of 47mmhr^{-1}.

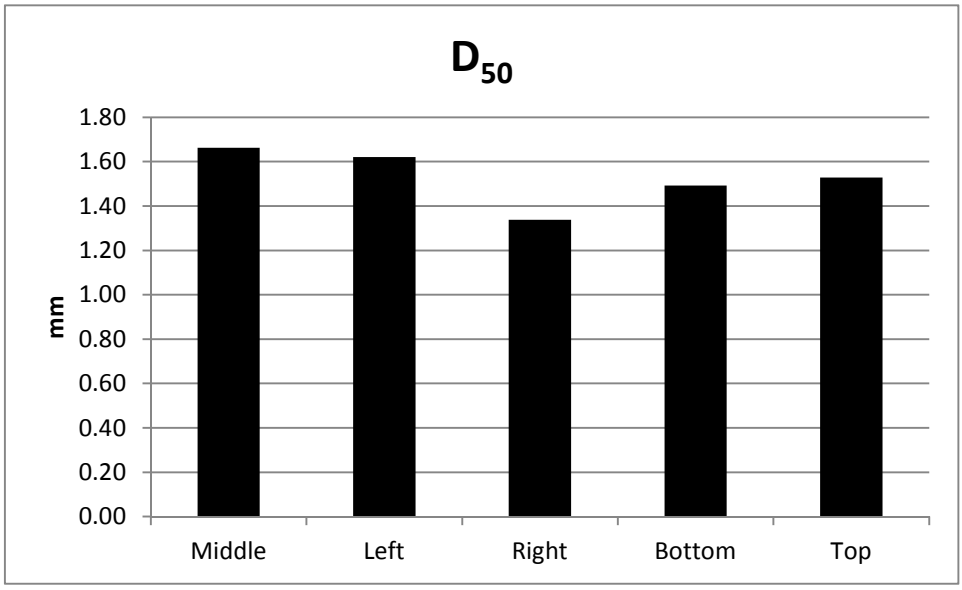

Figure 39 - Median drop size from each position of the LOD

A.3 Water content results

S2 soil did not dry out as much as S1 soil (Figure 40 a). In addition, S1 soil clearly shows a drying process occurring from the surface through the entire body of the core, whereas in

S2 the evaporative flux is somehow impeded and low water evaporation occurs thorough the depth profile (Figure 41). The fan drying regime was far more effective in drying out the soil and resulted in lower water content in both soils (Figure 40 b).

Figure 40 - Comparison of water content between two soil types (S1 and S2) and Soils (a) and water content within S1 and S2 for the two drying regimes (b)

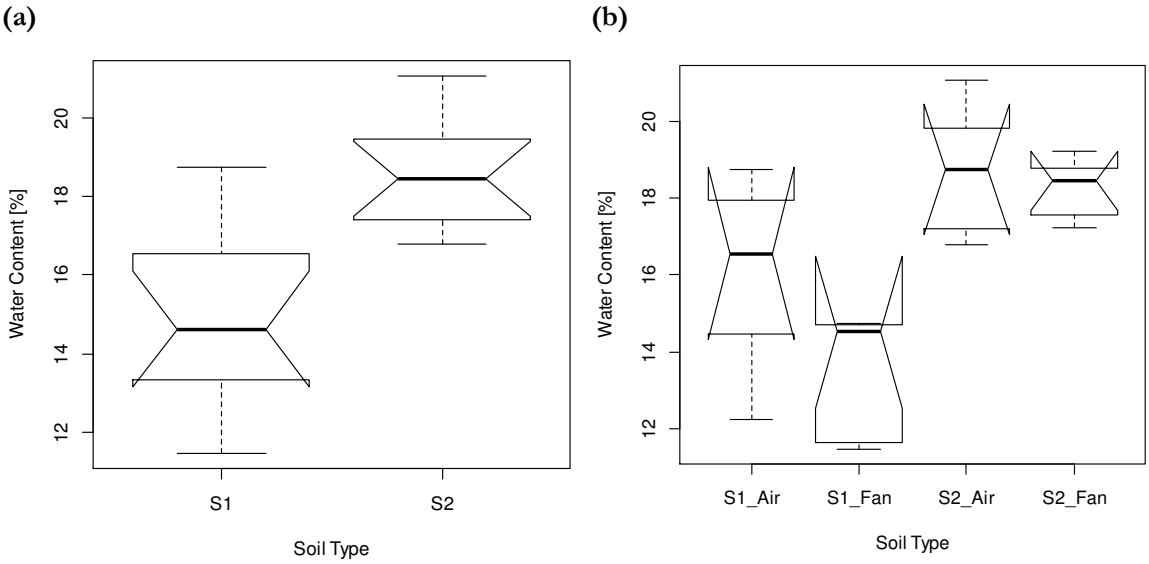

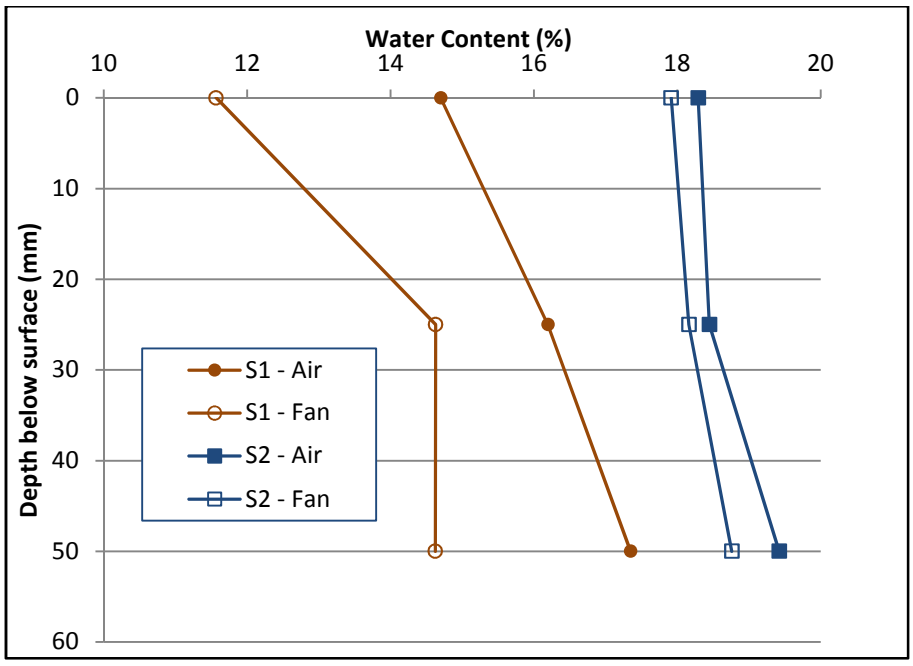

Figure 41 - Water content profile of S1 and S2

Appendix B – **FEA Study**

B.1 Drucker-Prager failure criterion

Under compression loading, soil usually exhibit material hardening, resulting in an increase in yield strength (Naderi-Boldaji et al., 2013). The extended Drucker Prager model is an elaboration of the Mohr-Coulomb model which includes material hardening characteristics. Drucker-Prager model is typically used to model granular materials which exhibit pressure dependant yield (material hardening) (ABAQUS, 2010). Using the linear form of the Drucker-Prager failure criteron is most appropriate for soil as parameters can be obtained using triaxial test data or with data in terms of Mohr-Coloumb cohesion and internal angle of friction (ABAQUS, 2010). The Drucker-Prager failure criterion as shown in is defined as:

$$F = t + p.tan\beta - d \quad \textbf{(B-1)}$$

where F is the yield function, p is he normal stress, t the deviatoric stress, β is the Drucker-Prager internal friction angle and d is the t-axis intercept in the p-t plane.The parameters β and d are similar but not exactly the same as ϕ and c in the Mohr-Coulomb criterion.

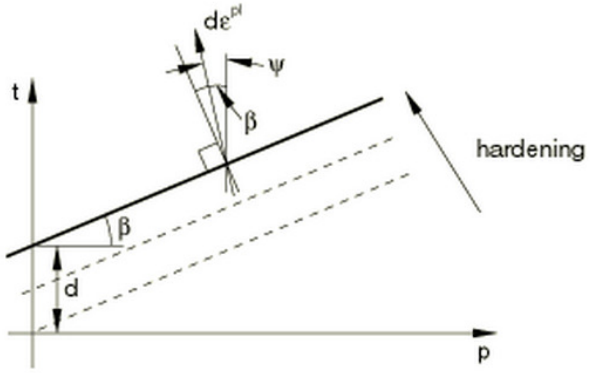

Figure 42 - Linear Drucker-Prager model: yield surface and flow direction in the p–t plane. Reproduced from (ABAQUS, 2010).

Where K (the flow stress ratio) is the ratio of yield stress in triaxial compression to yield stress in triaxial tension. K can be determined using the triaxial tests or using Eq.(B-2))

$$K = \frac{3 - sin\phi}{3 + sin\phi} \quad \textbf{(B-2)}$$

For the finite element analysis (FEA) modelling of the ascending and descending soil penetration with different shaped probes, the Drucker-Prager criterion was used.

B.2 Model geometry and boundary conditions

Due to symmetry of the soil sample the problem was simplified to an axisymmetric model of two bodies, the rigid probe and deformable soil body. The probe was modelled as a discrete rigid body of diameter 1.5mm as was used in the actual experiment. The soil body was meshed using CAX4R ABAQUS elements, while the probe was modelled as an analytical rigid body. Mesh refinement ensured that the elements potentially in contact with the probe were approximately one-fifteenth the probe diameter in order to make the explicit procedure stable and convergent. A velocity boundary condition was applied to the probe pushing it into the soil at a rate of 12mm/min for a penetration depth of 10mm. Thus the penetration through both crust layer and 5mm into the bulk soil were simulated. Ascending and descending penetration with a flat probe and a pointed probe with 30 degree cone angle were simulated.

Descending penetration

The soil body with radius of 25mm (radius of the soil cores) and depth of 50mm was partitioned into three layers. The first two layers formed the assumed 5mm crust and the bottom layer 45mm of the bulk soil (Figure 43(a)). The boundaries on the sides and bottom of the soil body were constrained in the radial (U1) and vertical (U2) degrees of freedom respectively. The top surface of the soil was left unconstrained. A reference node was attached to the probe to govern its motion.

Ascending penetration

For ascending penetration the soil body was 10mm deep. The probe was located 10mm below the surface and moved up into the soil (Figure 43b). Penetration was simulated to a probe displacement of 15mm. This increase in penetration depth was chosen to accommodate for the soil body being pushed up above the probe. Unlike the descending case, the ascending penetration meant that the surface was free to displace vertically,

making the simulation more complex than the descending case. Soil weight of the full volume of sample was applied to the top surface of the soil using a uniformly distributed pressure.

Several limitations of the ascending penetration soon emerged during the simulation:

- It became difficult to redefine the regions of the soil layers due to the vertical displacement of the soil body. For the purposes of simplicity the layer regions were chosen reference to the original undeformed soil body, making the final crust layers increase in thickness (Figure 48 and Figure 49)
- Even with increased penetration depth, the probe still did not exit the soil matrix as was the case in the pocket penetrometer experiment. Results would be higher than if the probe were to emerge.

(a)

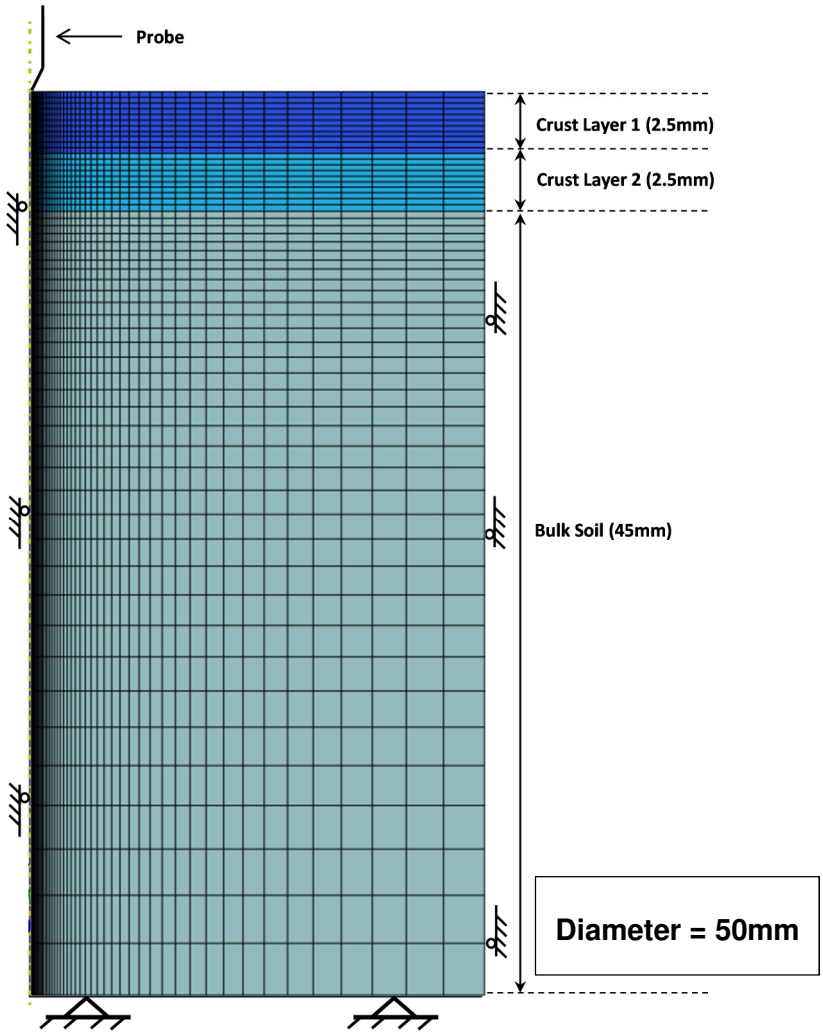

(b)

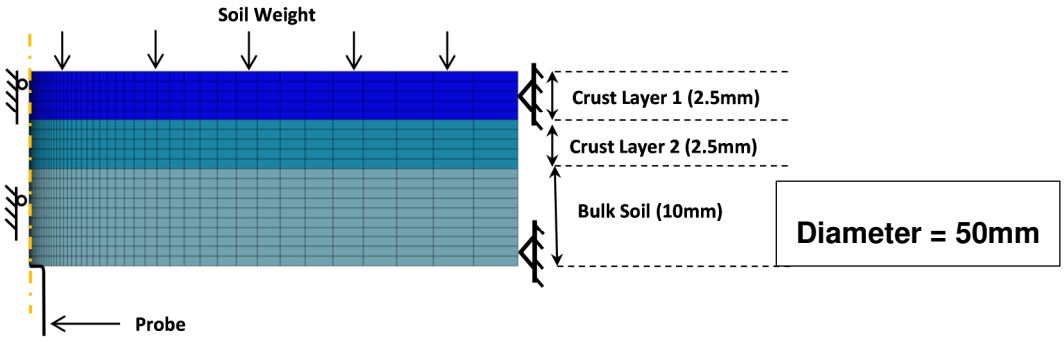

Figure 43 - Axisymmetric finite-element mesh and boundary conditions for (a) descending and (b) ascending penetration analysis

B.3 Adaptive meshing

The problem is broken done into several small steps allowing only a small amount of penetration during each simulation. This smaller penetration does not cause as much mesh distortion and the simulation will complete. Once the small penetration simulation is complete, the deformed mesh of the soil body is converted to a new geometric shape which is repartitioned into the bulk soil and crust layers. The deformed shape is then remeshed and the cone placed into the cavity left by the previous penetration. A new simulation is run, increasing the overall depth of penetration. This process is repeated until the full penetration depth is achieved. Each penetration was broken down into discrete steps (Table 16).

Table 16 - Penetration steps used in the simulation of ascending and descending penetration using two types of probe.

Increment	Descending Penetration		Ascending Penetration	
	Flat Probe	Pointed Probe (30◦ cone angle)	Flat Probe	Pointed Probe (30◦ cone angle)
Step 1.	0 - 4 mm	0 - 3mm	0 - 6mm	0 – 6mm
Step 2.	4 - 6 mm	3 – 5mm	6 – 9mm	6 – 10mm
Step 3.	6 -10mm	5 – 10mm	9 – 15mm	10 – 15mm

B.4 Assumptions of the model

There were assumptions made to this model in order to simplify the problem:

1. The Drucker-Prager model with hardening only models hydrostatic compaction behaviour. Other soil failure modes which occur in reality such as tension, shear and cutting have been ignored.
2. The soil properties were taken from literature and pertinent to a sandy loam soil (Tekeste et al., 2007). Although in a similar textural class to the soil used in the experiments (sandy-silt-loam), these properties could be significantly different in reality. For accurate soil properties tri-axial tests need to be performed on the soil.

3. Poisson's ratio was assumed constant at 0.3. It has been suggested that to better model soil strength the Poison's ratio should be varied with depth and soil strength (Raper and Erbach, 1990).
4. The two crust layers and bulk soil layer are assumed to be homogenous material. As discussed, in actual fact the strength of the crust layer decreases exponentially and layers are not discrete.
5. Manual adaptive remeshing required the partitions of the crust and soil body layers to be redefined after each step. This meant that, once the simulation had moved the probe past the initial depth of the discrete crust and soil layers, it was assumed that the probe had penetrated through the layer. In reality this is not strictly true and during penetration the advancing probe would compact the soil layer in front of the probe, pushing it into the sub-layers and the soil strength increases due to plastic hardening. Thus this assumption underestimates the PR.
6. The left boundary layer of the soil body restricts the movement of the soil horizontally. This boundary was required to keep the simulation stable, however, during actual penetration the soil would move horizontally past and around the advancing probe. This extra boundary condition is expected to increase the value of PR artificially.

B.5 Cone-soil interface

The soil-probe interface was simulated by surface to surface contact pair interaction with a frictional behaviour type. The frictional co-efficient of 0.5 was used based on Tekste et al. (2007). The relative motion of the probe and soil body surfaces was modelled using a finite sliding formulation that allows sliding, separation and rotation of the surfaces (ABAQUS, 2010). The kinematic contact algorithm was used to describe the contact interface. For this algorithm ABAQUS/Explicit calculates the value of the contact force at the mesh nodes from the mass of the node, the distance the node has slipped, and the time increment (ABAQUS, 2010).

B.6 Tekeste et al. (2007) case study

The FEA model was found to be effective in locating the transition interface between the three soil layers of varying hardness. The top soil layer was 5.15cm above the compacted hardpan layer, the hardpan layer was 4.09cm thick and the soil below the hardpan was the

remaining 15.87cm of soil profile. Penetration was modelled using a rigid 30° cone at a constant speed of 1.65cm/s to a depth of 12cm.

Due to the high level of signal noise obtained a moving average was required to smooth these data. Tekeste et al. (2007) did also use some moving average smoothing. The variation of the signal makes it quite difficult to reproduce exact results since the amount of smoothing is unknown. It was observed that the level of frequency of adaptive meshing significantly changed results. After consulting the author, it emerged that a low frequency of adaptive meshing was used. The model was also extremely unstable, failing due to excessive distortion. With improved mesh and increased adaptive meshing the model would likely improve, however, this would come at a computational cost.

Results from the validation show similar trends to those observed by Tekeste et al. (2007). The PR was, however, an order of magnitude out (Figure 44). This discrepancy is most likely due to the high sensitivity to changes in elastic modulus and hardening parameters. The results do, however, validate that the model can detect the location of the hardpan layer to within good proximity of Tekeste et al (2007). Since the purpose of the FEA model was to detect changes in the crust strength layers, the validation parameters were deemed sufficient for the full model of ascending and descending penetration study.

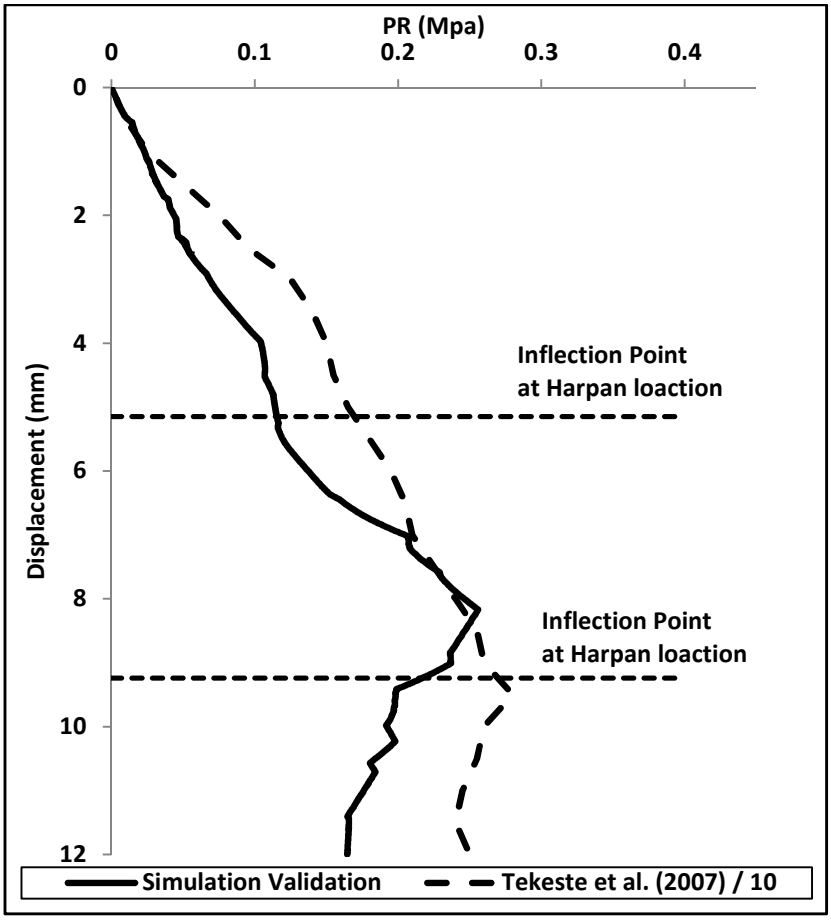

Figure 44 - Penetration resistance from FEA Model validated against Tekeste et al. (2007) figure 2, compaction III.

B.7 Results

Descending penetration

Figure 45 and Figure 46 display the results of the stress distributions from the descending penetration simulations. The plots clearly distinguish the differences in mechanical behaviour of the two cone shapes on the deformation of the soil. The flat cone (Figure 46) produces an area of compaction ahead of the advancing probe, consistent with discussed theory. Conversely, the pointed cone has more evenly distributed stresses, concentrated along the inclined length of the cone edge (Figure 45). This longer contact length indicates that the pointed cone is more affected by friction. The magnitudes of stresses produced were largely similar from the two shapes, with the pointed cone producing initially larger stresses at low depth. This is due to the smaller initial contact area of the cone. Stresses reduce throughout the depth profile which is to be expected due to the reduction in strength between the layers.

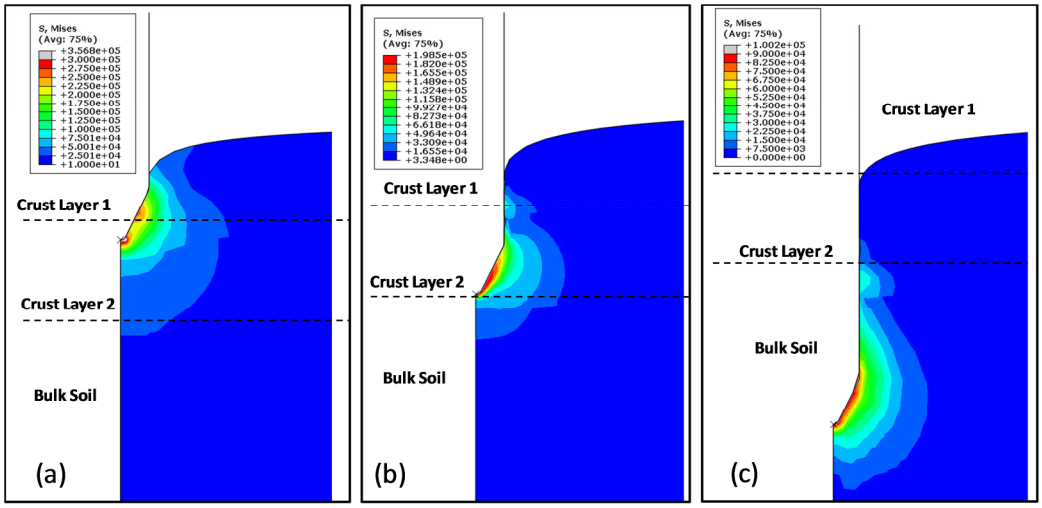

Figure 45 - Plots of stress distribution (Pa) from descending pointed probe showing plastic zone at cone penetration depths of (a) 3mm, (b) 5mm and (c) 10mm

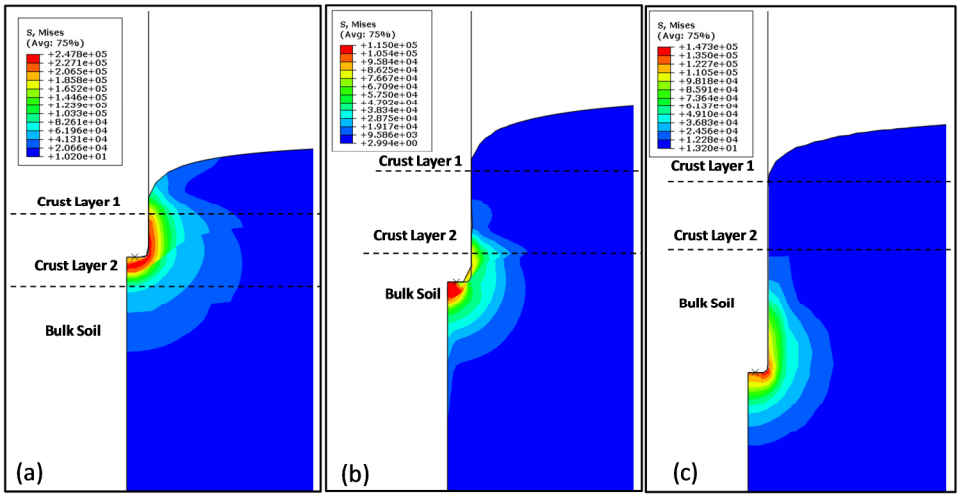

Figure 46 - Plots of stress distribution (Pa) from descending flat probe showing plastic zone at cone penetration depths of (a) 4mm, (b) 6mm and (c) 10mm

The PR results showed two deflection points, confirmed through the addition of trend lines, occurring where the material changes in the soil layers. At 2.5mm (depth of crust layer 1) the deflection is less apparent than the deflection when the probe moves from crust layer 2 into the soft bulk soil at 5.0mm depth (Figure 47).

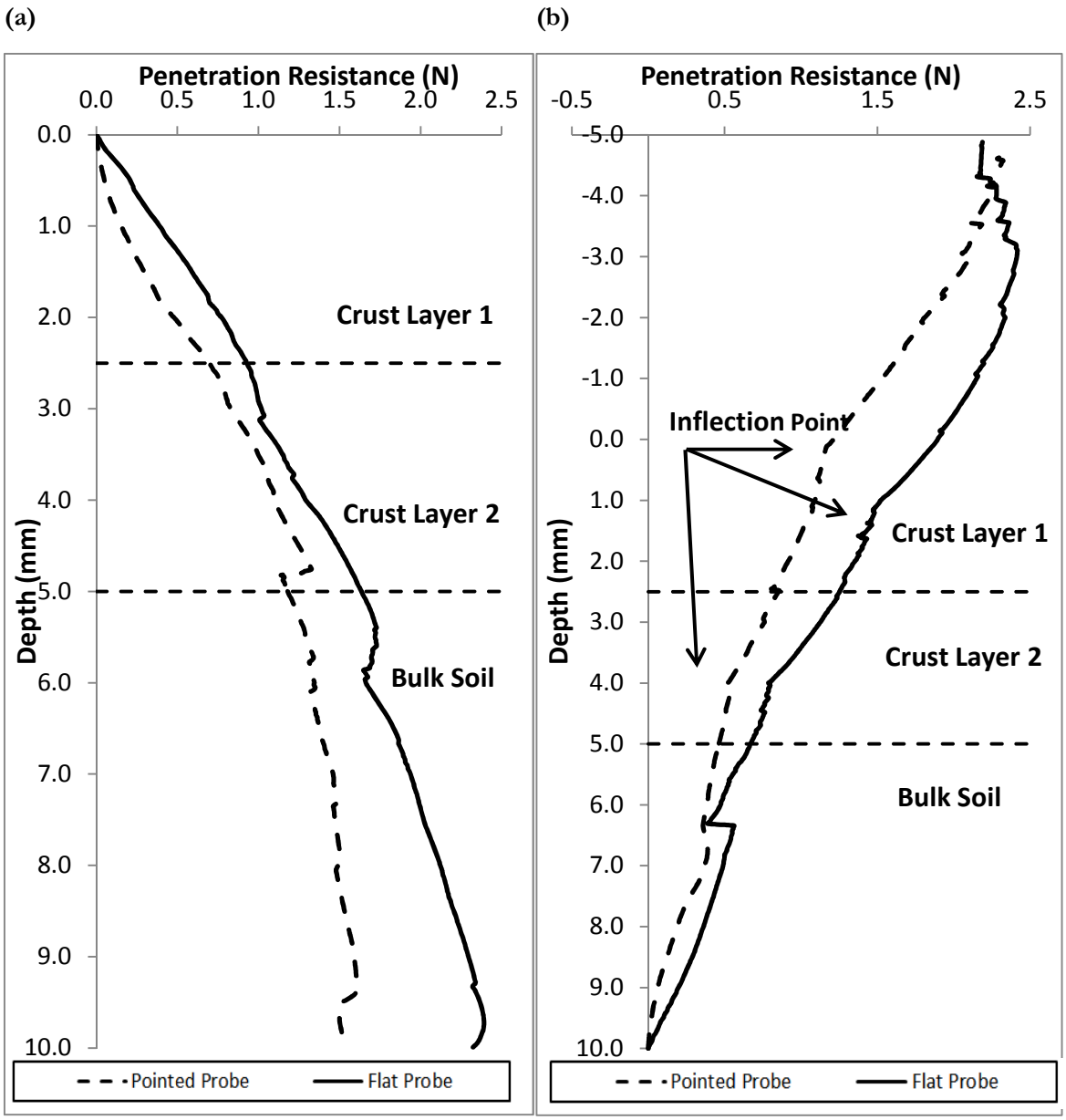

Figure 47 - Predicted penetration resistance (force) of the FE simulation for (a) descending and (b) ascending penetration using a flat and pointed probe.

Ascending penetration

Inflection points at the interface of the crust layers, during ascending penetration for the pointed needle, were less distinguishable compared to descending case (Figure 47). Soil stress distributions are similar to the descending penetration, with greater stresses localised in the harder crust layers (Figure 48 and Figure 49).

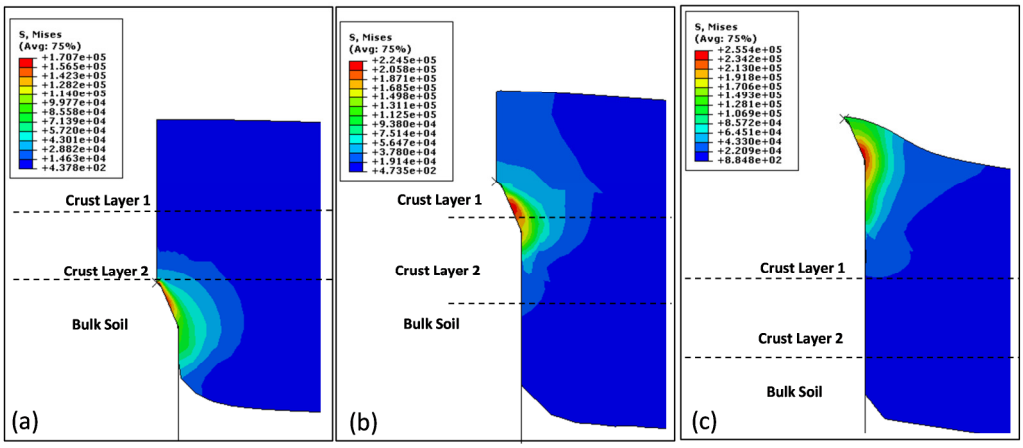

Figure 48 - Stress distribution (Pa) from ascending pointed probe showing plastic zone at cone penetration depths of (a) 6mm, (b) 10mm and (c) 15mm

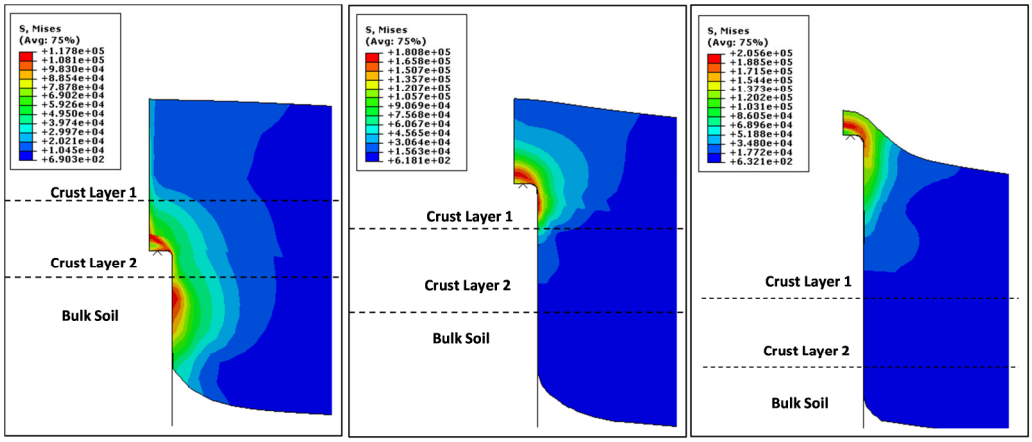

Figure 49 - Stress distribution (Pa) from ascending pointed probe showing plastic zone at cone penetration depths of (a) 6mm, (b) 9mm and (c) 15mm

In general, the flat probe shows the inflection points more clearly, whilst the pointed probe is more sensitive showing a greater change in gradient between layers (Table 17). Descending penetration leads to more distinct change in PR gradient between the layers.

Table 17 - Change in gradient between the crust and bulk soil layers for ascending and descending penetration.

Penetration application	Layer Interface	Flat Probe Change in gradient (%)	Pointed Probe Change in gradient (%)
Descending	Crust Layer1 – Crust Layer 2	22	17
	Crust Layer 2 – Bulk Soil	78	210
Ascending	Crust Layer1 – Crust Layer 2	1	35
	Crust Layer 2 – Bulk Soil	108	59

B.8 Drucker-Prager hardening characteristics

Figure 50 was used to calculate the Young's moduli and stress vs. plastic strain hardening characteristics for the soil used in the FEA modelling.

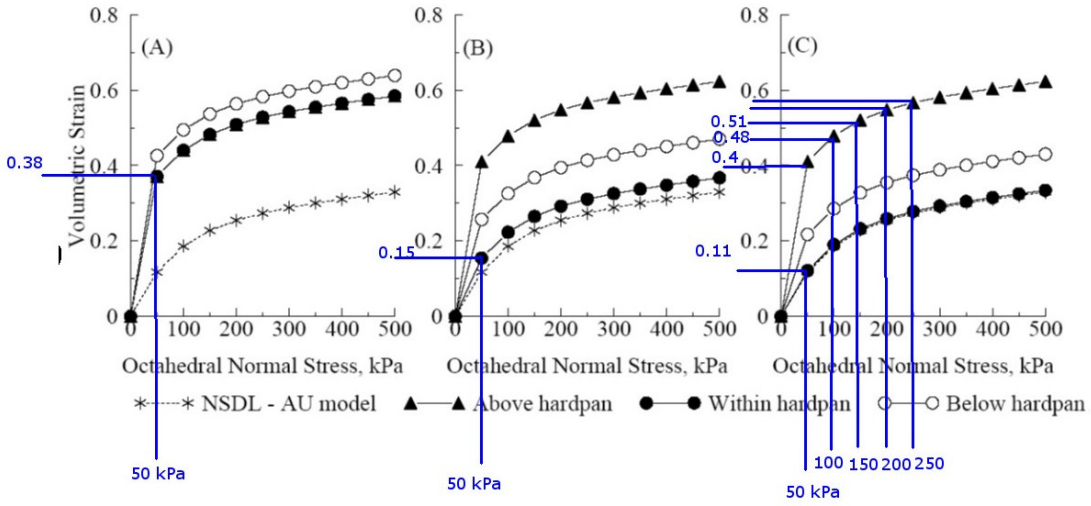

Figure 50 – Natural volumetric strains vs. stress for (a) Compaction I, (b) Compaction II and (c) Compaction III. Modified Figure 2 reproduced from Tekeste et al. (2007)

E averaged from Volumetric Strain Graphs – Example for Within Hardpan

Compaction I – Volumetric strain = 0.38, Stress = 50kpa

Convert Vol. Strain to Plastic Volumetric Strain → 0.38 x 0.926 = 0.35

Since have plastic volumetric strain can work out Bulk Modulus

Bulk Modulus K = (Normal Stress)/(Volumetric Plastic Strain)=50/0.35=142 kPa

Convert Bulk Modulus to Elastic Modulus →E=3K(1-2ν) = 3*142(1-2*0.3) = 171 kPa

Did this procedure for each compaction curve and averaged the values to get the average Young's modulus for each soil section.

Curves also yielded strains at rated stresses for each soil section. The results are tabulated in

Soil Layer Depth	**Bulk Density ρ (g.cm)^3**	**Elastic modulus (kPa) Young's modulus**	**Plastic Strain**	**Stress (kPa)**
Crust Layer1	1.71	364	0	45
0 -2.5mm			0.10	50
			0.17	100
			0.21	150
			0.23	200
			0.26	250
Crust Layer 2	1.54	222	0	45
2.5-5.0mm			0.19	50
			0.27	100
			0.30	150
			0.33	200
			0.35	250
Bulk Soil	1.20	134	0	45
5mm–50mm			0.37	50
			0.44	100
			0.48	150
			0.54	200
			0.55	250

Appendix C **- TOPSIS**

C.1 TOPSIS Method

For the TOPSIS analysis the design options and criteria against which they are evaluated make up the decision matrix.

Step 1. Decision Matrix

The alternatives of m design options (vector A) and n design criteria (vector C) form the decision matrix [X]. The decision matrix is presented in the following matrix format:

$$X = \begin{array}{c} \\ A_1 \\ A_2 \\ \vdots \\ A_m \end{array} \begin{array}{c} \begin{array}{cccc} C_1 & C_2 & \cdots & C_n \end{array} \\ \begin{bmatrix} x_{11} & x_{12} & \cdots & x_{1n} \\ x_{21} & x_{22} & \cdots & x_{2n} \\ \vdots & \vdots & \ddots & \vdots \\ x_{m1} & x_{m2} & \cdots & x_{mn} \end{bmatrix} \end{array}$$

In the m x n decision matrix each element represents the score given to the j-th option with respect to the i-th criterion. In this TOPSIS analysis experts in the Soil Science and Engineering field were asked to score the concepts relative to one another against the given criteria. These results were then averaged to form the decision matrix.

Step 2. – Normalise the decision matrix. This step transforms the various attribute dimensions into non-dimensional attributes, which allows comparisons across criteria. Each element of the decision matrix is normalised using the following formula:

$$r_{ij} = \frac{x_{ij}}{\sum x_{ij}^2}$$

The r_{ij} elements form the normalised matrix [R]

Step 2. – Construct weighted normalised decision matrix. The weighting vector [W] is formed by assigning a weight to each criterion, w_j for j = 1,…,n criteria. Multiply each column of the normalised decision matric by its associated weight. Each element of the new matrix [V] is:

$$v_{ij} = w_j \cdot r_{ij}$$

Step 3. – Determine the ideal and negative ideal solutions.

The ideal solution [A*] is defined as the solution which has the best score for every criterion, regardless if the scores are from different options/concepts. In this study the maximum score is always the best.

$A^* = \{v_1^*, \dots, v_n^*\}$, where $v_1^* = \{\max(v_{ij})\ if\ j \in J; \min(v_{ij})\ \ if\ j \in J'\}$

Negative ideal solution [A'] is defined as the solution which has the worst score for every criterion, regardless if the scores are from different options/concepts. In this study the minimum score is always the worst.

$A' = \{v_1', \dots, v_n'\}$, where $v_1' = \{\min(v_{ij})\ if\ j \in J; \max(v_{ij})\ \ if\ j \in J'\}$

Step 4. - Calculate the separation measures for each alternative.

This is the distance from the positive and negative ideal solution of each solution.

Distance from ideal solution for the i-th solution is calculated as follows:

$$S_i^* = [\sum (v_j^* - v_{ij})^2]^{\frac{1}{2}}$$

Distance from ideal negative solution for the i-th solution is calculated as follows:

$$S_i' = [\sum (v_j' - v_{ij})^2]^{\frac{1}{2}}$$

Step 5. – Calculate the relative closeness to the ideal solution

The relative closeness of each solution C* is calculated as follows:

$$C_i^* = \frac{S_i'}{(S_i^* + S_i')}$$

C.2 TOPSIS Questionnaire

Micropenetrometer for soil crust penetration resistance measurement.

Traditional penetrometer devices which measure soil penetration resistance do so by forcing a probe into the soil from above and recording the reaction force. In an attempt to mimic the real forces which a seedling would encounter during emergence through the soil crust, ascending probe penetration is suggested.

This questionnaire proposes several concepts which are seen to fulfil the design purpose. The TOPSIS study is a way to obtain an objective opinion from several experts. This will highlight which design criteria are most important and which design should be developed for the final solution.

The micropenetrometer will need to fulfil the following technical requirements:

- **Hold soil sample core of 50mm diameter**
- **Detect resistance force within 3mm soil crust. Expected forces 0 – 5N**
- **Force resolution of 0.1N**
- **Probe (1.5mm diameter) driven into crust at constant speed between 8 – 16mm/min**
- **Ascending measurement, probe forced through crust from base of sample**

Secondary requirements (not essential but ideal)

- **Depth resolution 0.1mm**
- **Descending measurement capability**

Rating criteria definitions

1. **Accuracy - Ability of device to measure force and displacement precisely**
2. **Repeatability – Ability of device to repeat the exact same measurement consistently**
3. **Durability – Robustness of device, strength and resistance to environmental factors such as rust and dirt**
4. **Manufacture and Integration – Ease of manufacture and integration of components into assembly**
5. **Adjustment and Control – Ease of adjustment and control of components within assembly**
6. **Ease of use - Ability of end user to perform measurements**
7. **Adaptability – Ability to change and adapt configuration**
8. **Low Cost – Relative price of device**

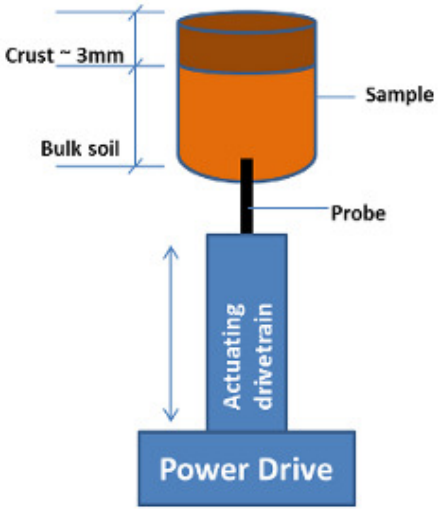

Part A – Relative weighting of criteria

Experts are asked to rate the criteria by importance for the design. The importance should be judged from the point of view of the expert and their expertise. A score of between 1 and 10 is assigned, 10 being highly important, 1 being low.

Criteria	Score (1 – 10) 10 being high
Accuracy	
Repeatability	
Durability	
Manufacture and Integration	
Adjustment and Control	
Ease of Use	
Adaptability	
Low Cost	

Example: Scoring the relative importance of the criteria from the perspective of a scientist, accuracy and repeatability could be viewed as far more important than cost or ease of use. Please score the criteria from your own view point.

Criteria	Score (1 – 10) 10 being high
Accuracy	10
Repeatability	9
Durability	5
Manufacture and Integration	3
Adjustment and Control	8
Ease of Use	3
Adaptability	3
Low Cost	2

Part B – Scoring concepts against criteria

Concepts and descriptions are presented. Experts are then asked to score the concepts against the criteria**. In some cases modifications to the original concepts are proposed.** This is a comparative study, so the concepts are scored relative to each other. A score between 1 and 10 is given, 10 being high and 1 being low.

PLEASE NOTE: This is not mandatory for the study. Please only complete this part of the survey if you feel you have the expertise to be able to do so. Not all criteria need to be scored, only the criteria you feel are applicable to your expertise.

CONCEPT 1

A - Electric motor mounted on side of simple mild steel frame and drives pinion gear
B - Rack and pinion gear mounted on vertical slide drives probe upwards into the sample
C - Inner rail (orange) slides vertically between outer guide rail (red)
D - Sample clamped at the top of frame
E - Load cell located beneath probe
F - Displacement measured by potentiometer which measures rotation of the motor shaft
G - Load cell and probe could be detachable and mounted on bottom of rack for descending measurement

Potential Modifications to Concept 1

Modification 1 - replaces potentiometer described in point (**F**) with accurate motor control to measure displacement

Modification 2 - replaces potentiometer described in point (**F**) with an LVDT (Linear variable differential transformer) to measure displacement between load cell and reference point at base of the sample

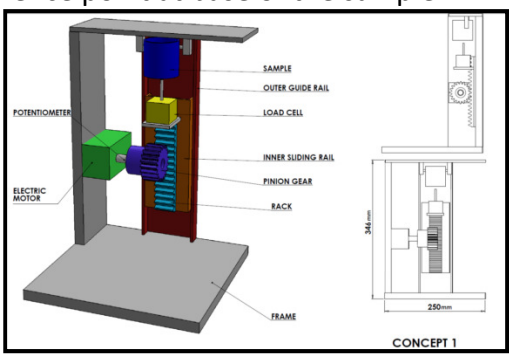

CONCEPT 2

A - Simple mild steel frame with vertical shafts over which crossbeam can slide vertically
B - Soil sample clamped to crossbeam
C - Crossbeam and sample pushed down onto probe by small hydraulic actuator.
D - Actuator shaft extends from actuator body to push crossbeam down.
E - Force measured by load cell. Probe and load cell fixed to frame at the base
F - Displacement measured by Linear variable differential transformer (LVDT)

Potential Modification to Concept 2

Modification 1 - replaces hydraulic actuator described in point (**C**) with a pneumatic actuator

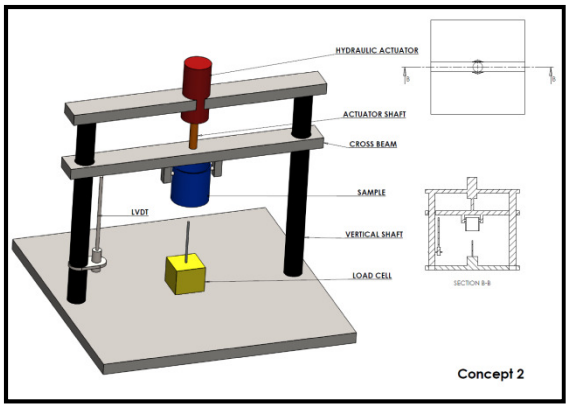

CONCEPT 3

A - Electric motor driven
B - Motor housed between guide rails, shaft with bearings allow for vertical travel of the motor and leadscrew
C - Motor guide rails are clamped to instrument frame
D - Motor directly drives a leadscrew. The leadscrew is held in place by leadscrew nut fixed to cross bar. Leadscrew advances upwards through the nut, pulling the motor with it.
E - Crossbar fitted with pin and pivot which allows the motor, leadscrew and probe to rotate. This means that descending measurements could also be achieved. The motor housing will pivot and then be clamped at the top of the frame. Sample clamp detachable so that sample can be clamped at the base of frame.
F - Load cell mounted to the end of leadscrew and probe mounted to load cell. A slip ring and or thrust bearing located at the base of the leadscrew so that the load cell and probe do not rotate with the rotating leadscrew.

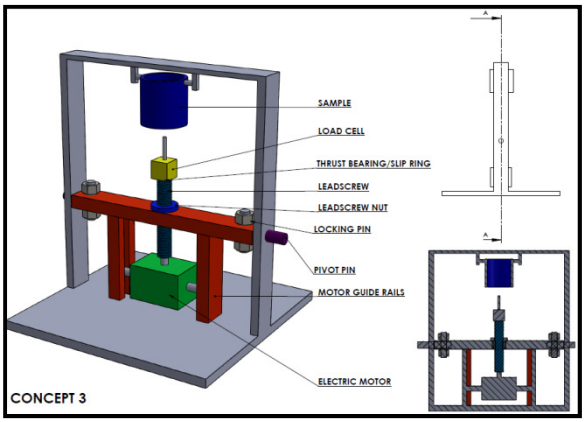

CONCEPT 4

A - Electric motor driven.
B - Similar concept to concept 3, however, instead of the leadscrew turning, the leadscrew nut turns.
C - Motor fitted with pinion gear which drives threaded leadscrew nut. The nut rotates pushing leadscrew vertically. Thrust bearing connects rotating leadscrew nut to the frame crossbar to allow rotation.

D - Leadscrew is prevented from rotating with the nut by the guide rail crossbar which is attached to the leadscrew. The guide rails allow for vertical movement of the leadscrew.
E - Whole unit can pivot around to allow for descending measurement if desired.
F - Displacement measured through control of the motor.

Potential Modifications to Concept 4:

Modification 1 - measures displacement using potentiometer that measures motor shaft rotation, replacing measurement by motor control described in (**F**)**.**

Modification 2 - measures displacement using LVDT located between load cell and sample base (not shown in drawing), replacing measurement by motor control described in (**F**)**.**

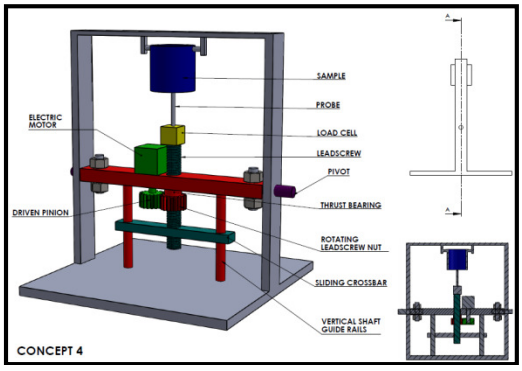

CONCEPT 5

A - Electric motor driven.
B - Similar in design to traditional axial load frames or universal testing devices.
C - Motor housed inside the base of the load frame.
D - Pulley drive belt system rotates leadscrews in each of the vertical support columns.
E - Leadscrew nuts fixed to the cross beam convert the rotation of leadscrew into vertical translation.
F - Sample is lowered onto probe and load cell at the base of the frame.
G- Displacement measured using precise motor control.
Potential Modification to Concept 5:
Modification 1 - LVDT measures displacement between crossbar and reference point on vertical column. Replaces precise motor measurement (**G**). (Not shown on drawing)

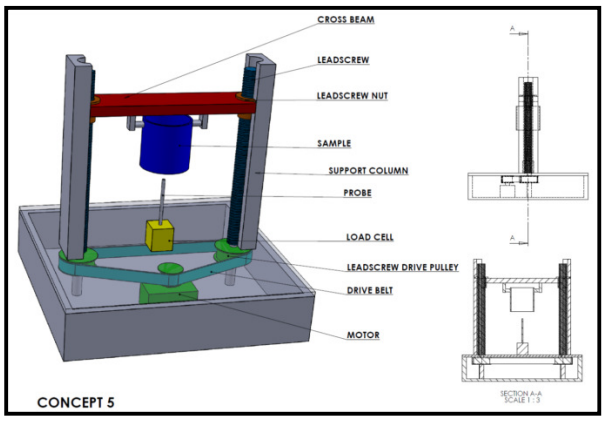

Scoring of Main Concepts – Please score concepts relative to each other, score between 1 (low) and 10 (high)

• Criteria	Concept 1	Concept 2	Concept 3	Concept 4	Concept 5
Accuracy					
Repeatability					
Durability					
Manufacture and Integration					
Adjustment and Control					
Ease of Use					
Adaptability					
Cost					

Criteria	Concept 1 Modification 1 replaces potentiometer with accurate motor control to measure displacement	Concept 1 Modification 2 replaces potentiometer with an LVDT to measure displacement	Concept 2 Modification 1 replaces hydraulic actuator with a pneumatic actuator	Concept 4 Modification 1 measures displacement using potentiometer that measures motor shaft rotation, replacing measurement by motor control	Concept 4 Modification 2 measures displacement using LVDT, replacing measurement by motor control	Concept 5 Modification 1 LVDT measures displacement between crossbar and reference point on vertical column. Replaces precise motor measurement
Accuracy						
Repeatability						
Durability						
Manufacture and Integration						
Adjustment and Control						
Ease of Use						
Adaptability						
Cost						

Appendix D - **Design Characteristics**

D.1 Lead screw design parameters

$$d_2 = n_0 l = n_0 mp \quad \textbf{(D-1)}$$

m = number of threads
n_0 = number of revolutions
p = pitch
d_2= axial displacement

Design proposal: for one full rotation displacement of

- Equation relating torque required to drive lead screw to the pitch/lead of leadscrew

$$T(Nm) = \frac{F(N) \times l(m)}{2 \times Pi \times \eta}$$

η = Efficiency, for Ball Lead Screw 0.9 and for leadscrew 0.4 recommended

Must consider application demands, including thrust, speed of linear motion required, accuracy, repeatability and resolution before choosing suitable leadscrew. There are friction losses in the lead screw this decreases the efficiency of the lead screw and therefore increases the amount of torque required to drive the lead screw.

Maximum lead screw load is calculated using Euler buckling formula

$$P_{CR} = \frac{n\pi^2 EI}{L^2} \quad \textbf{(D-2)}$$

Where n is the load factor, for column with 1 end fixed and other free n = 0.25
For stainless steel lead screw the equation is as follows:

$$P_{CR} = \frac{n\pi^2 EI}{L^2}$$

For circular lead screw
Accuracy and repeatability
Accuracy is the ability to of the lead screw to move within a desired tolerance. While repeatability is the how well the lead screw can move the load to the exact same location. It is possible for leadscrews to have good repeatability but low accuracy. For the application of the micropenetrometer good accuracy is required.

D.2 Motor torque calculations

Figure 51 - Torque calculations using (a) (THK CO., 2011; Altintas, 2000) and (b) Altintas, (2000) and (c) results.

(a)

Motor Torque Calculations

Method 1.

$$T=\frac{F*p}{2\pi*\eta}$$

$$\tan\beta=\frac{p}{\pi*d}$$

d=Mean diameter lead screw
p= lead screw pitch
β =lead screw angle

η=Efficiency lead screw
p= lead screw pitch
F=Force to overcome

From graph obtain η
With μ=0.2 – Co-efficient friction (conservative)
Get η=0.28 from Graph

FORCE BODY DIAGRAM

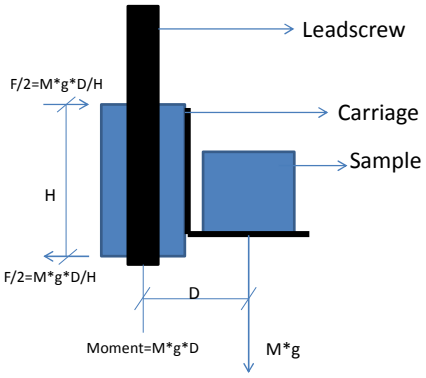

Worst load case
- Weight + Force onto needle (during pull up)

(b)

Motor Torque Calculations

Method 2.

$$T_d=J_e\frac{dw}{dt}+Bw+T_{sr}$$

Je=Total inertia on motor shaft
B= viscous damping co-efficient =0
Tsr=Total static force = Tgf+Tlf +Tf
Tf=cutting forces
Tlf=Torque in bearing
Tgf=Torque to overcome guide friction

$$T_{gf}=\frac{p}{2*pi}\mu_{gf}[(mt+mw)*g+Fz]$$

$$T_{lf}=\frac{d}{2}\mu_b(Ff)$$

Ff =- feed force
μ_b = bearing friction = 0.2 (conservative)

$$T_f=\frac{p}{2+pi}(Ff)$$

J_{le}=Jtw + Jl +Jm

p=leadscrwew pitch
Fz= normal cutting force on table = 10%of max resultant cutting force
μ_{gf} =guide friction = 0.1 usually
Mt = table mass – negligible
Mw = workpiece mass

Jtw= inertia of table and workpiece
Jl= inertia of leadscrew
Jm = inertia of motor shaft

$$J_{tw}=(\frac{p}{2*pi})\text{^}2(mt+mw)$$

$$J_l=(\frac{d}{2})\text{^}2(0.5*ml)$$

Worst load case
- Weight + Force onto needle (during pull up)

(c)

Method 1 - THK Ball Screw Torque		
Lead Screw Angle [degree]		4.76721654
Force to Overcome [N]		11.772
Static Torque [N.mm]		13.38265707
Dynamic Torque	From Book Manu. Automation	
Moment inertia (Load) [kg.mm^2]		0.070924829
Moment inertia (Leadscrew) [kg.mm^2]		2.349008097
Angular Acceleration [rad/s^2]		1308.996939
Dynamic Torque [N.m]		0.101342455
Total Torque [Nm]		0.115

Method 2 - Book Manu. Automation	
Torque guideway (Tgf) [N.mm]	0.237319119
Torque bearings (Tlf) [N.mm]	11.772
Torque leadscrew (Tf) [N.mm]	3.74714398
Static Torque [N.mm]	15.7564631
Inertia workpiece (Jtw) [kg.mm^2]	0.070924829
Inertia leadscrew (Jl) [kg.mm^2]	2.349008097
Total Inertia [kg.mm^2]	7.74E+01
Total Dynamic Torque [N.m]	1.17E-01
Total Torque [N.m]	0.133

Method 3 - Cool Muscle Software	
Total Torque [N.m]	0.115

Linear Table Parameters	
Diamter [mm]	10
Pitch [mm]	2
Leadscrew travel [mm]	200
Leadscrew length [mm]	304.8
Efficiency - From Graph	0.28
Co-eff. Friction Bearing/Leadscrew	0.2
Gravity [m/s^2]	9.81
Carriage Length (H) [mm]	50
Mass of table [kg]	0.1
Material density [kg/m^2]	7850
Motor shaft Inertia [kg/m^2]	7.50E-05
Motor rotation speed [revs/sec]	0.83333333
Maximum Speed [mm/min]	100
Time to accelerate [s]	0.004
Angluar velocity [rad/s]	5.23598776
Mass leadscrew [kg]	0.18792065
Guideway friction coefficient (ugf)	0.1
Sample Parameters	
Mass Sample [kg]	0.6
Maximum Applied Force [kg]	0.6
Offset Dist (D) [mm]	50

D.3 – System Options

Configuration and component details of the three proposed systems are shown in Figure 52.

Figure 52 – Micropenetrometersystem options (a) Most Expensive "Ferrari" version (b) Intermediate version and (c) Economical version.

(a)

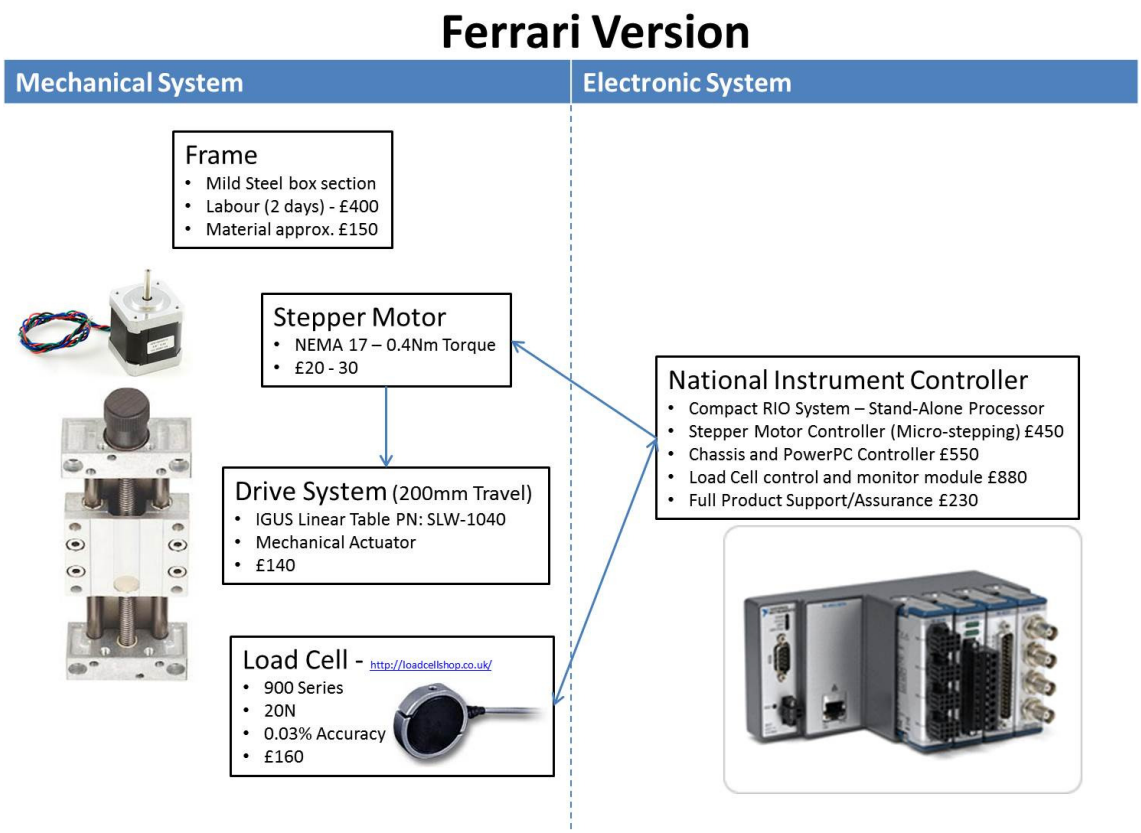

(b)

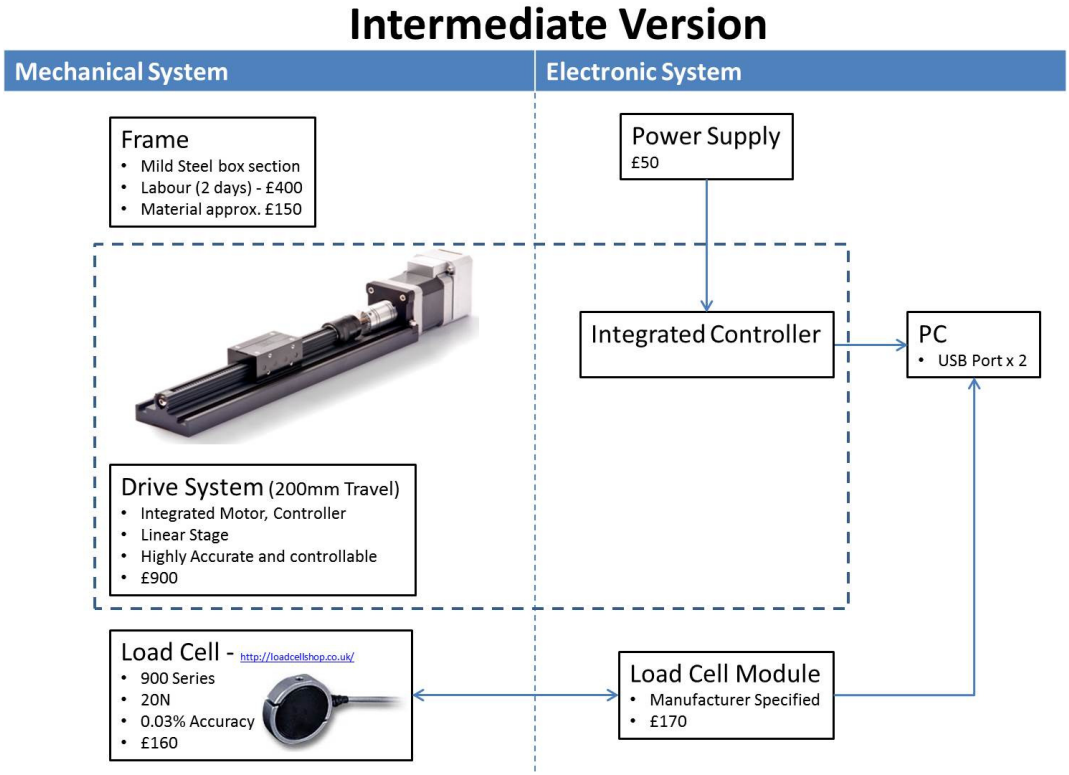
Intermediate Version
Mechanical System
Electronic System
Frame
• Mild Steel box section
• Labour (2 days) - £400
• Material approx. £150
Power Supply
£50
Integrated Controller
PC
• USB Port x 2
Drive System (200mm Travel)
• Integrated Motor, Controller
• Linear Stage
• Highly Accurate and controllable
• £900
Load Cell - http://loadcellshop.co.uk/
• 900 Series
• 20N
• 0.03% Accuracy
• £160
Load Cell Module
• Manufacturer Specified
• £170

(c)

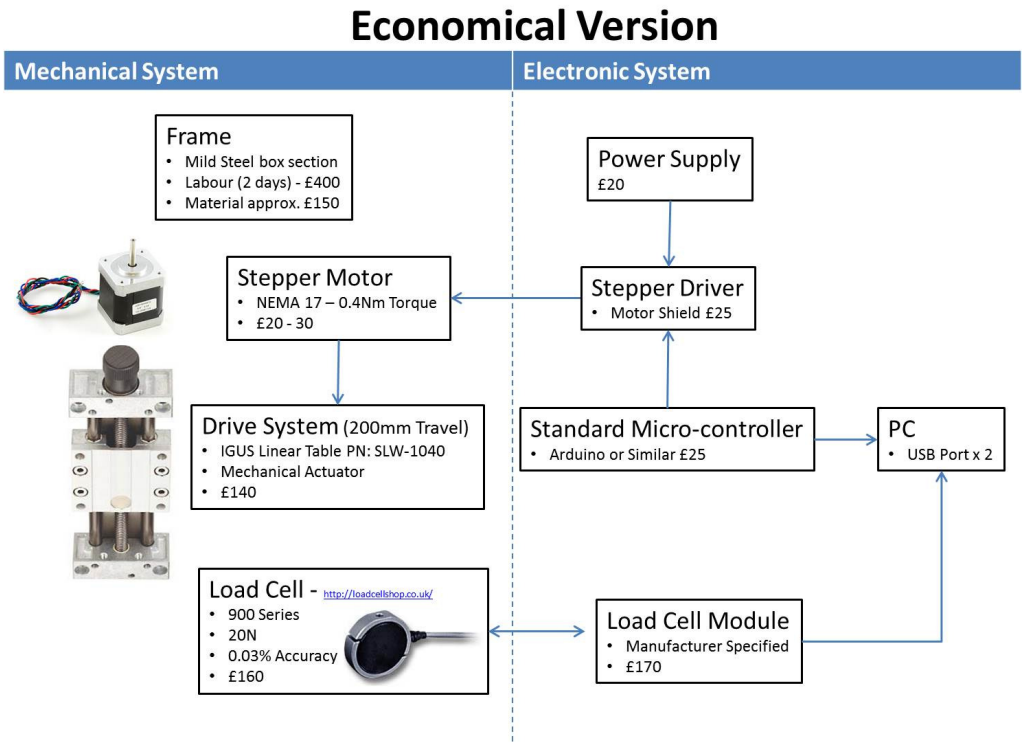
Economical Version
Mechanical System
Electronic System
Frame
• Mild Steel box section
• Labour (2 days) - £400
• Material approx. £150
Power Supply
£20
Stepper Motor
• NEMA 17 – 0.4Nm Torque
• £20 - 30
Stepper Driver
• Motor Shield £25
Drive System (200mm Travel)
• IGUS Linear Table PN: SLW-1040
• Mechanical Actuator
• £140
Standard Micro-controller
• Arduino or Similar £25
PC
• USB Port x 2
Load Cell - http://loadcellshop.co.uk/
• 900 Series
• 20N
• 0.03% Accuracy
• £160
Load Cell Module
• Manufacturer Specified
• £170

D.4 – Component Specifications

Load Cell

Richmond Industries Series 900 – 20N Capacity.

Specification: (Standard Output)

Standard Ranges	0 to 5, 10, 20, 50, 100, 250, 500N
Excitation Voltage	10V (normal), 15V (max) DC*
Sensitivity	2.0 mV/V (nominal)*
Non-Linearity	0.03% of F.R.O or Better
Hysteresis	0.03% of F.R.O or Better
Zero Balance	0.50% of F.R.O
Bridge Resistance	350 Ohm
Over Load Characteristics	500% with no loss in Calibration (300% > 250N) 500% with no Structural failure (300% > 250N)
Insulation Resistance	> 1000M Ohm
Storage Temp	-40 to +70 Degrees C
Operating Temp	-20 to +70 Degrees C
Compensated Temp	+20 to +70 Degrees C (Standard)
Electrical Connections	Integral Screened Cable
Thermal Sensitivity	0.005% of F.R.O/Degrees C

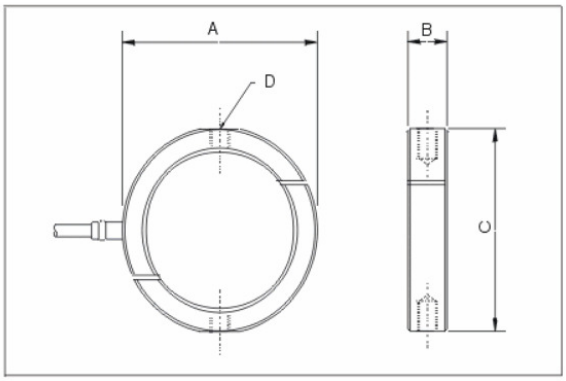

A=50mm

B=12.5mm

C=48mm

Reliance Cool Muscle Motorised Stage PN: RCMS17L-M02-C-1-12

Size 17

Reliance Cool Motion Stage
RCMS Leadscrew Actuator

All dimensions in mm
unless otherwise stated

Associated Products
Hardware: page 13-1

1

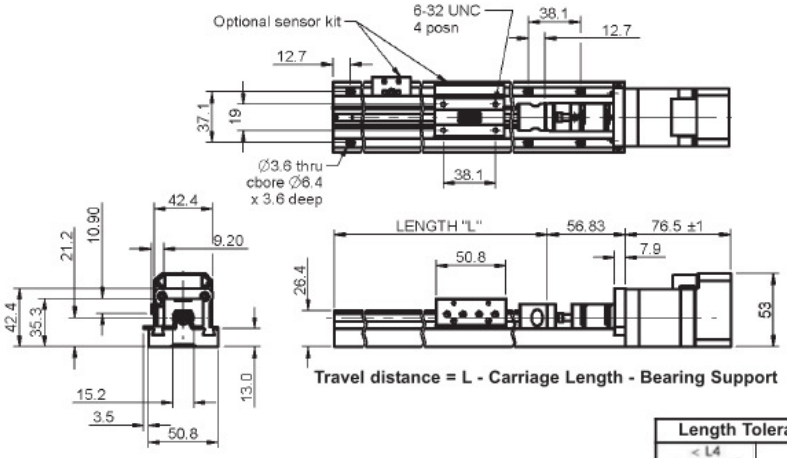

Travel distance = L - Carriage Length - Bearing Support

Length Tolerances	
< L4	± 0.1
4 < L ≤ 16	± 0.15
16 < L ≤ 63	± 0.2
63 < L ≤ 250	± 0.3

Part number selection table

Example Part No. RCMS17L-M04-(C/P)-1-18-S — Denotes Sensor Kit

Basic Part Number	Screw Lead mm (Inch)	Motor Interface	No. Carriages #	Linear Resolution (Default) mm	Max Drag Torque Nm	Standard Guide Lengths `L` Inch
RCMS17L-M02	2.0	C (Computer) P (Pulse)	1	0.002	0.03	12 18
RCMS17L-M04	4.0			0.004	0.04	12 18
RCMS17L-M012	12.0			0.012	0.04	12 24
RCMS17L-M25	25.0		2	0.025	0.05	18 24
RCMS17L-0100	(0.100)			0.00254	0.03	10 12 15 18 24
RCMS17L-0200	(0.200)		3	0.00508	0.04	10 12 15 18 24
RCMS17L-0500	(0.500)			0.0127	0.04	12 15 18 24
RCMS17L-1000	(1.000)			0.0254	0.05	12 18 24 36

#Carriage information:
1 = 1 driven carriage
2 = 1 driven and 1 passive carriage
3 = 1 driven and 2 passive carriages

Slide manufactured by Haydon Kerk Motion Solutions

- The RCMS17 assembly combines the high speeds, linear accuracy and reliability of a screw driven linear slide with the intelligence of the Reliance Cool Muscle motor
- The size 17 Reliance Cool Muscle motor encompasses an integrated vector drive, amplifier, H-infinity control, 50,000 count magnetic encoder and a 0-3000 rpm high torque motor into one package
- High performance proprietary polymers and TFE coating extends the life of the slides moving parts
- Precision aluminium guide and carriage, driven by a precision rolled stainless steel leadscrew

Standard Product Sales : +44 (0)1484 601060 +44 (0)1484 601061
www.rpmechatronics.co.uk sales@rpmechatronics.co.uk

D.5 - Design Drawings

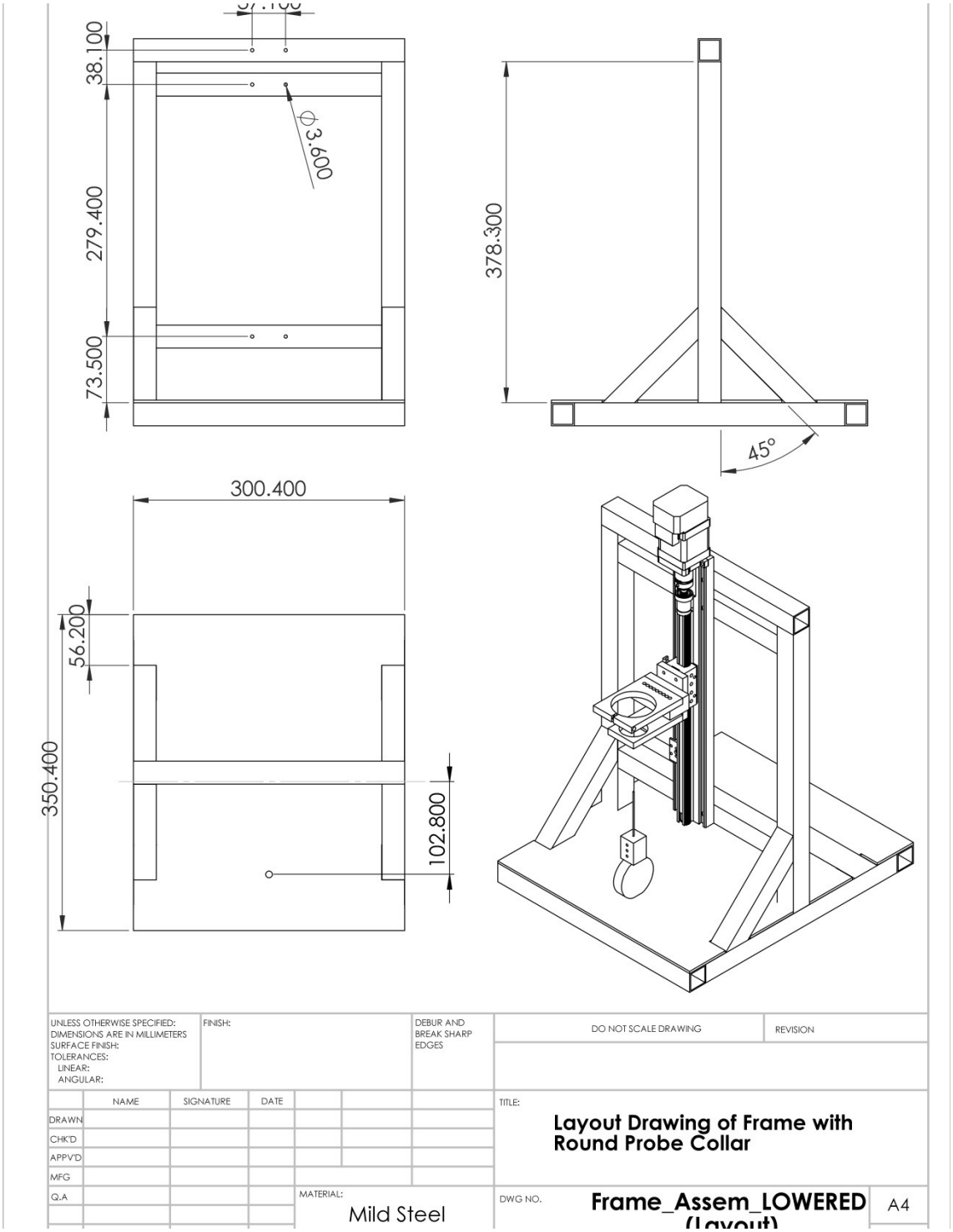

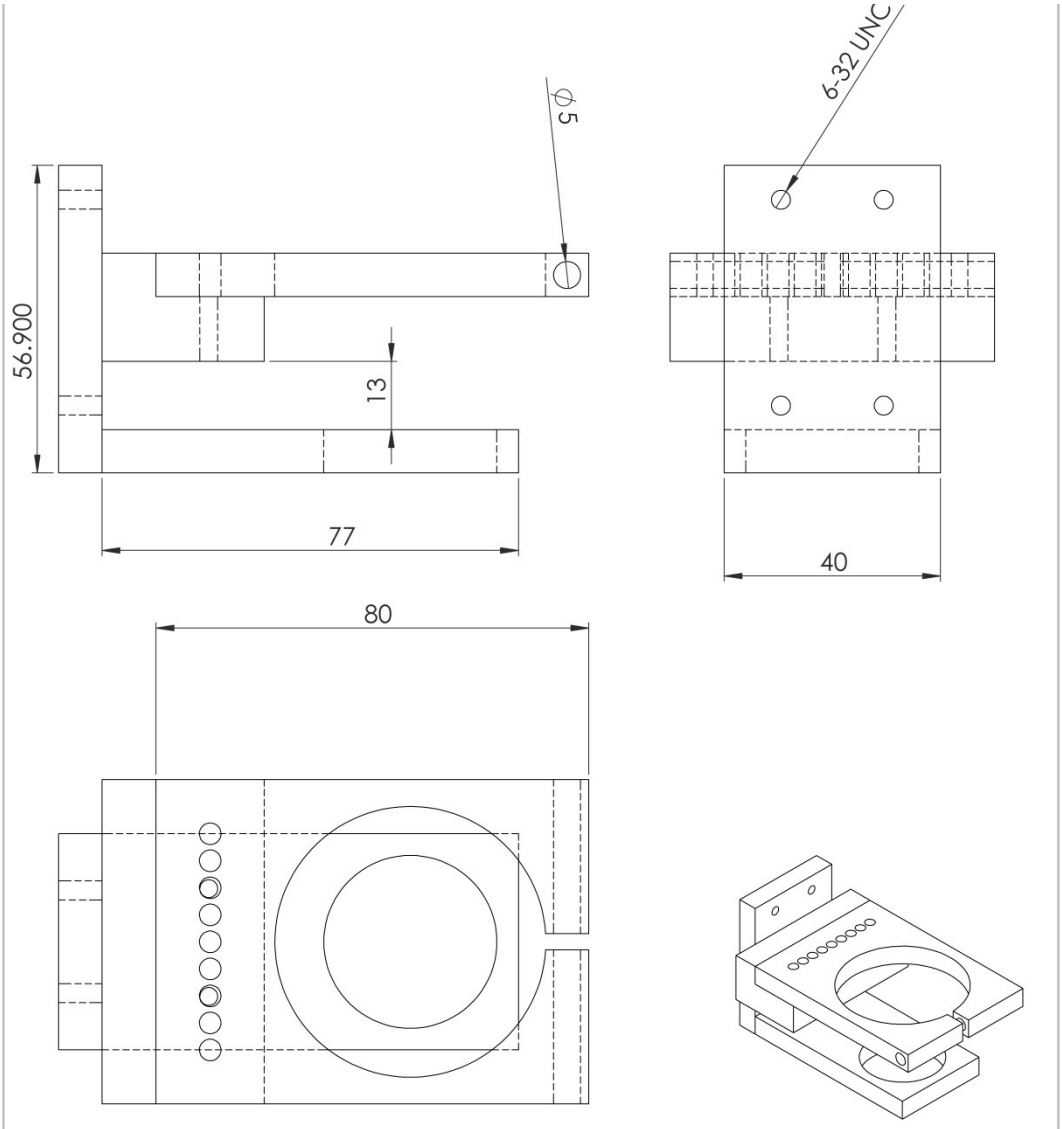

UNLESS OTHERWISE SPECIFIED: DIMENSIONS ARE IN MILLIMETERS SURFACE FINISH: TOLERANCES: LINEAR: ANGULAR:		FINISH:		DEBUR AND BREAK SHARP EDGES	DO NOT SCALE DRAWING	REVISION
	NAME	SIGNATURE	DATE		TITLE:	
DRAWN						
CHK'D						
APPV'D						
MFG						
Q.A				MATERIAL:	DWG NO. **Clamp_Final_171013 (20mm) v2**	A4

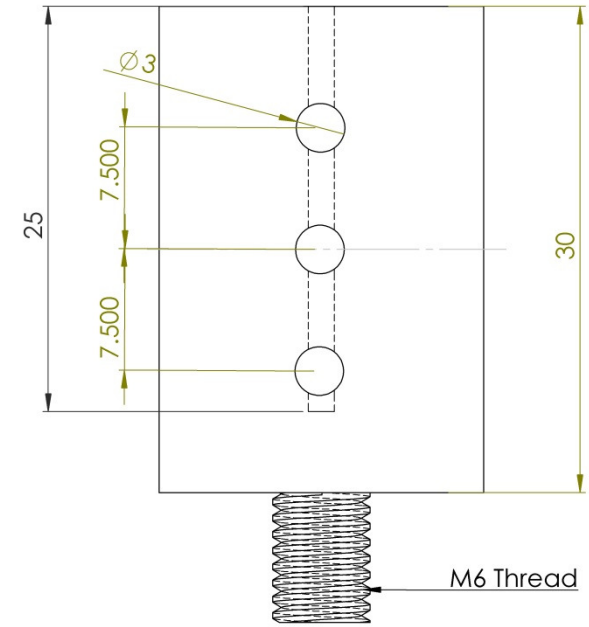

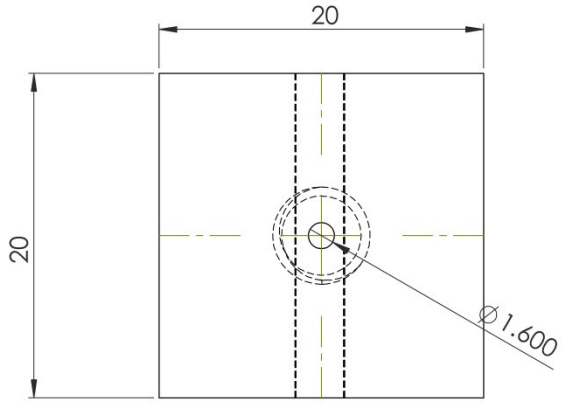

UNLESS OTHERWISE SPECIFIED: DIMENSIONS ARE IN MILLIMETERS SURFACE FINISH: TOLERANCES: LINEAR: ANGULAR:	FINISH:	DEBUR AND BREAK SHARP EDGES	DO NOT SCALE DRAWING — REVISION **230913**

	NAME	SIGNATURE	DATE
DRAWN			
CHK'D			
APP'V'D			
MFG			
Q.A			

MATERIAL: 6061 Aluminium

TITLE: Round Collar - Directly Attaches Probe to Load Cell

DWG NO. **Collar_Square_230913** — A4

Appendix E **- Calibration**

Calibration of the load cell was achieved by comparing the load call force readings with calibrated weights converted to force using gravity at 9.80665m/s^2. At weights above 20g the error in the readings dropped significantly to below 1%. The final calibration curve is presented below together with the obtained calibration conversion equation and confirmation of 100% linear correlation.